Uranium and Molybdenum Isotope Constraints on Ocean Redox Conditions During Deposition of the Upper Devonian Kettle Point Formation, Ontario

by

Jieying Wang

A thesis
presented to the University of Waterloo
in fulfillment of the
thesis requirement for the degree of
Master of Science
in
Earth Sciences

Waterloo, Ontario, Canada, 2016

© Jieying Wang

Authors Declaration

I hereby declare that I am the sole author of this thesis. This is a true copy of the thesis, including any required final revisions, as accepted by my examiners.

I understand that my thesis may be made electronically available to the public.

Abstract

The Late Devonian extinction event was among the most severe Phanerozoic mass extinction events, which led to a decline in the abundance and diversity of marine and terrestrial ecosystems, particularly tropical shallow-marine faunas. However, the key trigger of this event is still being debated. Here, a multi-proxy study using Mo and U isotopes and elemental data from black shales of the Kettle Point Formation (southwestern Ontario, Canada) has been carried out to evaluate the role of local versus global ocean redox conditions on the Frasnian-Famennian mass extinction event. High total organic carbon (TOC) (3.1-15.6 wt%) and total sulfur contents (1.2-6.0 wt%) as well as high Mo (38–448) and U enrichments (3-27) and high Mo EF / U EF ratios (average = 10.3 ± 2.4, 1 SD, about 3× the modern seawater weight ratio) are observed in the black shales, suggesting a locally euxinic depositional environment with Fe-limitation. The high Mo/U ratios also suggest operation of an Fe-Mn particulate shuttle that accelerated transfer of Mo to the sediments. A distinctive change in the Mo/TOC slope from the lower-middle Kettle Point Formation (~8 ppm/wt% in Units 1–3) to the upper Kettle Point Formation (~35 ppm/wt% in Unit 4) may reflect a transition from moderate to weak basin restriction from the open ocean. The δ^{98}Mo values in the Kettle Point Formation range from 0.55‰ to 1.73‰ (average = 0.96‰), and display an upward decreasing trend from Units 1–3 (0.62-1.73‰, average = 1.21‰) to Unit 4 (0.55-0.98‰, average = 0.78‰). The δ^{238}U values vary from –0.14‰ to 0.54‰, exhibiting an upward increasing trend from –0.14‰ to 0.20‰ (average = –0.02‰) in Units 1–3, and from 0.11‰ to 0.54‰ (average = 0.34‰) in Unit 4. Based on the Mo and U isotope data and their stratigraphic trends, two scenarios are proposed: 1) a greater global extent of ocean anoxia occurred during Units 1–3, and was followed by a switch to a more oxygenated global ocean during Unit 4; and 2) the extent of local basin restriction from the open ocean changed, whereas the global ocean redox state was relatively invariant. The second scenario is preferred because a moderate negative correlation is observed between the Mo and U isotope compositions, which is more easily explained by a change in the extent of basin restriction rather than global ocean redox conditions. Our data permit a slightly greater extent of ocean anoxia/euxinia compared with today, but the relatively widespread ocean oxygenation suggests that ocean anoxia was not the key driver of the Late Devonian mass extinction event.

Acknowledgements

I wish to express my sincere gratitude to my supervisor, Dr. Brian Kendall, for his expertise, patience, and understanding. I have always been touched by his dedication and great heart to help his students. The successful and final outcome of this thesis cannot be achieved without his precious guidance and assistance on both lab work and writing. Above all, I will never have this chance to do this project without him providing me opportunities.

I'm grateful to my lab manager, Liyan Xing, for her kind help which ensured the smooth running of my laboratory work. I benefited a lot from her guidance, especially when doing the Mo and U column chemistry. Joy Hu and Wang Zheng are thanked for assistance with elemental and isotope measurements. Charles Wu is acknowledged for assistance with total organic carbon and total sulfur measurements.

I would like to thank my committee members Dr. Lingling Wu and Dr. Chris Yakymchuk for their generous time, comments, and support that have helped to improve my thesis project. Many thanks to them being my committee members.

I would like to thank Mr. Jordan Clark, the manager of Ontario Oil, Gas and Salt Resources Library, for providing me the Kettle Point black shale samples. I also thank Catherine Beland-Otis for suggestions on drill core sampling and for constructive comments that improved this thesis.

I would also like to thank the following colleagues and school mates for their love and support (including but not limited to): Xinze Lu, Ryan Truong, Su Wang, Wanqing Lu, Ying Wang, Shuai Yang, Lingyi Kong, Kai Liu, Fanlong Meng, and Yan Zhang.

This research was financially supported by a NSERC Discovery Grant and a University of Waterloo faculty startup grant to Dr. Brian Kendall.

Table of Contents

List of Figures

List of Tables

1. Introduction

The Late Devonian extinction event is recognized as one of the most prominent Phanerozoic mass extinction events (McGhee, 1996; Ryder, 1996; Sepkoski, 1986; Stearn, 1987; McGhee et al., 2013; Formolo et. al., 2014). This severe event led to a decline in the abundance and diversity of marine and terrestrial ecosystems, particularly tropical shallow-marine reef communities, and occurred in multiple pulses, including the Givetian-Frasnian Taghanic, Frasnian-Famennian Kellwasser, and end-Devonian Hangenberg events (Sepkoski, 1986; Stearn, 1987; Droser et al., 2000; Alroy et al., 2008; Stigall, 2012; McGhee et al., 2013). The most pronounced mass extinction, the Kellwasser event, is estimated to have lasted 16-18 kyr (Sepkoski, 1986; McGhee et al., 2013; George et al., 2014; Huang and Gong, 2016). The cause of this mass extinction event is controversial and has been proposed to involve one or more of the following factors: expanded ocean anoxia/euxinia, sea-level changes, global cooling, eutrophication, tectonism, climate change, biogeochemical cycle perturbations, submarine hydrothermal activity, or volcanism (Joachimski and Buggisch, 1993; Copper, 2002; Racki et al., 2002; Yudina et al., 2002; Tribovillard et al., 2004; Averbuch et al., 2005; John et al., 2010; George et al., 2014).

The expansion of ocean anoxia/euxinia is commonly invoked as a key trigger of the Frasnian-Famennian mass extinction event due to the close stratigraphic association between the extinction event and the Kellwasser Anoxia Events (Wignall and Hallam, 1992; McGhee, 1996; Wignall and Twitchett, 1996; Jin et al., 2000; Tribovillard et al., 2004; Riquier et al., 2006; Carmichael et al., 2014; Formolo et al., 2014; George et al., 2014). Although various approaches (e.g., carbon isotopes, oxygen isotopes, iron speciation, and trace metal geochemistry) have been conducted to evaluate the role of anoxia in triggering the Frasnian-Famennian extinction event (Joachimski, 1997; Joachimski and Buggisch, 2002; Yudina et al., 2002; Bond et al., 2004; Tribovillard et al., 2004; Formolo et. al., 2014; George et al., 2014; Ma et al., 2016), these techniques are better suited for inferring local rather than global ocean redox conditions. Hence, no consensus has been reached because of the lack of geochemical data that enables more quantitative constraints to be placed on the extent of global ocean anoxia before, during, and after the extinction event.

For instance, Formolo at al. (2014) associated the establishment and expansion of euxinic conditions with the Kellwasser extinction on the basis of TOC contents, carbon and

sulfur isotope compositions, sedimentary iron speciation, and Mo and U concentrations preserved in the Antrim Formation (Michigan Basin, U.S.A.). The coeval Upper Devonian Woodford Shale (Permian Basin, west Texas) is significantly enriched in redox-sensitive metals such as Mo, U, S and Se, suggesting the development of water column anoxia around the Frasnian-Famennian boundary (Harris et al., 2013). The development of water column anoxia in the Permian Basin may reflect a greater extent of basin restriction from the open ocean as a result of a short-lived but significant fall in sea level. Organic geochemical data from a Late Devonian reef system (Canning Basin, Australia) suggest that photic zone euxinia contributed to the mass extinction (Tulipani et al., 2015). Similar examples of photic zone euxinia have been described from other Late Devonian sections (Summons and Powell, 1986, 1987; Requejo et al., 1992; Marynowski et al., 2000; Joachimski et al., 2001; Brown and Kenig, 2004; Marynowski and Filipiak, 2007; Marynowski et al., 2011; Melendez et al., 2013).

However, a number of studies argue against a significant expansion of ocean anoxia/euxinia. Benthic cyanobacterial mats present in Late Devonian black shales and limestones from Poland are more consistent with fluctuating redox conditions than persistent anoxia or euxinia (Kazmierczak et al., 2012). George et al. (2014) concluded that anoxia was not a major driver of the mass extinction based on the limited correlation between positive carbon isotope excursions and peaks in the total organic carbon (TOC) contents of sedimentary rocks, and instead highlighted the importance of regional changes in tectonism, sealevel, and nutrient supply. Fossil charcoal (i.e., inertinite) in Late Devonian marine black shales provides evidence of continuous and sustained fire events, which in turn indicates high atmospheric O_2 levels during Late Devonian time (Rimmer et al., 2015). Hence, the inferred expansion of ocean anoxia and euxinia inferred by previous studies may have been confined to local continental margin basins and epicontinental seaways rather than occurring globally throughout the open oceans. A better understanding of the environmental changes in the Late Devonian is needed, which requires the application of new tools (e.g., geochemical redox proxies applicable to global ocean chemistry) to help test these hypotheses.

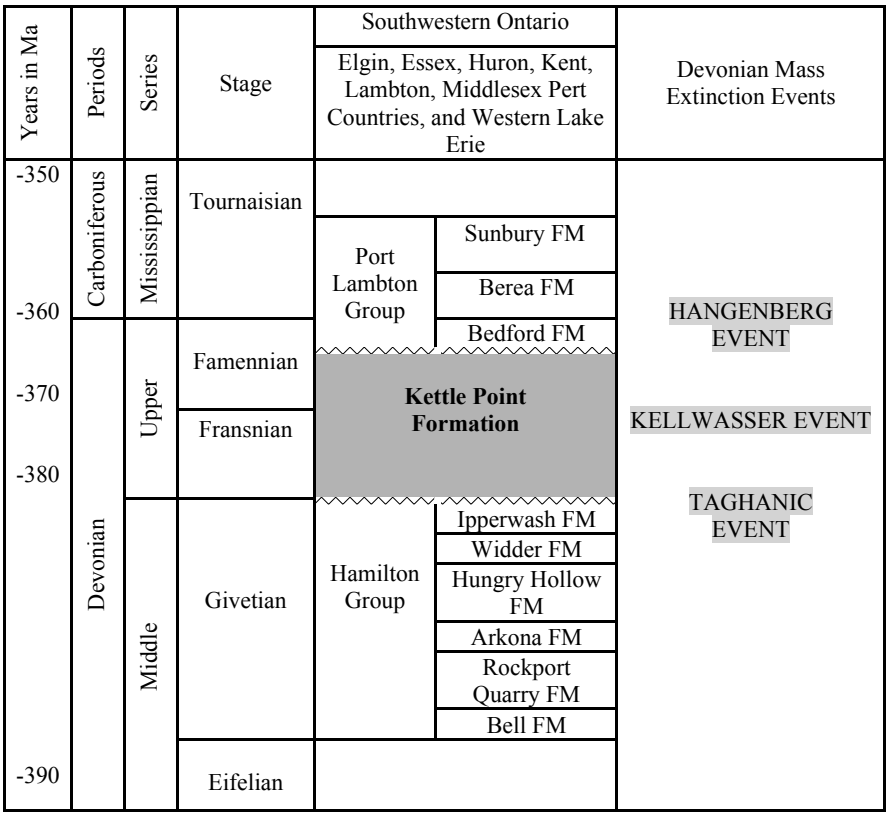

Fig. 1. Stratigraphic section for southwestern Ontario showing the Kettle Point Formation. The locations of the Late Devonian mass extinction events are plotted (modified from Haq and Schutter, 2008; Armstrong and Carter, 2010; Béland Otis, 2013).

The concentration and isotopic composition of redox-sensitive trace metals in black shales are utilized in this thesis as paleoceanographic proxies. Recent studies have shown that such measurements on black shales and carbonates are particularly valuable for reconstructing local and global ocean paleoredox conditions and the extent of paleoproductivity at the time of deposition (Tribovillard et al., 2006; Weyer et al., 2008; Algeo and Tribovillard, 2009; Scott and Lyons, 2012; Kendall at al., 2015). In terms of dissolved O_2 concentrations, waters can be classified into oxic (> 2.0 ml O_2/L), suboxic (~0.2-2.0 ml O_2/L), anoxic/non-sulfidic (< 0.2 ml O_2/L, 0 ml H_2S/L), and anoxic/sulfidic or euxinic (0 ml O_2/L, > 0 ml H_2S/L) (Tyson and Pearson, 1991). The conservative behavior of Mo and U under oxic conditions and their long oceanic residence time (10^5 years) compared to the global ocean mixing time (10^3 years), make them particularly convincing proxies for global paleoenvironmental analysis (e.g., Scott et al., 2008; Partin et al., 2013). The geochemical behavior of Mo in Earth surface environments is intimately linked to the

relative availability of dissolved H_2S and O_2, with the rate of Mo removal to sediments strongly tied to dissolved H_2S concentrations (Emerson and Huested, 1991; Crusius et al., 1996; Morford and Emerson, 1999; Morford et al., 2005; Scott et al., 2008; Scott and Lyons, 2012). Hence, the Mo isotope compositions of Mo-rich black shales deposited from euxinic waters are best used to place constraints on the extent of ocean euxinia (Arnold et al., 2004; Neubert et al., 2008; Gordon et al., 2009). By contrast, the removal of U to sediments occurs under O_2–deficient conditions independent of the amount of dissolved H_2S (Morford and Emerson, 1999; Morford et al., 2005), and thus the U isotope composition of black shales is more indicative of the extent of general ocean anoxia (both sulfidic and non-sulfidic) (Weyer et al., 2008; Montoya-Pino et al., 2010). Based on the analysis of Mo and U isotopic compositions, the long-term evolution of global ocean oxygenation and atmospheric O_2 levels can be tracked (e.g., Arnold et al., 2004; Weyer et al., 2008; Dahl at al., 2010; Montoya-Pino et al., 2010; Kendall et al., 2015). For instance, an early Devonian rise in atmospheric and ocean O_2 concentrations by no later than 400 Ma was inferred based on a compilation of Mo isotope data for black shales (Dahl at al., 2010).

No previous studies have attempted to use both Mo and U isotopes to constrain the global ocean redox conditions during the Late Devonian. In addition, the time resolution of existing Mo isotope data for the Devonian is low (Dahl et al., 2010). Combined U and Mo isotope analyses of the Frasnian-Famennian Kettle Point Formation (southwestern Ontario, Canada) are used in this study to determine the extent of ocean anoxia and euxinia at this time, respectively, which in turn is used to infer the role of ocean redox conditions on the Frasnian-Famennian mass extinction.

The Kettle Point Formation is also of great interest because of its shale gas potential in southwestern Ontario. However, due to environmental concerns (e.g., contamination of drinking water supplies), the exploitation of shale gas in Ontario is still limited (Béland-Otis, 2013). A better understanding of the depositional environment of the Kettle Point Formation is of vital significance. The local redox conditions during deposition may provide useful information about the source rock and shale gas quality. For example, accumulation of abundant sulfur-rich organic matter may occur in sediments because of anoxic, sulfide-rich, and iron-limited conditions, which prevents all sulfide produced from microbial sulfate reduction from being locked up in pyrite (Dean and Arthur, 1989). During catagenesis, sulfur-rich kerogen may be thermally cracked to produce hydrocarbons, which

can thus include sour gas that is detrimental economically and environmentally (Waples, 2013). In contrast, deposition from mildly oxygenated bottom waters (with limited O_2 penetration into sediments but also low H_2S concentrations in sediment pore waters) would lead to deposition of organic matter that is not as sulfur-rich and thus the thermogenic shale gas produced is more economically and environmentally beneficial.

The main goals of this study are to: 1) reconstruct and characterize the local and global paleoredox conditions through analysis of the Fe-TOC-S systematics, Mo and U abundances, Mo/U ratios, and Mo and U isotope compositions in the Kettle Point Formation, in order to evaluate the role of local versus global ocean redox conditions on the Late Devonian mass extinction events; and 2) infer the economic and environmental implications of local ocean redox conditions for the quality of shale gas at the study site.

2. Geological Setting

The Kettle Point Formation is dominated by fissile, petroliferous, organic-rich, dark grey to black mudstone (i.e., black shale) and is known as a potential shale gas resource in southwestern Ontario (Harris, 1985; Russell, 1985; Armstrong, 1986; Armstrong and Dodge, 2007; Armstrong and Carter, 2010; Hamblin, 2010; Béland-Otis, 2013). It is named after the large semispheroidal carbonate concretions (called kettles) composed of fibrous and carbonate cement that formed during early diagenesis (Coniglio and Cameron, 1990; Béland-Otis, 2013). The Kettle Point Formation is preserved between the Algonquin and Findlay arches in a structural depression called the Chatham Sag that separates the Appalachian and Michigan basins (Fig. 2). The Kettle Point Formation was deposited as the distal portion of the Catskill deltaic wedge complex in an epeiric sea within the Appalachian Foreland Basin during the Acadian Orogeny (Broadhead et al., 1982; Klemme and Ulmishek, 1991; Gutschick and Sandberg, 1991; Ettensohn, 1992; Hamblin, 2010). The Middle-Late Devonian Acadian Orogeny is part of the larger Appalachian Orogeny (which lasted from the Ordovician to Permian), and is reflected in the transition from Early Devonian carbonate-dominated deposits (Bois Blanc Formation) to the Middle Devonian siliciclastic-dominated deposits (Hamilton Group), and the Late Devonian black shales (Kettle Point Formation) (Bingham-Koslowski et al., 2016). Eustatic sea-level rise, foreland subsidence, and associated transgression over the Middle Devonian platform ultimately led to the deposition of the Kettle Point Formation (Ettensohn, 1992; Roen, 1984; Bingham-Koslowski et al., 2016).

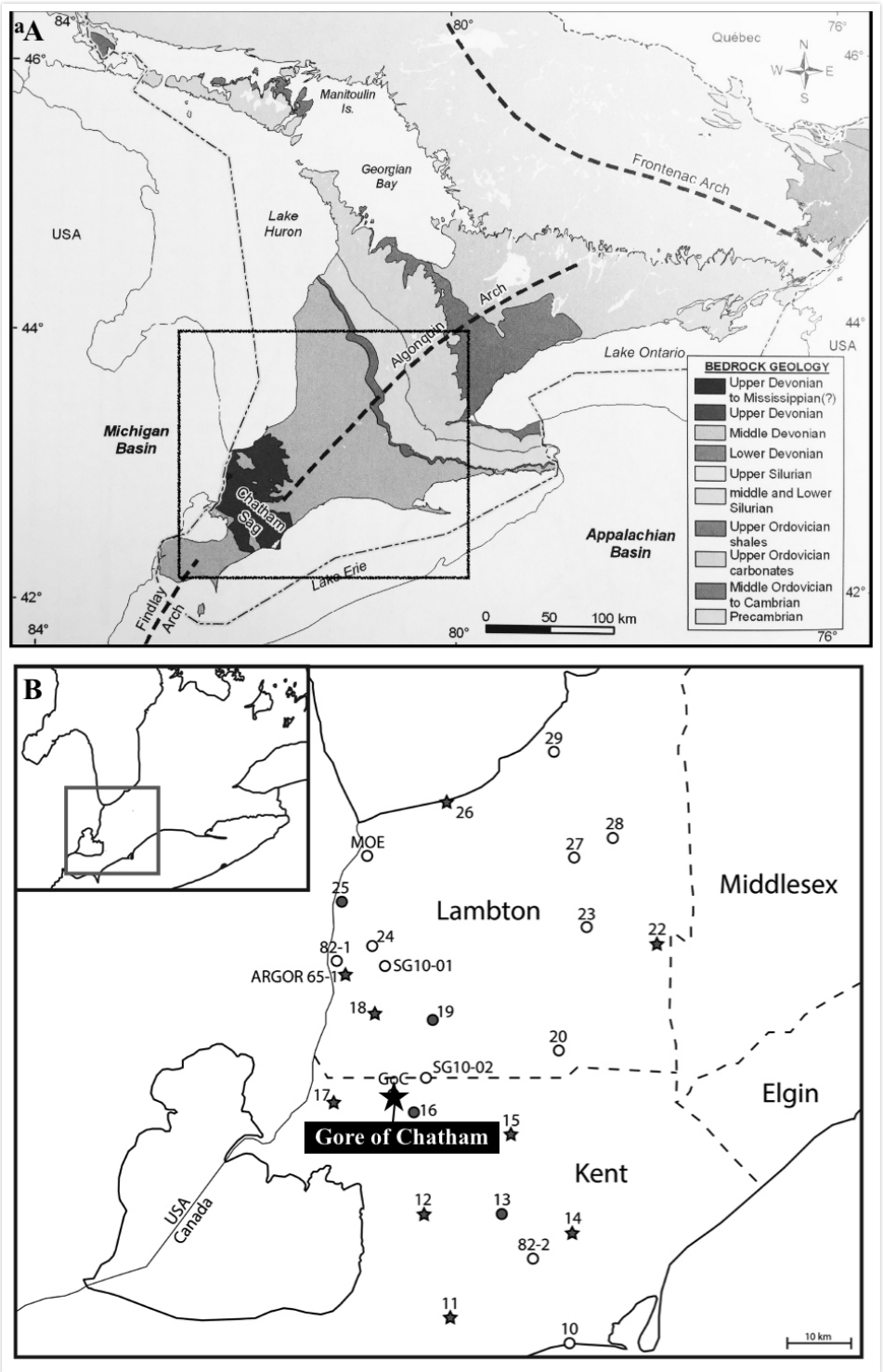

Fig. 2. A. Geological map showing the location of the Chatham Sag in which the Kettle Point Formation was deposited. The enclosed region is expanded in B. B. Drill core sites in Ontario containing the Kettle Point Formation. Black star is the 'Gore of Chatham' core where samples were obtained for this study. Modified from Armstrong and Carter (2010) and Bingham-Koslowski et al. (2016).

The Frasnian-Famennian Kettle Point Formation disconformably underlies the Famennian/Mississippian Bedford Formation of the Port Lambton Group in a small area near the St. Clair River and disconformably overlies the Givetian Hamilton Group (Sanford and Brady, 1955; Russell, 1985; Hamblin, 1998; Béland-Otis, 2013; Bingham-Koslowski et al., 2016). The Kettle Point Formation has a limited outcrop area in southwestern Ontario, as most of it is covered by Quaternary sediments (Hamblin, 2010; Bingham-Koslowski et al., 2016). The stratigraphically equivalent shale unit of the Kettle Point Formation to the south in the U.S.A., the Antrim Shale in the Michigan Basin, has been a target for shale gas since the late 1980s (Witt, 1986; Agrawal, 2009; Hamblin, 2010; Béland-Otis, 2013; Bingham-Koslowski et al., 2016). Moreover, the Kettle Point Formation is lithologically and stratigraphically equivalent to the Ohio Shale (Ohio) and the New Albany Shale (New York), which is supported by gamma-ray log correlations (Uyeno et al., 1982; Russell, 1985; Hamblin, 2010; Béland-Otis, 2013). As the equivalents of these productive units in adjacent sedimentary basins, the Kettle Point Formation has previously been identified as having the same oil and gas potential in the 1980s by the Ontario Geological Survey as part of the Hydrocarbon Energy Resources Program (Johnson et al., 1983; Stromquist et al., 1984; Powell et al., 1984).

In previous studies, much attention focused on the sedimentary depositional environments of the Kettle Point black shales, as well as their potential as hydrocarbon source rocks. After Caley (1943, 1945) first gave the Kettle Point Formation a stratigraphic definition, the stratigraphy of the unit was successively studied by many workers, including Sanford and Brady (1955), Macdonald (1960), Russell and Barker (1983), Armstrong (1986), Coniglio and Cameron (1990), and Russell (1985, 1993). Many wells were cored in order to study and evaluate the oil and gas resource potential in the Kettle Point Formation by the Ontario Geological Survey (OGS). A detailed lithological examination of the Kettle Point Formation in 21 cores was published by Harris (1985), containing a characterization of bed thicknesses, grain size, bioturbation, pyrite nodules, and fossils. Based on the core descriptions by Harris (1985), Russell (1985) divided the Kettle Point Formation into subunits using gamma ray signatures. More core and outcrop descriptions were completed by Hamblin (2010) on the Kettle Point Formation, who identified the facies of the formation as: (A) abundant black laminated mudstone, (B) minor greenish grey silty mudstone and muddy siltstone, (C) rare reddish siltstone and mudstone, and (D) rare grey fine-grained limestone. Source rock potential, mechanical properties, petrology,

paleontology, and geochemistry of the Kettle Point Formation have all been explored in many studies (Loftsson, 1984; Powell et al., 1984; Delitala, 1984; Armstrong, 1986; Dusseault at al., 1986; Hamblin, 2006, 2010; Béland-Otis, 2013; Bingham-Koslowski et al., 2016).

There are 26 cores in Ontario reported to contain the Kettle Point Formation. Recently, nine cores were logged in detail (OGS KP-11, OGS KP-12, OGS KP-14, OGS KP-15, OGS KP-17, OGS KP-18, OGS KP-22, OGS KP-26, and ARGOR 65-1) by Bingham-Koslowski et al. (2016), complementing the efforts of previous workers. The thicknesses of the cores vary from several meters to over a hundred meters, and the average thickness is about 28 m, although it is noted that the upper contact of the Kettle Point Formation is not usually preserved in the cores (Armstrong and Carter, 2010; Bingham-Koslowski et al., 2016). The thickest and most complete sections of the Kettle Point Formation occur in the middle of the Chatham Sag, whereas thinner sections occur along the basin margins. All the samples in this study are taken from the Gore of Chatham in the middle of the basin, which contains one of the thickest intervals of the Kettle Point Formation at 111.10 m.

Detailed core and thin section analysis of multiple cores previously showed that the Kettle Point Formation mainly consists of laminated to non-laminated black shale with subordinate amounts of interbedded grayish green silty mudstone (Harris, 1985; Armstrong, 1986; Hamblin, 2010; Béland-Otis, 2013; Bingham-Koslowski et al., 2016). In terms of mineralogy, the Kettle Point Formation mainly contains quartz (27-63 wt.%), clay minerals such as illite and chlorite (18-55 wt.%), dolomite (0-25 wt.%), organic carbon (up to 15 wt.%), pyrite (1-12 wt.%), potassium feldspar (1-6 wt.%), and rutile (0.4 wt.%) (Russell, 1985; Armstrong, 1986; Béland-Otis, 2013; Bingham-Koslowski et al., 2016). Pyrite is found in black shales as finely disseminated crystals and mm- to cm-scale nodules or lenses. Minor minerals include calcite, siderite, gypsum, barite, marcasite, and apatite (Russell, 1985; Armstrong, 1986; Béland-Otis, 2013; Bingham-Koslowski et al., 2016).

The lithostratigraphy of the most complete and thickest sections of the Kettle Point Formation can be subdivided into four units that, in ascending order, include: 1) interbedded green-grey mudstones and black shales containing carbonate concretions; 2) a thick lower black shale unit; 3) interbedded green-grey mudstones and black shales lacking

carbonate concretions; and 4) a thick upper black shale unit (Bingham-Koslowski et al., 2016). These units were interpreted to capture changes in relative sea level during deposition of the Kettle Point Formation, with the thick black shale intervals (Units 2 and 4) deposited in deeper waters and the intervals containing abundant green-grey mudstone (Units 1 and 3) deposited in shallower waters. Black shales from Units 1 and 3 commonly contain laminations rich in silt-sized quartz that may represent higher energy storm or distal turbidite deposits that interrupted periods of quiet-water deposition. These silty laminations are not typically observed in the black shales of Units 2 and 4, consistent with deeper-water deposition of these units (Bingham-Koslowski et al., 2016). Terrestrial fossils, notably the plant fossil *Callixylon*, and coal layers are known from Units 2 and 4, and may originate from the surrounding highlands that were flooded during sea level rise (Harris, 1985; Bingham-Koslowski et al., 2016).

In the Kettle Point Formation, the Frasnian-Famennian boundary is placed approximately at the contact between Units 1 and 2, based on conodont data (Winder, 1966; Uyeno et al., 1982) and the occurrence of the Famennian fossil *Protosalvinia (Foerstia)* in Unit 2 (Bingham-Koslowski et al., 2016). This placement is consistent with the position of the Frasnian-Famennian boundary in the stratigraphically equivalent and lithologically similar Long Rapids Formation (northern Ontario; Levman and von Bitter, 2002).

The black shales of the Kettle Point Formation have the highest pyrite and total organic carbon (TOC) contents of the formation and the lowest sulfur isotope compositions (average $\delta^{34}S$ of about –20‰), indicating preservation of organic matter in the sediments due to an anoxic environment. This interpretation is consistent with the lack of bioturbation, especially in Units 2 and 4 (Delitala, 1984; Samson, 2007; Hamblin, 2010; Bingham-Koslowski et al., 2016). The organic-poor gray-green mudstones in Units 1 and 3 contain no body fossils but do show evidence of bioturbation (*Chondrites* and *Zoophycos* ichnofossils are common in these mudstones and in the immediately underlying interlaminated black shales) and have less negative to positive sulfur isotope compositions, thus indicating a periodic switch to mildly oxygenated bottom waters and surface sediments (Béland-Otis, 2013; Bingham-Koslowski et al., 2016). Water column stratification (well-oxygenated surface waters and anoxic deeper waters) is implied by the presence of *Tasmanites* (algae) and rare fish scale fossils in the black shales (Bingham-Koslowski et al., 2016). In reducing depositional environments, metal fixation in sediments is enhanced

because of the lower solubility and higher particle reactivity of many redox-sensitive metals, resulting in their removal from the water column to sulfide minerals, organic matter, clay minerals, or other authigenic mineral phases (e.g., Tribovillard et al., 2006). Hence, Devonian black shales are characterized by their enrichment in trace metals such as Mo, U, V, Re, Ni, Cu, and Zn (e.g., Harris at al., 2013), including the black shales of the Kettle Point Formation (Armstrong, 1986).

The distinct geochemical properties contribute to the potentially significant economic value of black shales in the Kettle Point Formation. Based on Rock-Eval pyrolysis parameters (e.g., density, saturation, matrix permeability, and porosity) and TOC analysis, the Kettle Point Formation is thought to have very good source rock potential (Béland-Otis, 2013). The Kettle Point Formation predominantly contains Type I (algae/bacteria) and II (zooplankton/phytoplankton/bacteria) kerogen from marine sources, which is characterized as having high and intermediate hydrogen/carbon ratios, respectively, and possibly also contains minor amounts of Type III kerogen with low hydrogen/carbon ratios (derived from terrigenous woody plant matter) (Tissot and Welte, 1978; Wignall, 1994; Hamblin, 2010; Béland-Otis, 2013). According to previously published data (Snowdon, 1984; Obermajer, 1997; Béland-Otis, 2013), the T_{max} (i.e., the temperature at which cracking of kerogen during pyrolysis generates the maximum amount of hydrocarbons), and vitrinite reflectance (i.e., %Ro) values associated with the Kettle Point Formation are 424–440°C and 0.42–0.70, respectively (Obermajer, 1997; Obermajer et al., 1997; Béland-Otis, 2013). With respect to thermal maturity for petroleum production, these parameters suggest that the organic matter in the Kettle Point Formation is immature to early mature. Hence, only limited quantities of thermogenic gas is inferred to have been produced (Obermajer 1997; Samson, 2007; Béland-Otis, 2013). Instead, the gas may dominantly be of biogenic (microbial) origin, consistent with the carbon and deuterium isotope compositions of methane. The gas composition is dominated by methane with minor amounts of heavier hydrocarbons and carbon dioxide (Coleman et al., 1995; Béland-Otis, 2013). Similarly, the natural gas produced from the correlative Antrim Shale appears to be biogenic gas mainly composed of methane with variable amounts of carbon dioxide and ethane based on methane isotope analysis and gas composition analysis (Martini et al., 1998; Béland-Otis, 2013).

Despite previous lithological, stratigraphic, organic geochemistry, and light stable

isotope analyses, redox-sensitive trace metals have not been extensively studied in the Kettle Point Formation despite their value for constraining the local and global ocean paleoredox conditions during deposition. Armstrong (1986) examined the trace metal geochemistry (including U, Th, Mo, Fe, Cu, and Zn contents), and interpreted the high enrichments of trace metals and organic matter (including good Mo-TOC and U-TOC correlations) in the black shales to reflect deposition from anoxic bottom waters in a stratified epeiric sea. Algeo and Tribovillard (2009) used the Kettle Point Formation data from Armstrong (1986) to examine covariation in Mo and U concentrations, which were consistent with deposition from predominantly anoxic bottom waters, although low Mo and U enrichments and low Mo/U ratios from a small subset of samples pointed to suboxic bottom waters (see below). Neither Mo or U isotope compositions have been measured previously on the black shales of the Kettle Point Formation.

3. Background: Molybdenum and Uranium Geochemistry

3.1 Molybdenum Geochemistry

Molybdenum concentrations and isotope compositions preserved in ancient black shales represent a significant paleoredox proxy that has provided valuable insights on the Earth's oxygenation history and biogeochemical evolution (Arnold et al., 2004; Algeo and Lyons, 2006; Scott et al., 2008; Dahl et al., 2010; Scott and Lyons, 2012; Reinhard et al., 2013; Chen et al., 2015; Kendall et al., 2015). Molybdenum possesses a long ocean residence time of approximately 440 kyr and a relatively invariant seawater concentration of approximately 105 nmol kg^{-1} (Collier, 1985; Miller et al., 2011). The major source of Mo to modern seawater is the oxidative weathering of crustal sulfides and to a lesser extent black shales, which supplies Mo to rivers, and a minor input flux of Mo comes from low-temperature hydrothermal systems on the ocean floor (Wheat et al., 2002; Miller et al., 2011; Reinhard et al., 2013).

Molybdenum has a distinctive bi-modal geochemical behavior in Earth surface environments, including the oceans, that is controlled by the relative availability of dissolved H_2S and O_2. As the most abundant transition metal in the oceans, Mo displays conservative behavior as soluble MoO_4^{2-} in oxygenated seawater. Despite the conservative behavior of Mo in oxygenated settings, Mo is removed to Mn-oxides and to a lesser extent Fe-oxides in sediments (e.g., Bertine and Turekian, 1973; Shimmield and Price, 1986). However, the adsorption and/or co-precipitation of Mo to Mn nodules and ferromanganese crusts in deep-sea oxic environments is a slow and inefficient process because of the low sedimentation rates in such environments (Morford and Emerson, 1999; Scott et al., 2008).

By contrast, in anoxic and sulfidic (euxinic) settings, the removal of Mo from seawater to sediments is highly efficient (e.g., Bertine and Turekian, 1973; Emerson and Huested, 1991; Crusius et al., 1996; Morford and Emerson, 1999). The presence of dissolved H_2S dramatically increases the reactivity of Mo by converting the relatively unreactive MoO_4^{2-} to particle-reactive thiomolybdate ions ($MoO_{4-x}S_x^{2-}$). When $[H_2S]_{aq}$ is greater than 11 μM, MoO_4^{2-} will be converted to MoS_4^{2-} and then to Mo polysulfide species (Helz et al., 1996; Erickson and Helz, 2000; Zheng et al., 2000; Vorlicek et al., 2004; Dahl et al., 2013). These particle-reactive species are then removed to Fe sulfide minerals, clay minerals, and/or organic matter (Helz et al., 1996, 2004, 2011; Bostick et al., 2003;

Tribovillard et al., 2004; Biswas et al., 2009; Chappaz et al., 2014). With increasing depth in the water column, the concentration of Mo in the Black Sea decreases sharply with increasing concentrations of dissolved H_2S, reflecting the removal of Mo from the euxinic deep waters (Emerson and Huested, 1991; Neubert et al., 2008). Relative to the average Mo abundance in the upper continental crust of 1.5 ppm (McLennan, 2001), Mo is strongly enriched in modern organic-rich sediments deposited from euxinic bottom waters, with concentrations usually greater than 25 ppm and often exceeding 100 ppm (Scott and Lyons, 2012). Hence, high enrichments of Mo in black shales are considered representative of euxinic depositional conditions (Algeo and Maynard, 2004; Tribovillard et al., 2006; Scott et al., 2008; Algeo and Rowe, 2012; Scott and Lyons, 2012).

In euxinic environments, the rate of Mo burial in sediments is two to three orders of magnitude higher than in oxic environments (Bertine and Turekian, 1973; Scott et al., 2008; Reinhard et al., 2013). In environments where bottom waters are weakly oxygenated and sulfide is confined to sediment pore waters, the rate of Mo burial is intermediate between the oxygenated and euxinic end-members (Scott et al., 2008; Scott and Lyons, 2012; Reinhard et al., 2013). Therefore, in oceans that are primarily well-oxygenated like today, the seawater Mo concentration is high because of the large areal extent of oxygenated waters where Mo removal rates to sediments are slow. By contrast, at times of expanded ocean anoxia relative to today, the seawater Mo concentration is lower because of a greater extent of seafloor where Mo is being removed to anoxic (and especially euxinic) sediments more rapidly (Scott et al., 2008; Reinhard et al., 2013).

In addition to global ocean redox conditions, the extent of basin restriction from the open ocean exerts a significant influence on the degree of Mo enrichment in euxinic organic-rich sediments (Algeo and Lyons, 2006). Because Mo and TOC contents are commonly well-correlated for euxinic organic-rich sediments, the Mo/TOC ratio of such sediments is a function of the uptake of Mo per unit organic matter, which has a positive correlation with aqueous Mo concentrations in deep waters. In anoxic silled basin environments with strong restriction, depletion of aqueous Mo occurs as a result of constant Mo removal to sediments without adequate resupply of Mo from the open ocean, leading to a reduced Mo/TOC ratio in euxinic sediments (Algeo and Lyons, 2006). By contrast, in a more open basin, aqueous Mo is always available to be removed to sediments because the rate of Mo recharge to the bottom waters can keep pace with the rate of Mo removal to

sediments, thus yielding a higher Mo/TOC ratio in euxinic sediments. Therefore, the slope of Mo-TOC covariation from euxinic black shales is useful to distinguish degrees of basin restriction in anoxic marine environments, as distinctly increasing Mo/TOC ratios are observed from the strongly restricted Black Sea (4.5 ± 1 ppm/wt%) to the moderately restricted Cariaco Basin (25 ± 5 ppm/wt%) to the weakly restricted Saanich Inlet (45 ± 5 ppm/wt%) (Algeo and Lyons, 2006). The degree of basin restriction also influences the H_2S concentrations of deep waters. The strongly restricted Black Sea and moderately restricted Cariaco Basin are considered modern analogs of ancient strongly and weakly euxinic marine settings, respectively (Anbar and Knoll, 2002; Algeo and Lyons, 2006; Scott et al., 2008; Algeo and Tribovillard, 2009; Lyons et al., 2009).

As a maturing stable isotope system in paleoceanography and biogeochemistry, Mo isotopes have received special attention because of their strong redox sensitivity in marine systems (Fig. 3). Modern global seawater has a high and essentially uniform δ^{98}Mo of 2.34 ± 0.10‰ (Barling et al., 2001; Siebert et al., 2003; Nakagawa et al., 2012). For the main marine source of Mo (rivers), the average δ^{98}Mo is approximately 0.7‰ (Archer and Vance, 2008), whereas the δ^{98}Mo of fluids from low-temperature hydrothermal systems is poorly constrained (McManus et al., 2002). Due to the Mo isotope fractionation caused by adsorption of Mo to Fe-Mn oxides, non-quantitative conversion of molybdate to thiomolybdate in weakly oxygenated to weakly sulfidic systems ($H_2S_{aq} < 11$ μM), and non-quantitative removal of Mo from bottom waters, the lighter Mo isotopes are preferentially removed to sediments, leading to a high modern seawater δ^{98}Mo value (Barling et al., 2001; Barling and Anbar, 2004; Arnold et al., 2004; Poulson et al., 2006; Siebert et al., 2006; Neubert et al., 2008; Poulson Brucker et al., 2009). There is no modern setting in which the heavier Mo isotopes are preferentially removed from seawater to sediments.

In the modern oceans, the magnitude of Mo isotope fractionation between global seawater and sediments varies as a function of O_2 and H_2S contents in the water column and sediment pore waters. Molybdenum burial in the strongly euxinic Black Sea and Kyllaren fjord (Norway) is associated with the smallest extent of isotope fractionation because of high $[H_2S]_{aq}$ (> 11 μM) and strong basin restriction, which together promote both quantitative conversion of molybdate to tetrathiomolybdate and quantitative removal of Mo from bottom waters (Barling et al., 2001; Arnold et al., 2004; Neubert et al., 2008; Noordmann et al., 2015). Euxinic sediments in restricted basins may thus serve as a

recorder of global seawater δ^{98}Mo since the removal of Mo from bottom waters to sediments in strongly euxinic environments can be near quantitative, which is revealed by low Mo/TOC ratios in the sediments (Barling et al., 2001; Algeo and Lyons, 2006). The long oceanic residence time of Mo enables the global seawater δ^{98}Mo to be preserved in such sediments despite the significant degree of basin restriction from the open ocean. However, there is a Mo isotope fractionation of up to ~0.5 ± 0.3 ‰ between seawater and sediments in strongly euxinic settings when Mo removal from bottom waters is not quantitative (Nägler et al., 2011). In weakly euxinic environments ($[H_2S]_{aq}$ <11 μM), the fractionation factor between seawater and sediments can be significant because of incomplete conversion of molybdate to tetrathiomolybdate (i.e., formation of intermediate thiomolybdate complexes; Arnold et al., 2004; Neubert et al., 2008). The magnitude of Mo isotope fractionation in weakly euxinic settings varies from ~0.5‰ in the deep Cariaco Basin to ~3‰ just below the chemocline in the shallow Black Sea (Arnold et al., 2004; Neubert et al., 2008). The reasons for the significant difference in isotope fractionation between these two weakly euxinic settings is poorly understood.

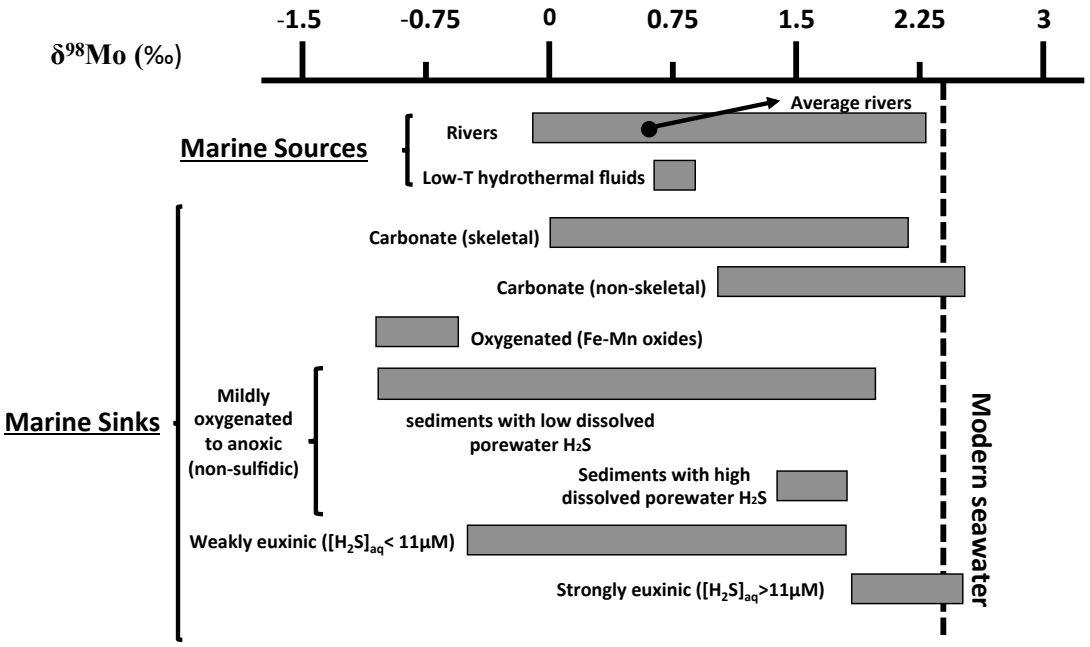

Fig. 3. Molybdenum isotope budget of the modern oceans, including major marine sources and sinks (modified from Kendall at al., 2011, in press).

An appreciable and relatively consistent extent of Mo isotope fractionation (~ 0.7‰)

also occurs between seawater and sediments when the conversion of molybdate to thiomolybdate is incomplete in sediment pore waters (i.e., deposition from anoxic/non-sulfidic and weakly oxygenated bottom waters) along continental margins (Siebert et al., 2006; Poulson et al., 2006; Poulson Brucker et al., 2009). Higher fractionation factors generally occur with increasing O_2 concentrations in the bottom waters, which are associated with slower rates of Mo removal to sediments (Poulson et al., 2006; Siebert et al., 2006; Poulson Brucker et al., 2009; Goldberg et al., 2009, 2012). The adsorption of Mo onto well-oxygenated sediments (i.e. Mn or Fe-Mn oxides/crusts/nodules) leads to a high Mo isotope fractionation of ~3‰ (Barling et al., 2001; Siebert et al., 2003; Barling and Anbar, 2004; Wasylenki et al., 2008; Poulson Brucker et al., 2009). Hence, the extent of Mo isotope fractionation between seawater and sediments is generally greater in oxygenated versus anoxic environments (Barling et al., 2001; Arnold et al., 2004; Poulson et al., 2006; Neubert et al., 2008; Poulson Brucker et al., 2009). Because of widespread oxygenation in the modern oceans, the preferential removal of lighter Mo isotopes into oxic sediments plays an important role in driving modern global seawater δ^{98}Mo to high values.

High seawater Mo concentrations and high δ^{98}Mo points to globally O_2-rich oceans whereas low seawater Mo concentrations and low δ^{98}Mo can represent extensive ocean anoxia (Barling et al., 2001; Arnold et al., 2004; Scott et al., 2008). Because Mo removal to sediments is highly sensitive to the presence of dissolved H_2S, the concentration and isotopic composition of seawater Mo is more sensitive to the extent of ocean euxinia rather than general ocean anoxia (i.e., euxinic and anoxic/Fe(II)-rich [ferruginous]) (Neubert et al., 2008). Strongly euxinic black shales deposited in restricted basins represent the best opportunity to capture the seawater δ^{98}Mo and thus the global ocean paleoredox conditions (Arnold et al., 2004; Neubert et al., 2008; Gordon et al., 2009; Noordmann et al., 2015). Euxinic black shales with high Mo/TOC ratios and high δ^{98}Mo are thus considered excellent indicators for widespread ocean oxygenation (Barling et al., 2001; Arnold et al., 2004; Dahl et al., 2010; Kendall et al., 2015). Evidence for local bottom water euxinia can be readily inferred from high Mo concentrations, high TOC contents, and/or sedimentary Fe speciation (Poulton and Canfield, 2011; Scott and Lyons, 2012). However, it is difficult to infer whether bottom waters in ancient ocean basins were weakly or strongly euxinic using geochemical redox proxies, and Mo removal from bottom waters is not always quantitative (e.g., high Mo/TOC ratios in black shales). If the bottom waters were weakly euxinic or if Mo removal from the bottom waters was not quantitative, then the δ^{98}Mo of

black shales will be somewhat lower than coeval global seawater. Hence, the heaviest δ^{98}Mo from a stratigraphic interval of euxinic Mo-rich black shales can be regarded as the most conservative estimate for global seawater δ^{98}Mo (Dahl et al., 2010).

3.2 Uranium Geochemistry

Compared to Mo, the application of U isotopes as an ocean paleoredox proxy is not as advanced because the first papers were published only recently in 2007-2008 (Stirling et al., 2007; Weyer et al., 2008). Nevertheless, the concentration and isotope composition of U in black shales is rapidly emerging as a complementary tool for tracing the global extent of ocean anoxia. There are two valence states of U in surface environments: reduced and insoluble U(IV) and oxidized and soluble U(VI) (Langmuir, 1978). The residence time of U in the modern ocean is ~450 kyr, which is 2 orders of magnitude longer compared to the timescale of ocean mixing (~1.6 kyr), thus yielding a relatively homogeneous seawater U concentration of ~14 nmol kg^{-1} (Ku et al., 1977; Broecker and Peng, 1982; Dunk et al., 2002). Uranium is mobilized from a variety of accessory phases (e.g., zircon, sphene, apatite, magnetite, uraninite) in the upper continental crust by oxidative weathering and is transported by rivers to the oceans where it accumulates in oxygenated seawater as soluble U(VI) and exhibits conservative behavior (Langmuir, 1978; Dunk et al., 2002; Algeo and Tribovillard, 2009). Rivers are the only major source of U to seawater (Dunk et al., 2002).

Multiple sinks for U are proposed (Morford and Emerson, 1999; Dunk et al., 2002; Partin et al., 2013; Tissot and Dauphas, 2015; Andersen et al., 2016; Noordmann et al., 2016; Wang et al., 2016). Biogenic carbonates, sediments deposited from suboxic waters, sediments deposited from anoxic (including euxinic) waters, and hydrothermally altered oceanic crust are the four major sinks for U, whereas metalliferous sediments (e.g., Fe-Mn oxides, nodules, and crusts deposited from well-oxygenated bottom waters) is only a minor sink for U. A detailed description of the U isotope mass balance containing the U flux and isotopic composition of modern oceanic sources and sinks is provided by Tissot and Dauphas (2015), Wang et al. (2016), and Noordmann et al. (2016).

Local redox conditions exert a pronounced control on the magnitude of U enrichments in organic-rich sediments. Reducing conditions enhance the sedimentation of U as UO_2, U_3O_7, or U_3O_8 as well as adsorption of U to organic matter because soluble U(VI) is reduced to insoluble U(IV) below the sediment-water interface (Tribovillard et al., 2006;

Algeo and Tribovillard, 2009). Reduced U(IV) accumulation in anoxic sediments occurs through diffusion of seawater U into anoxic pore waters, followed by the microbially mediated reduction of U(VI) (Anderson et al., 1989; Barnes and Cochran, 1990; Klinkhammer and Palmer, 1991; Andersen et al., 2014). Uranium sequestration in suboxic sediments (i.e., O_2 penetration is < 1 cm below the sediment-water interface) occurs at a rate ~14 times lower than in sediments overlain by anoxic bottom waters, as calculated by Tissot and Dauphas (2015). The typical range of U enrichments in anoxic Phanerozoic black shales spans tens of ppm up to several hundred ppm, with an overall average of 26 ppm, which is an order of magnitude greater than the average upper crust concentration of 2.8 ppm (McLennan, 2001; Partin et al., 2013). In contrast with Mo, the presence of dissolved H_2S is less important for the burial rate of U in sediments, rather it is the extent of reducing conditions in sediment pore waters that is important (Algeo and Tribovillard, 2009). Indeed, U enrichment in suboxic continental margin sediments can occur without Mo enrichment (Morford and Emerson, 1999; Morford et al., 2005).

As for Mo, a higher seawater U concentration is expected at times of globally widespread ocean oxygenation, whereas lower seawater U concentrations should occur at times of expanded ocean anoxia because the seawater U reservoir would be depleted by U removal to anoxic sediments. Such changes in the global oceanic U inventory should be reflected in the U concentrations of black shales (Partin et al., 2013). Basin restriction will result in lower U enrichments in black shales, although the effect is less severe compared with Mo owing to the slower rate of U removal to sediments. For example, ~40% depletion of U is observed in the deep euxinic waters of the Black Sea, whereas Mo depletion is ≥95% (e.g., Anderson et al., 1989; Algeo and Lyons, 2006; Andersen et al., 2014). Local effects (i.e., sedimentation rates) may complicate the use of U abundances as an ocean paleoredox tracer (Zheng et al., 2002). For instance, slower sedimentation rates will contribute to greater authigenic U accumulation as sediments reside in the anoxic pore water zone in the upper part of the sediment column for a longer time interval (Andersen et al., 2016).

Because of the long oceanic residence time of U, global seawater $\delta^{238}U$ is invariant and thus provides a promising tool to infer global ocean paleoredox conditions. It has been applied to Fe-Mn crusts, carbonates, and black shales (Weyer et al., 2008; Montoya-Pino et al., 2010; Brennecka et al., 2011a; Asael et al., 2013; Kendall et al., 2013, 2015; Romaniello et al., 2013; Dahl et al., 2014; Goto et al., 2014; Lau et al., 2016; Noordmann et

al., 2016; Wang et al., 2016). The $\delta^{238}U$ of modern seawater is –0.39 ± 0.02‰ (2σ) (Stirling et al., 2007; Weyer et al., 2008; Tissot and Dauphas, 2015; Andersen et al., 2016; Noordmann et al., 2016), and the average $\delta^{238}U$ of the upper continental crust (as inferred from basalts and granites) was recently estimated to be –0.30 ± 0.04‰ by Tissot and Dauphas (2015), or ~0.1‰ higher than modern seawater. The average $\delta^{238}U$ of the upper continental crust is similar to the average $\delta^{238}U$ of rivers (–0.24‰ to –0.34‰; Tissot and Dauphas, 2015; Andersen et al., 2016; Noordmann et al., 2016).

In contrast with the near quantitative removal of Mo to strongly euxinic sediments in highly restricted basins (e.g., the Black Sea), the reduction and removal of U in such settings is kinetically slow and characterized by the preferential removal of heavier U isotopes in the water column to sediments (Schauble, 2007; Weyer et al., 2008; Montoya-Pino et al., 2010; Noordmann et al., 2015; Stylo et al., 2015; Andersen et al., 2014, 2016). This process is suggested to be driven by a large volume-dependent equilibrium isotope fractionation (i.e., nuclear field shift) (Schauble, 2007; Weyer et al., 2008; Andersen et al., 2014). Volume-dependent U isotope fractionation dominates over mass-dependent U isotope fractionation because of the high mass of the U isotopes. Natural U is manifested in the two long-lived radioactive isotopes ^{235}U (half life of ~0.7 Ga) and ^{238}U (half life of ~4.5 Ga) as well as small amounts of the short-lived radioactive ^{234}U (half life of ~0.246 Ma) that is continuously generated by alpha decay of ^{238}U (Jaffey et al., 1971; Andersen et al., 2014; Tissot and Dauphas, 2015). Although the U isotopes are radioactive, the decay of U isotopes to intermediate daughter isotopes to stable Pb isotopes does not eradicate volume-dependent U isotope variations in nature that are reported as per mil deviations relative to a standard (i.e., as done for stable isotope variations of other elements) because radioactive decay of U isotopes affects both the sample and standard.

The magnitude of U isotope fractionation between euxinic organic-rich sediments and modern seawater varies with the degree of basin restriction and local U recharge conditions (Fig, 4; Andersen et al., 2014, 2016; Noordmann et al., 2015; Tissot and Dauphas, 2015). A full fractionation factor of +1.2‰ was suggested during the reduction of U(VI) to U(IV) by Andersen et al. (2014) based on the relationship between authigenic U concentrations and $\delta^{238}U$ of Black Sea sediments. The fractionation factor may be relatively constant when U sedimentation is at a steady state (e.g., persistently anoxic/euxinic conditions), but will change as a result of variations in local depositional conditions (e.g., settings with

bioirrigation, periodic water column ventilation, degree of basin restriction, primary productivity, and sorption of U onto plankton; Anderson et al., 2014, 2016; Holmden et al., 2015; Hinojosa et al., 2016). Based on the latest studies on modern euxinic U sinks such as the Black Sea, Cariaco Basin, and Saanich Inlet with relatively persistent steady state conditions, an average authigenic $\delta^{238}U$ of 0.62 ± 0.17 ‰ higher than global seawater was suggested for euxinic sediments deposited in relatively open marine settings (Saanich Inlet) whereas smaller U isotope fractionation factors of ~0.4-0.5‰ were observed in more restricted settings (Black Sea and Cariaco Basin) (Andersen et al., 2014, 2016; Holmden et al., 2015; Noordmann et al., 2015; Tissot and Dauphas, 2015). However, these fractionation factors are lower than the inferred full fractionation factor of 1.2‰ (Andersen et al., 2014).

There are three potential end-member scenarios linked to basin restriction that could affect U isotope fractionation between seawater and organic-rich sediments (Andersen et al., 2014). First, in a fully open ocean setting where U is continuously recharged into bottom waters without depletion, authigenic U accumulation occurs in the presence of an unlimited reservoir of U. In such a scenario, half of the full reductive isotope fractionation factor may be observed in the final accumulation product, based on a mathematic diffusion-reaction-transport model (Clark and Johnson, 2008). Thus the U isotope fractionation between global seawater and sediments would be equal to +0.6‰ (Andersen et al., 2014, 2016). Second, in an open-ocean setting where U extraction from pore waters to sediments only partially occurs, the heavy U isotopes are depleted from porewaters at a lower rate (Andersen et al., 2014). In this scenario, the U isotope fractionation will be larger than 0.6‰, but still somewhat smaller than the full isotope fractionation factor (+1.2‰) (Andersen et al., 2014). Third, in a fully restricted setting, where there is continuous extraction of heavier ^{238}U from seawater to sediments through reduction, the water column and porewaters become more and more depleted in U and thus take on a lighter U isotopic composition without further replenishment of U to the water column (Andersen et al., 2014, 2016). In this scenario, increasingly lighter U is progressively removed into sediments, ultimately leading to a negligible isotope fractionation between sediments and seawater when U is almost completely removed from the water column and porewaters (Andersen et al., 2014, 2016). Hence, in a significantly restricted basin, the observed $\delta^{238}U$ offset between global seawater and sediments will be less than 0.6‰.

Recent studies show that it is crucial to consider the biotic U isotope fractionation that occurs during microbially-mediated U reduction, a process not considered in Andersen et al. (2014). In laboratory-controlled microbial experiments conducted by Stirling et al. (2015) where unreacted growth medium U(VI) is reduced to U(IV)-bearing precipitates in the presence of gram-negative sulfate-reducing bacteria, the $\delta^{238}U$ is higher in the precipitates, which is consistent with the observations in anoxic marine systems. The magnitude of the biotic U isotope fractionation was estimated to have an average of around 0.85‰, with a range of 0.68‰ to 0.99‰ (Basu et al., 2014; Stirling et al., 2015; Stylo et al., 2015). Microbially mediated U(VI) reduction likely plays an important role in the removal of U to sediments in anoxic settings because the experimental magnitude and direction of biotic isotope fractionation matches natural observations in modern anoxic basins better than abiotic U reduction (Stylo et al., 2015). Indeed, the observed isotopic offset between the euxinic bottom waters of the Black Sea and the underlying sediments averages around 0.7–0.8‰ (the bottom waters are isotopically lighter than global seawater because of strongly restricted conditions and preferential removal of isotopically heavy U to the underlying sediments; Romaniello et al., 2009; Andersen et al., 2014; Noordmann et al., 2015). Therefore, the representative U isotope fractionation between seawater and fully open ocean euxinic sediments may be ~0.85‰ instead of the ~0.6‰ used in previous paleoredox studies (e.g., Montoya-Pino et al., 2010; Brennecka et al., 2011; Andersen et al., 2014; Kendall et al., 2015).

Other U sinks are associated with smaller U isotope fractionations. Uranium isotope fractionation between global seawater and oxygenated sediments is observed to be small compared to anoxic settings, with Fe-Mn oxides (metalliferous sediments) having $\delta^{238}U$ that is about 0.25‰ lower than global seawater (Weyer et al., 2008; Brennecka et al., 2011; Goto et al., 2014; Wang et al., 2016). The $\delta^{238}U$ of continental margin sediments off the coasts of Peru and Washington State, U.S.A., that underlie weakly oxygenated waters is only 0.1–0.2‰ higher than the modern seawater value (Weyer et al., 2008; Andersen et al., 2016). Uranium removal into carbonates is generally associated with a low U isotope fractionation factor, except for when there are sulfidic pore waters in the carbonate sediments (0.2–0.4‰) (Romaniello et al., 2013; Stirling et al., 2015; Chen et al., 2016). A small net U isotope fractionation of 0.25‰ favoring removal of isotopically heavy U from seawater may occur during the low-temperature hydrothermal alteration of oceanic basalts (Andersen et al., 2015; Tissot and Dauphas, 2015; Noordmann et al., 2016).

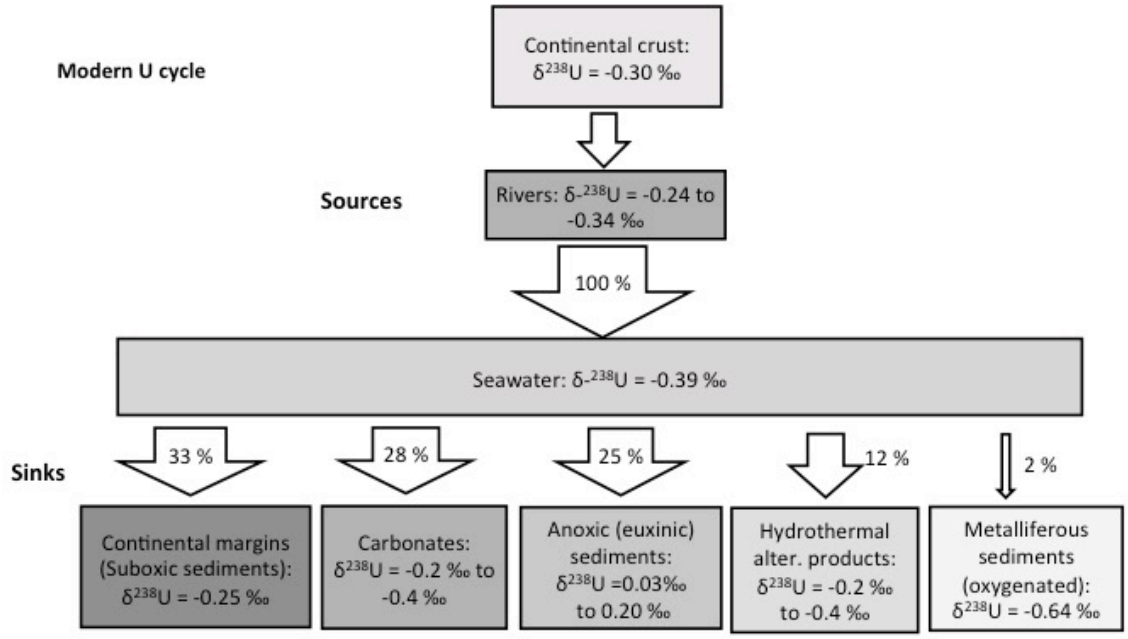

Fig. 4. Uranium isotope mass balance for the modern oceans with relative abundances of sources and sinks, modified from the compilations of Tissot and Dauphas (2015), Wang et al. (2016), and Noordmann et al. (2016).

In light of the observations from modern environments, it is clear that the greatest extent of U isotope fractionation occurs in anoxic/euxinic settings. Therefore, high $\delta^{238}U$ in ancient global seawater and in coeval black shales can be interpreted as evidence for greater global ocean oxygenation. In contrast, lower $\delta^{238}U$ in black shales represents evidence for greater global ocean anoxia because it indicates that a greater proportion of the heavier U isotopes have already been depleted from seawater by sequestration in anoxic sediments that cover a greater areal extent of seafloor, thus shifting global seawater to lower $\delta^{238}U$ (i.e., assuming a similar river U isotope composition and U isotope fractionation factor for each oceanic U sink as today). Accurately inferring global seawater $\delta^{238}U$ from black shales depends on a good understanding of local depositional conditions. This includes evaluation of the degree of basin restriction from the open ocean, which is necessary to estimate the seawater-sediment U isotope fractionation factor, and confirmation of persistently anoxic (i.e., steady-state) conditions that will minimize local redox-related changes in the U isotope fractionation factor during U removal to sediments.

4. Methodology

4.1 Samples

Sixty-five samples of organic-rich black shale from the OGS Gore of Chatham core were collected from the Ontario Oil, Gas, and Salt Resources Library in London, Ontario. In this core, the Kettle Point Formation is 111.1 m thick, and occurs at a depth of 26.8 m to 137.9 m. The Gore of Chatham core has a similar lithostratigraphy as other thick sections located elsewhere in the middle of the Chatham Sag, such that Units 1-4 defined by Bingham-Koslowski et al. (2016) can be easily identified. Specifically, Units 1 and 3 consist of interlaminated black shales interbedded with grey-green mudstone and are located at 120–138 m and 64–91 m, respectively. Units 2 and 4 consist of nonlaminated black shales and occur at 91–120 m and 27–64 m, respectively. The upper contact of the Kettle Point Formation is not preserved in the Gore of Chatham core.

Table 1. Core log for the Gore of Chatham

	Top depth (m)	Bottom depth (m)	Interval (m)	Lithology
	26	27	1	Breccia
	27	27	<1	Greyish green mudstone
	27	41	14	Black shale
Unit 4	**41**	41	<1	Carbonate
	41	43	2	Black shale
	43	44	<1	Carbonate
	44	64	20	Black shale
	64	77	13	Interbedded green shale with black shale
	77	83	7	Greyish green mudstone
	83	86	2	Interbedded green shale with black shale
	86	87	1	Black shale
Unit 3	**87**	87	1	Greyish green mudstone
	87	88	1	Black shale
	88	89	1	Greyish green mudstone
	89	91	2	Interbedded green shale with black shale
Unit 2	**91**	120	29	Black shale
	120	127	7	Interbedded green shale with black shale
	127	132	5	Black shale
Unit 1	**132**	134	1	Greyish green mudstone
	134	137	3	Black shale
	137	138	1	Carbonate

Samples were taken from a depth of 27.99 to 135.32 m. Throughout the core, the sampling resolution ranged from 1 sample per ~0.5 to 4.3 m (depending on the stratigraphic continuity of the black shales), and averaged 1 sample per 1.7 m. When selecting samples, material with diagenetic macroscopic pyrite nodules and carbonate/quartz veins were carefully avoided because the goal of the study is to reconstruct depositional rather than diagenetic conditions. Black shale samples lacking these features typically preserve depositional geochemical signatures owing to their relatively low porosity and permeability, as confirmed by precise and accurate Re-Os depositional ages from many black shale units of Archean to Phanerozoic age (e.g., Kendall et al., 2009 and references therein). Samples were also selected away from the lower contacts of green mudstone beds. These beds likely represent deposition from oxidizing bottom waters (Béland-Otis, 2013; Bingham-Koslowski et al., 2016). During deposition of the organic-poor green sediments, penetration of dissolved O_2 into the immediately underlying black sediments can remobilize redox-sensitive metals (resulting in re-deposition of the metals at deeper depths in anoxic sediments or loss of the metal to the overlying water column) and thus obscure the geochemical signature of depositional conditions. Because the Kettle Point Formation is thermally immature to early mature, thermal remobilization of redox-sensitive metals (such as that associated with thermochemical sulfate reduction; Ardakani et al., 2016) should be minimal. The samples were analyzed for total organic carbon content, total sulfur content, major/minor/trace element abundances, and Mo and U isotope compositions.

4.2 Analytical Methods

4.2.1 Elemental Analyses

Dissolution of samples for measurement of metal concentration and isotope data was carried out at the Metal Isotope Geochemistry Laboratory, Department of Earth and Environmental Sciences, University of Waterloo. All samples were powdered using metal-free methods in an automated agate ball mill. About 100-150 mg of powder was ashed at 550°C overnight to destroy organic matter. In a clean lab, the ashed samples were transferred to 22 ml Savillex Teflon beakers and fully dissolved in concentrated trace-metal grade acids, specifically 2.5 ml HNO_3 plus 0.5 ml HF at 110°C for over 48 h, followed by 3 ml HCl plus 1 ml HNO_3 at 110°C for over 48 h, and finally 2 ml of HCl at 110°C for 24 h. The digested solution was then stored in 5 ml 6M HCl and 3 drops of 0.5% HF.

For analysis of metal concentrations, a weighed portion of the digested sample solution was dried, and re-dissolved in 2% HNO_3. Major elements were measured using a Thermo iCAP 6000 Duo inductively coupled plasma optical emission spectrometer (ICP-OES). Major, minor, and trace element concentrations were measured on a Thermo X Series 2 quadrupole inductively coupled plasma mass spectrometer (Q-ICP-MS). Both instruments are housed in the clean laboratory of the Groundwater Geochemistry and Remediation group at the University of Waterloo. The measured elemental concentration data were standardized against quality control standards (QCS-26 and IV-ICPMS-71A), which were verified against the SRM 3100 series developed by the National Institute of Standards and Technology (NIST). External quality control standards used to verify instrument accuracy included 6020 CAL-1 for ICP-OES and the Standard Reference Material 1643e or 1640a for ICP-MS, both of which are also verified against the SRM 3100 series. Instrument accuracy was further verified by analysis of the United States Geological Survey (USGS) shale standards SGR-1b (Eocene Green River Shale) and SBC-1 (Pennsylvanian Brush Creek Shale). Elements In and Bi were used to correct for instrumental drift during the course of Q-ICP-MS analysis. The reproducibility of elemental concentrations for each sample, measured three times during a single session, is typically <5%. The Mo and U concentrations measured via Q-ICP-MS were used to calculate the optimal amount of Mo and U double spike to be added to sample solutions (prior to ion exchange chromatography), which facilitates acquisition of high-precision isotope data. The double spike technique also enables more precise calculation of the Mo and U concentrations of sample solutions via isotope dilution analysis.

In order to correct for variable detrital and carbonate contents in the samples, element enrichment factors (EF) for Mo and U were calculated for a better evaluation of local redox conditions during deposition. The EFs were calculated using the following equation (average upper crust concentrations are Mo = 1.5 ppm, U = 2.8 ppm, and Al = 80,400 ppm; McLennan, 2001; Tribovillard et al., 2006):

$$EF = [metal / Al]_{sample} / [metal / Al]_{average\ upper\ crust}$$

Total organic carbon (TOC) and total sulfur (TS) contents of the samples were measured at the Geoanalytical Laboratory, Department of Earth Sciences, University of Western Ontario. The TOC is measured as the difference between total carbon (TC)

determined by combustion in a Leco CS-244 analyzer and total inorganic carbon (TIC) determined by acidification (e.g., Scott et al., 2008). The TS contents were determined by combustion in the Leco CS-244 analyzer. Standards used in this study to verify the accuracy of the TOC and TS data included AR-4005, AR-4006, and AR-4007. Deviation of the TOC and TS content of these standards were <5% from recommended values during the course of this study.

4.2.2 Mo and U Isotopes

Purification of Mo and U from sample solutions and Mo and U isotope measurements were conducted following the experimental methods stated in previous papers such as Weyer et al. (2008), Kendall et al. (2009a), Duan et al. (2010), Herrmann et al. (2012), and Kendall et al. (2013). Based on the stratigraphic trends in Mo and U enrichments, a subset of samples was chosen for Mo and U isotope measurements. Ion exchange chromatography was used to isolate and purify Mo and U at the Metal Isotope Geochemistry Laboratory, University of Waterloo. To correct for laboratory mass fractionation (instrumental analysis and ion-exchange chromatography) of Mo and U isotopes, ^{97}Mo–^{100}Mo and ^{233}U–^{236}U double spikes were added to sample solutions before column chromatography. The Mo and U isotope analyses were measured on a Thermo Neptune multi-collector inductively coupled plasma mass spectrometer (MC-ICP-MS) at the W.M. Keck Foundation Laboratory for Environmental Biogeochemistry, School of Earth and Space Exploration, Arizona State University (ASU).

Prior to U column chemistry, samples were spiked with the IRMM3636 ^{233}U–^{236}U double spike to a final ^{233}U/^{235}U ratio of 2.5 for optimal precision during isotope analysis. The weighed spike solution was added to a sample solution containing 300 ng U. Eichrom® UTEVA resin was used in U column chemistry to isolate U from the sample–spike solution. Sample U isotope ratios (δ^{238}U) are reported relative to the CRM145 standard as follows:

$$\delta^{238}\text{U}\ (‰) = (^{238/235}\text{U sample} / {}^{238/235}\text{U}_{\text{CRM145}} - 1) \times 1000$$

The U isotope standards CRM145, CRM129a, and Ricca were measured repeatedly over the course of the study, yielding average δ^{238}U values of 0.00 ± 0.09‰ (2SD, n=130), –1.70 ± 0.09‰ (2SD, n=22), and –0.23 ± 0.07‰ (2SD, n=21), respectively. As expected,

the average $\delta^{238}U$ for CRM145 is 0‰ because this standard was measured relative to itself. The value for CRM129a is statistically identical to the values reported by previous studies (e.g., Weyer et al., 2008; Montoya-Pino et al., 2010; Brennecka et al., 2011a,b; Shiel et al., 2013; Kendall et al., 2013, 2015; Wang et al., 2015; Chen et al., 2016). Two replicate measurements on samples were conducted, and in both cases, the duplicate analysis yielded the same $\delta^{238}U$ as the original analysis within 2SD uncertainties. The 2SD uncertainty of a sample is reported as the 2SD uncertainty of sample replicate measurements or 0.09‰ (the average long-term uncertainty of CRM145, CRM129a, and Ricca), whichever is greater.

For Mo isotope analysis, samples were purified using a two-step column chemistry methodology (anion and cation exchange chromatography). Samples containing 250 ng of Mo were spiked with an appropriate amount of the ^{97}Mo–^{100}Mo double spike solution to achieve optimal precision during isotope analysis. BioRad AG1X8 100–200 mesh resin and BioRad AGWX8 200–400 mesh resin were used for Mo anion column chemistry and subsequent Mo cation column chemistry, respectively. Molybdenum isotope data are reported as follows (Goldberg et al., 2013; Nägler et al., 2014):

$$\delta^{98}Mo\ (‰) = \{[(^{98/95}Mo)_{sample}/(^{98/95}Mo)_{NIST\text{-}SRM\text{-}3134}) - 1] \times 1000\} + 0.25$$

The new international NIST SRM 3134 standard is set to 0.25‰ instead of 0‰ to enable Mo isotope data to be directly compared with the traditional seawater value of 2.34 ± 0.10‰ previously measured using most in-house standards in different laboratories (Barling et al., 2001; Siebert et al., 2003; Arnold et al., 2004; Nakagawa et al., 2012; Goldberg et al., 2013; Nägler et al., 2014). During the course of this study, the $\delta^{98}Mo$ value for NIST SRM 3134 was 0.33 ± 0.03‰, (2SD, n = 8) relative to ASU in-house standard RochMo2, which is 0.08‰ higher than 0.25‰. In this study, the $\delta^{98}Mo$ of samples are first measured relative to RochMo2, and then the sample $\delta^{98}Mo$ was recalculated by subtracting 0.08‰, in order for samples to be reported relative to NIST SRM 3134 = 0.25‰. The average $\delta^{98}Mo$ for the USGS Devonian black shale standard SDO-1 in this study was 0.82 ± 0.02‰ (2SD, n = 8) relative to NIST SRM 3134 = 0.0‰ and 1.07 ± 0.02‰ (2SD, n = 8) relative to NIST SRM 3134 = 0.25‰. The first value is in excellent agreement with the average $\delta^{98}Mo$ of 0.82 ± 0.11 ‰ (2SD, n = 145) for SDO-1 reported by Goldberg et al. (2013) using double spike analysis on the Thermo Neptune instrument at ASU. The 2SD uncertainty of a sample is the 2SD uncertainty of sample replicate measurements or 0.11‰ (the long-term uncertainty of SDO-1), whichever is greater.

5. Results

5.1 Elemental Concentrations

Elemental and isotopic data are shown in Table 2. The TOC contents of black shales from the Kettle Point Formation are high, with a range of 3.1 to 15.6 wt% and an average of 8.4 wt%. Sulfur contents in the black shales are also high and range between 1.2 and 6.0 wt%, with an average of 2.2 wt%. High and variable Mo (40–459 ppm; average = 121 ppm) and U (10–62 ppm; average = 27 ppm) concentrations are observed in the black shales (Table 2 and Fig. 5B). The corresponding EF values for Mo and U are 38–448 (average = 115) and 3–27 (average = 11), respectively (Table 2).

Both Mo and U EFs exhibit high stratigraphic variability over depth in the core (Fig. 5B). In the lower Kettle Point Formation between 135 and 64 m (Units 1-3), the Mo EFs are relatively lower and show a slight declining upward trend (38-178; average = 90) (Fig. 5B). In the upper Kettle Point Formation between 64 and 28 m (Unit 4), a much wider range of Mo EFs is observed (51-448; average = 141), and a significant increase in Mo EF values occurs upsection beginning at ~45 m, with values reaching as high as 448 at ~30 m (Fig. 5B). A broadly parallel, but more subtle, U EF pattern is also observed. From 135 to 64 m, U EFs range from 3 to 22 (average = 10) and show a slight decline upsection. From 64 to 28 m, the U EFs are slightly more elevated and have a range of 4 to 26 (average = 13; Fig. 5B). Like Mo, U EFs begin to increase at ~45 m and a peak in U EF occurs around 30 m. There is a strong correlation between Mo EF and U EF ($R^2 = 0.82$; Fig. 6). The samples from the Kettle Point Formation yield an average Mo EF / U EF ratio of 10.3 ± 2.4 (1 SD) that exceeds the modern seawater weight ratio (3.16; Algeo and Tribovillard, 2009) by a factor of about three. A slight increasing trend upsection in the Mo EF / U EF ratio is observed from an average of 9.3 in Units 1–3 to an average of 10.4 in Unit 4 (Table 2 and Fig. 5A).

With respect to Mo/TOC ratios (4.9-34.5 ppm/wt%; average = 15.3 ppm/wt%), a highly variable but generally increasing trend upsection is observed, with the highest ratio occurring at a depth of about 29 m. Overall, the Mo and TOC contents are moderately correlated ($R^2 = 0.56$; Fig. 7A). However, it is important to note that there are two distinct trends on the Mo-TOC cross-plot that correspond to Units 1-3 and Unit 4 (Fig. 7A). Linear regression of the two Mo-TOC trends yields a good correlation for both intervals ($R^2 = 0.59$

and 0.70 respectively). Unit 4 yields a much steeper slope (~35 ppm/wt%) than Units 1–3 (~8 ppm/wt%).

Uranium concentrations exhibit a slightly better correlation with TOC contents overall (R^2 = 0.67), and both Unit 4 and Units 1-3 show a good correlation between U and TOC content (R^2 = 0.68 and 0.76 respectively) (Fig. 7B). Like Mo, there is a difference between the slope of the U-TOC trends defined by Unit 4 versus Units 1–3, although it is more subtle. Namely, there is a slight increase in the slope from ~2.2 ppm/wt% in Units 1–3 to 4.0 ppm/wt% in Unit 4. The Mo and U EFs correlate with TOC content significantly better than with TS content, as no correlation between Mo EF and TS content, or between U EF and TS content is observed (R^2 = 0.06 and 0.02, respectively) (Fig. 8).

Table 2A. Elemental data for black shales from the Kettle Point Formation

Sample	Depth (m)	TOC[a] (%)	Al (wt%)	Mo (ppm)	U (ppm)	Mo/TOC (ppm/%)	Mo EF[b]	U EF[b]	Mo EF[b] /U EF[b]	Total S (%)	Fe (wt%)	Fe/Al
KPZ-1	28.0	12.9	8.4	346.2	45.0	26.9	280.9	15.8	17.8	1.7	3.6	0.4
KPZ-2	28.7	12.5	7.5	430.3	52.3	34.5	392.4	20.7	19.0	2.2	4.1	0.5
KPZ-3	29.4	15.6	7.0	458.7	62.0	29.4	447.6	26.2	17.1	1.8	3.3	0.5
KPZ-4	30.6	12.3	6.8	295.3	50.0	24.1	297.6	21.8	13.6	5.1	5.8	0.9
KPZ-5	31.4	10.0	7.7	241.7	45.2	24.1	215.2	17.4	12.3	2.8	4.2	0.5
KPZ-6	32.9	8.8	7.5	60.2	17.0	6.8	54.7	6.7	8.2	1.7	3.6	0.5
KPZ-7	34.4	11.0	6.5	164.6	33.9	15.0	172.7	15.4	11.2	1.4	3.0	0.5
KPW6	36.0	11.0	7.0	99.7	29.2	9.1	96.9	12.3	7.9	2.2	3.3	0.5
KPW4	37.5	8.8	7.0	235.4	38.7	26.8	229.5	16.3	14.0	3.4	4.3	0.6
KPW5	39.5	7.8	7.6	166.8	34.8	21.3	149.6	13.5	11.1	1.9	3.5	0.5
KPW3	41.2	6.9	8.7	116.0	26.3	16.9	91.0	8.9	10.2	1.8	3.5	0.4
KPW2	42.9	4.9	9.2	70.5	17.6	14.4	52.3	5.7	9.2	1.9	3.6	0.4
KPW1	44.1	4.2	9.4	59.4	13.4	14.3	43.2	4.2	10.2	2.0	3.6	0.4
KPR1	45.1	5.3	8.8	74.4	20.5	14.0	57.9	6.9	8.4	1.7	3.3	0.4
KPR2	46.4	6.4	7.8	105.9	19.3	16.5	92.6	7.3	12.6	1.5	3.1	0.4
KPR3	47.1	7.3	7.2	96.6	28.9	13.2	92.2	11.9	7.7	1.6	2.8	0.4
KPR4	47.9	8.3	7.1	123.6	25.3	15.0	119.9	10.6	11.3	1.4	2.5	0.4
KPR6	48.6	7.9	6.9	129.1	34.8	16.3	127.5	14.9	8.6	1.2	3.0	0.4
KPR5	48.8	7.9	2.8	40.2	10.5	5.1	99.8	11.2	8.9	1.6	1.0	0.4
KPR7	50.5	7.2	7.0	88.9	21.3	12.3	86.5	9.0	9.6	1.2	2.7	0.4
KPR8	51.4	8.2	5.8	92.0	22.7	11.2	107.6	11.5	9.4	1.2	2.3	0.4
KPR9	52.3	7.2	7.0	93.7	21.0	13.0	91.0	8.8	10.3	1.2	2.6	0.4
KPR10	53.1	6.3	7.4	73.3	18.9	11.6	67.9	7.6	9.0	1.4	2.7	0.4
KPR11	53.5	8.5	7.3	124.0	31.1	14.6	116.7	12.7	9.2	1.4	2.8	0.4
KPR12	54.8	9.2	6.0	130.1	33.6	14.2	147.9	16.5	8.9	2.2	2.9	0.5
KPR13	55.8	9.5	6.6	150.7	44.7	16.0	157.1	20.2	7.8	1.7	2.8	0.4
KPR14	56.8	7.3	7.1	100.9	27.7	13.8	97.2	11.6	8.4	1.2	2.7	0.4
KPR15	57.4	8.4	7.0	136.8	32.8	16.2	134.0	13.9	9.6	1.3	2.7	0.4
KPR16	57.9	8.1	7.4	123.6	30.2	15.3	114.7	12.2	9.4	1.4	2.9	0.4
KPR17	58.8	8.5	8.0	159.0	40.1	18.7	136.4	14.9	9.1	1.9	3.4	0.4
KPR18	59.7	8.8	7.4	102.0	28.3	11.6	93.9	11.3	8.3	1.7	3.2	0.4
KPP2	60.2	7.3	8.7	65.1	17.0	8.9	50.9	5.7	8.9	2.2	3.3	0.4
KPP11	61.6	7.0	7.8	106.6	28.3	15.2	93.6	10.8	8.7	1.6	3.2	0.4
KPP6	62.3	6.3	8.2	119.7	27.0	19.4	100.4	9.8	10.2	2.1	3.6	0.4
KPP1	63.2	7.3	7.9	106.6	27.3	14.6	92.4	10.3	9.0	2.2	3.5	0.4
KPP8	64.1	6.1	8.4	104.4	24.4	17.1	84.7	8.6	9.9	2.0	3.6	0.4
KPP9	64.6	8.4	8.1	158.8	32.9	19.0	133.6	12.0	11.1	1.5	3.3	0.4
KPP5	72.7	5.7	8.1	94.5	22.5	16.7	79.5	8.2	9.7	1.8	3.5	0.4
KPP4	73.9	6.4	7.6	91.7	25.9	14.3	83.0	10.2	8.2	1.3	3.0	0.4

KPP12	74.7	4.2	10.1	77.2	19.7	18.2	52.5	5.8	9.0	1.2	4.0	0.4
KPP10	75.4	5.3	8.0	89.3	18.1	16.9	76.5	6.7	11.4	1.5	3.4	0.4
KPP3	76.6	3.1	8.7	47.8	9.8	15.3	37.7	3.3	11.3	2.0	3.6	0.4
KPP7	78.2	4.5	8.9	73.8	16.6	16.2	57.0	5.5	10.3	2.5	4.3	0.5
KP22	83.1	5.3	9.2	73.8	16.0	13.9	54.8	5.1	10.7	2.3	3.8	0.4
KP21	85.8	7.3	7.3	90.6	23.5	12.4	84.4	9.5	8.9	1.8	3.5	0.5
KP20	87.7	5.8	8.2	76.4	19.8	13.1	63.7	7.2	8.9	1.9	3.8	0.5
KP19	90.7	6.9	8.3	95.3	21.3	13.7	78.6	7.6	10.3	3.1	4.7	0.6
KP18	92.0	4.5	8.3	66.3	20.7	14.9	54.8	7.4	7.4	2.2	4.1	0.5
KP17	95.0	6.8	7.7	83.1	21.8	12.2	73.7	8.4	8.8	2.2	3.7	0.5
KP16	96.5	6.0	6.8	65.6	18.7	10.9	65.8	8.1	8.1	2.3	3.5	0.5
KP15	98.1	5.7	6.7	61.1	18.5	10.8	61.9	8.1	7.6	2.0	3.2	0.5
KP14	99.7	7.4	6.8	69.7	22.2	9.4	70.5	9.7	7.3	2.7	3.7	0.5
KP13	101.2	10.5	6.9	55.1	18.3	5.2	54.5	7.9	6.9	2.3	3.5	0.5
KP10	103.1	7.7	6.3	123.9	24.5	16.0	134.6	11.5	11.7	2.9	3.7	0.6
KP12	105.1	7.7	6.1	107.0	24.1	14.0	120.9	11.8	10.2	3.5	3.9	0.6
KP9	108.3	5.0	5.5	71.5	17.6	14.4	89.2	9.5	9.4	3.3	3.9	0.7
KP8	110.1	7.1	6.8	91.4	24.0	12.9	91.7	10.4	8.8	3.6	4.7	0.7
KP7	114.2	5.5	4.6	66.1	14.7	12.0	98.2	9.5	10.3	3.0	3.4	0.7
KP6	118.2	9.3	4.8	124.1	32.0	13.4	177.6	19.9	8.9	4.2	4.7	1.0
KP5	120.2	9.9	6.1	134.7	29.5	13.6	150.2	14.3	10.5	4.8	5.2	0.8
KP4	123.0	12.2	6.4	56.9	28.4	4.7	60.7	13.2	4.6	6.0	6.0	0.9
KP3	126.1	8.2	7.1	131.7	29.9	16.0	127.3	12.5	10.2	2.9	4.2	0.6
KP2	128.6	13.1	6.5	111.8	27.2	8.5	117.8	12.4	9.5	3.2	4.2	0.6
KP11	130.9	7.2	7.5	117.6	23.1	16.4	106.6	9.1	11.8	3.0	4.1	0.5
KP1	135.3	14.4	7.0	150.5	41.6	10.5	146.5	17.5	8.4	2.3	3.5	0.5

[a] TOC = Total organic carbon

[b] EF = enrichment factor

Table 2B. Mo and U Isotope data for black shales from the Kettle Point Formation

Sample	Depth (m)	$\delta^{98}Mo$[c]	2SD Measured	2SD[d] Reported	n[e]	$\delta^{238}U$[f]	2SD Measured	2SD[g] Reported	n[e]
KPZ-1	28.0	0.82	0.05	0.11	3	0.54	0.07	0.09	3
KPZ-2	28.7	0.98	0.02	0.11	3	0.40	0.02	0.09	3
KPZ-2'	28.7					0.39	0.01	0.09	2
KPZ-3	29.4	0.95	0.03	0.11	3	0.46	0.04	0.09	3
KPZ-4	30.6	0.85	0.03	0.11	3	0.40	0.01	0.09	3
KPZ-4'	30.6	0.90	0.03	0.11	3				
KPZ-5	31.4	0.95	0.03	0.11	3	0.37	0.10	0.10	3
KPZ-6	32.9	0.76	0.00	0.11	3	0.18	0.03	0.09	3
KPZ-7	34.4	0.71	0.04	0.11	3	0.53	0.06	0.09	3
KPW6	36.0	0.68	0.04	0.11	3	0.44	0.06	0.09	3
KPW4	37.5	0.76	0.03	0.11	3	0.39	0.04	0.09	3
KPW5	39.5	0.78	0.05	0.11	3	0.41	0.03	0.09	3
KPW5'	39.5					0.37	0.26	0.26	2
KPW3	41.2	0.69	0.05	0.11	3	0.42	0.08	0.09	3
KPW2	42.9	0.71	0.05	0.11	3	0.32	0.07	0.09	3
KPW1	44.1	0.68	0.03	0.11	3	0.30	0.04	0.09	3
KPR2	46.4	0.55	0.04	0.11	3	0.34	0.14	0.14	3
KPR6	48.6	0.88	0.03	0.11	3	0.35	0.07	0.09	3
KPR8	51.4	0.77	0.03	0.11	3	0.34	0.11	0.11	3
KPR11	53.5	0.79	0.11	0.11	3	0.32	0.10	0.10	3
KPR14	56.8	0.86	0.01	0.11	3	0.20	0.06	0.09	3
KPR17	58.8	1.29	0.02	0.11	3	0.12	0.02	0.09	3
KPR-17'	58.8	1.33	0.04	0.11	3				
KPP11	61.6	1.26	0.01	0.11	3	0.11	0.11	0.11	3
KPP8	64.1	1.31	0.03	0.11	3				
KPP4	73.9	1.06	0.07	0.11	3	0.20	0.04	0.09	3
KPP3	76.6	0.77	0.02	0.11	3	0.04	0.04	0.09	3
KP21	85.8	0.62	0.02	0.11	3				
KP18	92.0	1.17	0.03	0.11	3	-0.06	0.08	0.09	3

KP15	98.1	0.96	0.05	0.11	3	0.01	0.07	0.09	3
KP10	103.1	1.60	0.05	0.11	3	-0.06	0.05	0.09	3
KP8	110.1	1.45	0.03	0.11	3	-0.14	0.11	0.11	3
KP5	120.2	1.27	0.02	0.11	3	-0.03	0.03	0.09	2
KP2	128.6	1.73	0.01	0.11	3	-0.11	0.02	0.09	2

[c] Mo isotope data reported relative to NIST SRM 3134 = +0.25‰

[d] Reported uncertainty is the 2SD of replicate measurements or 0.11‰, whichever is greater

[e] Number of times MC-ICP-MS analysis was carried out on the sample solutions

[f] U isotope data reported relative to CRM 145

[g] Reported uncertainty is the 2SD of replicate measurements or 0.09‰, whichever is greater

’ denotes a replicate analysis

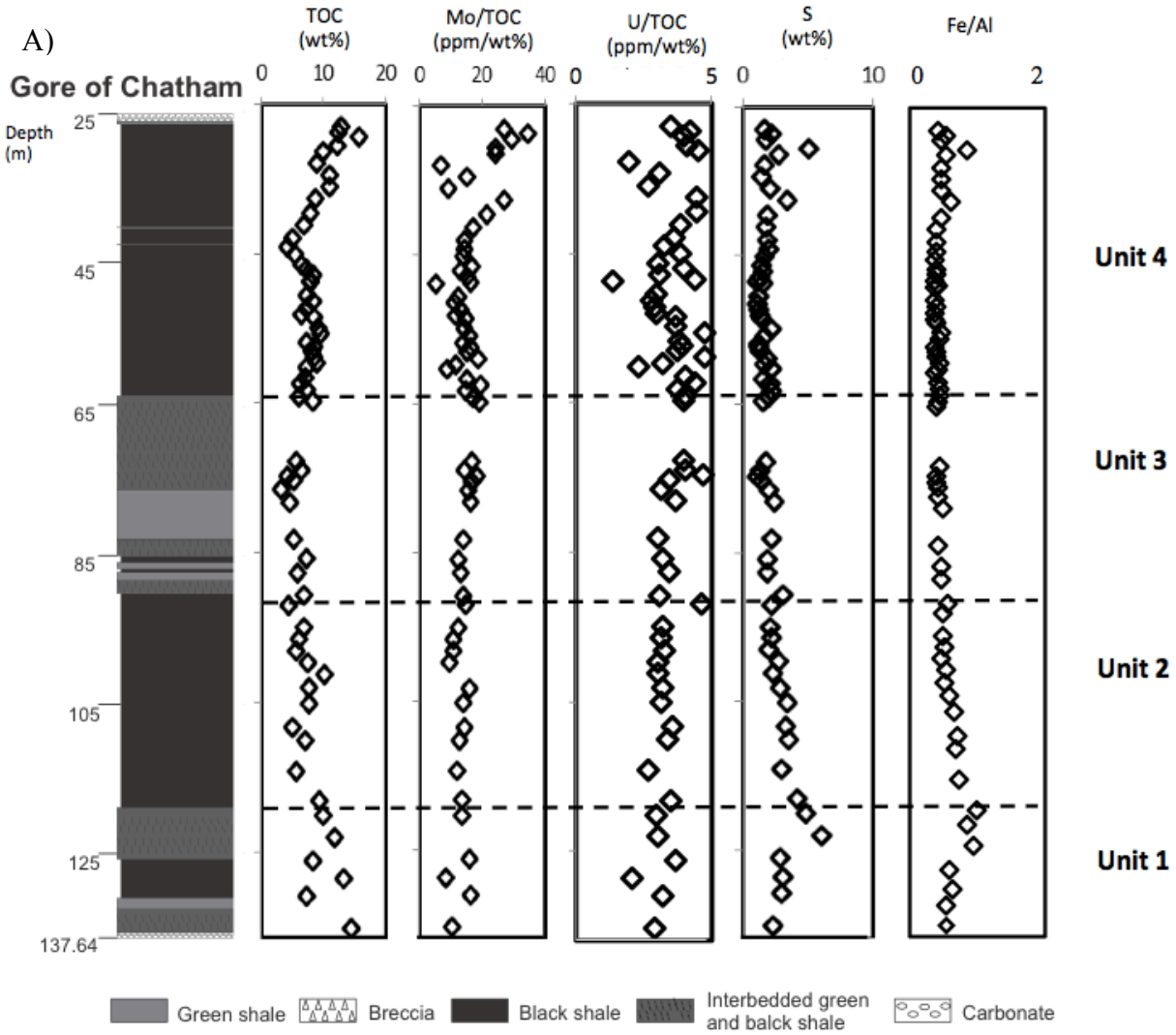

B)

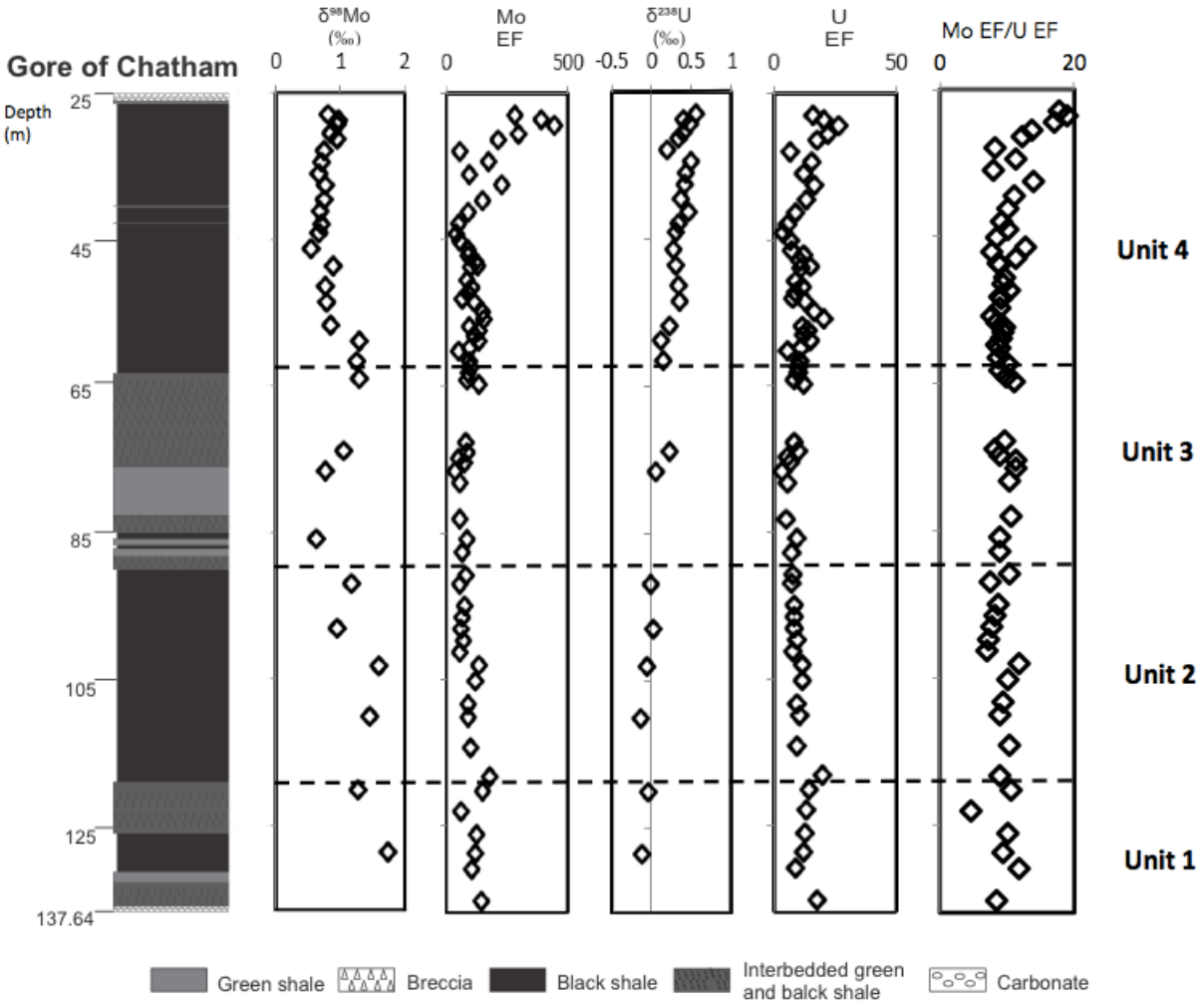

Fig. 5. Stratigraphic and geochemical profiles through the Gore of Chatham core. A lithological legend for the stratigraphic column is shown beneath the geochemical profiles. A. Elemental data. B. Mo and U enrichment factors and isotope compositions.

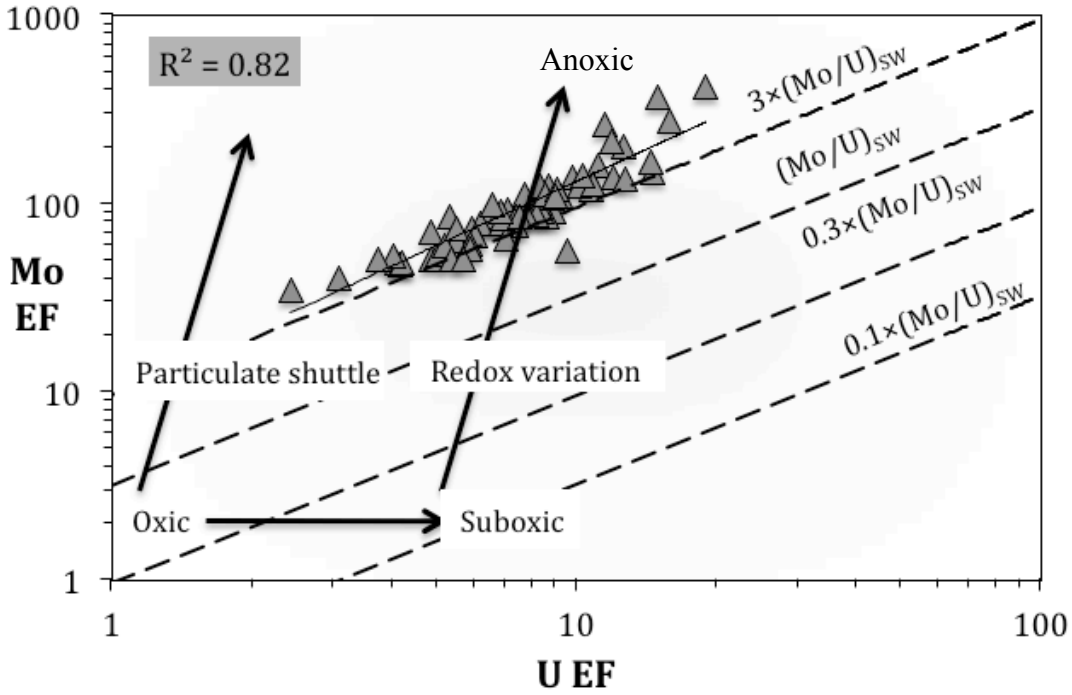

Fig. 6. Cross-plot of Mo EF versus U EF. The dashed lines are weight equivalents of the molar Mo/U ratio of modern seawater (1×SW), and various fractions of modern seawater (0.1×SW, 0.3×SW, and 3×SW) (Algeo and Tribovillard, 2009). Enrichment patterns and their corresponding controls are illustrated following Algeo and Tribovillard (2009).

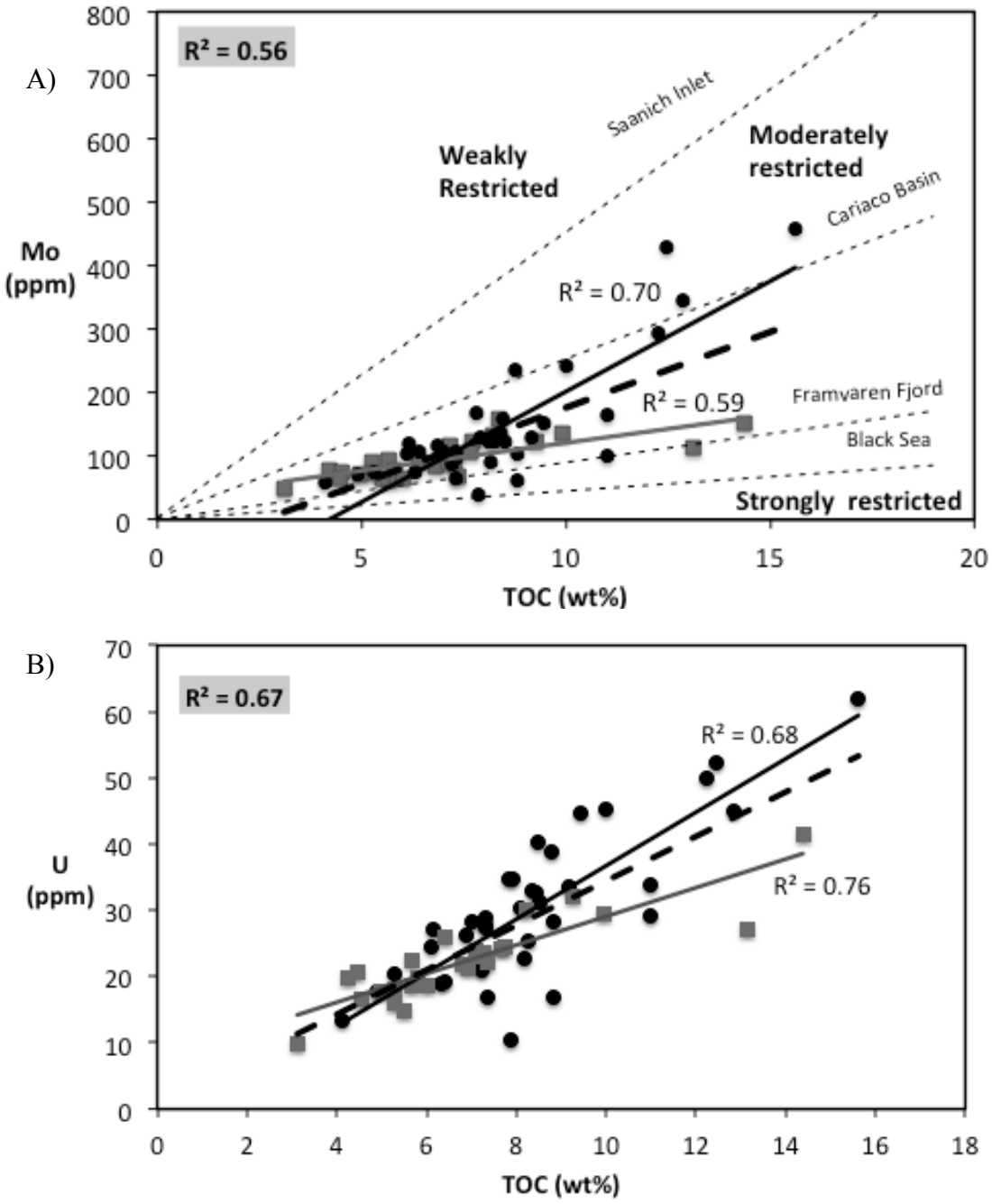

Fig. 7. Geochemical diagrams showing the relationship between Mo and U concentrations versus TOC. The grey trendline and grey dots represent Units 1–3 (135-64 m); the black trendline and black dots represent Unit 4 (64-28 m); the heavy dashed line represents the overall trendline for all samples; and the R^2 for all samples is shown in the grey box. A. Mo vs TOC. Thin dashed lines represent regression slopes for four modern anoxic basins from Algeo and Lyons (2006) (Saanich Inlet: 45 ± 5; Cariaco Basin: 25 ± 5; Framvaren Fjord: 9 ± 2; Black Sea: 4.5 ± 1; in ppm/wt%). B. U vs TOC.

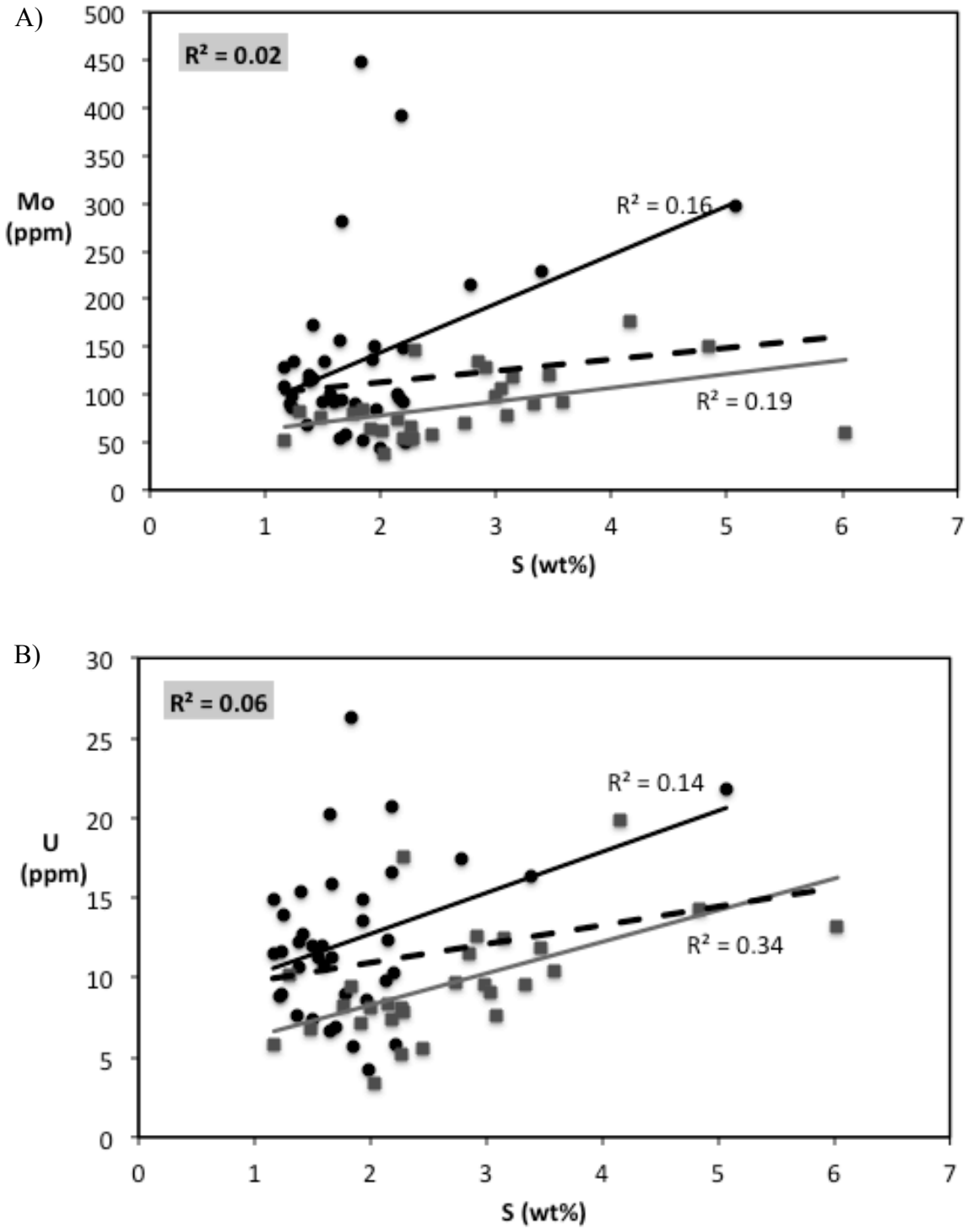

Fig. 8. Geochemical diagrams showing the relationship between Mo and U concentrations versus S content. The grey trendline and grey dots represent Units 1–3 (135-64 m); the black trendline and black dots represent Unit 4 (64-28 m); the heavy dashed line represents the overall trendline for all samples; and the R^2 for all samples is shown in the grey box. A. Mo vs S. B. U vs S.

5.2 Molybdenum and Uranium Isotope Compositions

The δ^{98}Mo values in the Kettle Point Formation span a wide range from 0.55‰ to 1.73‰, yielding an overall average of 0.96‰ (Table 2 and Fig. 5B). By comparison, the δ^{238}U values vary from –0.14‰ to 0.54‰ (average = 0.24‰) (Table 2). There is no significant overall correlation between U EF and δ^{238}U (R^2 = 0.18; Fig. 9B) or between Mo EF and δ^{98}Mo (R^2 = 0; Fig. 9A). Similarly, poor correlations are observed between Mo EF and δ^{98}Mo, and between U EF and δ^{238}U for the Units 1-3 and 4 subdivisions (Fig. 9).

Overall, an upward decreasing trend in δ^{98}Mo values is observed, particularly through Units 1–3, albeit with large oscillations (0.62-1.73‰, average = 1.21‰) (Fig. 5B). Unit 4 displays more uniform δ^{98}Mo from 0.55‰ to 0.98‰ (average = 0.78‰), but also exhibits a declining upward trend (Fig. 5B). By contrast, δ^{238}U values exhibit an increasing trend from stratigraphically deeper depth to shallower depth (Fig. 5B). A progressive increase of δ^{238}U from –0.14‰ to 0.20‰ (average = –0.02‰) occurs in Units 1–3, whereas in Unit 4, the δ^{238}U values are higher and increase gradually from 0.11‰ to 0.54‰ (average = 0.34‰) (Fig. 5B). The stratigraphic trends of δ^{98}Mo and δ^{238}U are thus reversed, as indicated by a moderate negative correlation between δ^{98}Mo and δ^{238}U (R^2 = 0.58) (Fig. 9C). The correlation between δ^{98}Mo and δ^{238}U is strongly reduced for the two individual groups of samples, especially for Unit 4 (R^2 = 0.13) compared with Units 1–3 (R^2 = 0.29).

A)

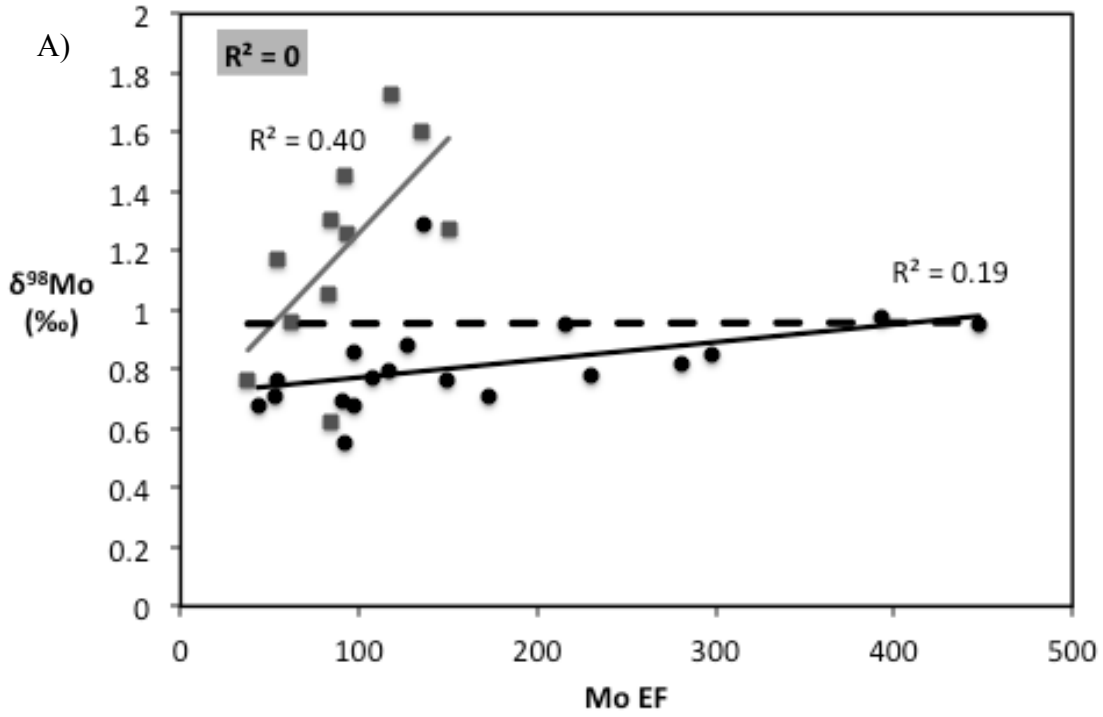
R² = 0
R² = 0.40
R² = 0.19
δ98Mo (‰)
Mo EF
0
0.2
0.4
0.6
0.8
1
1.2
1.4
1.6
1.8
2
0
100
200
300
400
500

B)

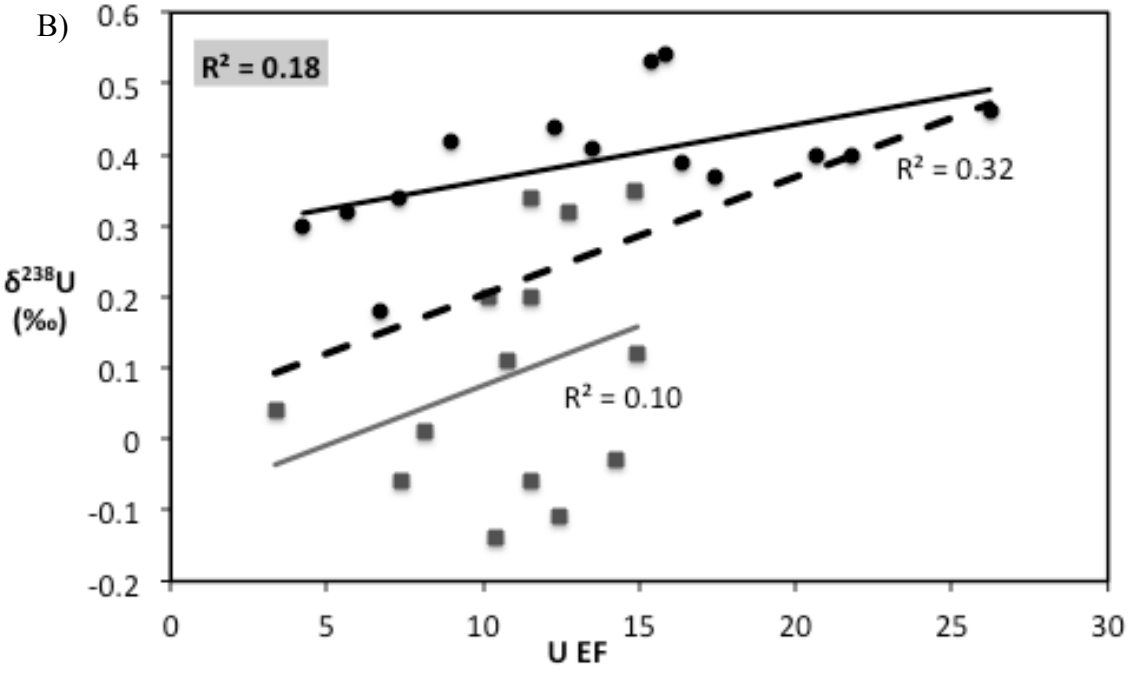
R² = 0.18
R² = 0.32
R² = 0.10
δ238U (‰)
U EF
-0.2
-0.1
0
0.1
0.2
0.3
0.4
0.5
0.6
0
5
10
15
20
25
30

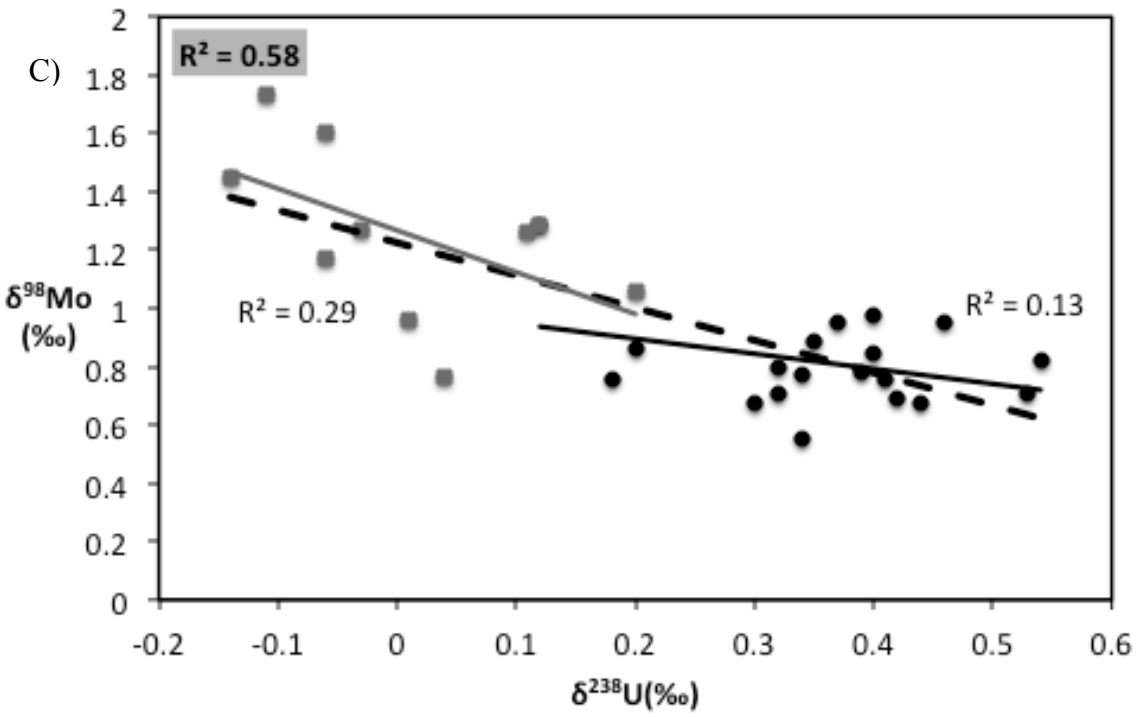

Fig. 9. Geochemical diagrams showing A) δ^{98}Mo versus Mo EF; B) δ^{238}U versus U EF; and C) δ^{98}Mo versus δ^{238}U. In all three panels, grey squares and trendlines represent Units 1-3 (135-64 m); black circles and trendlines represent Unit 4 (64-28 m); and the dashed trendline and R^2 in the grey box are for all samples.

6. Discussion

6.1 Elemental Constraints on Local Redox Conditions During Deposition of the Kettle Point Formation

In order to properly use the Mo and U isotope records in the Kettle Point black shales for inferring global ocean paleoredox conditions, a combination of Fe-TOC-S systematics, Mo and U enrichments, and Mo/U ratios are used to constrain the local water column paleoredox conditions. In addition, Mo/TOC and Mo/U ratios are used to place constraints on the extent of local basin restriction from the open ocean, which is important because the Kettle Point Formation was most likely deposited in a relatively shallow epeiric sea rather than along an open-ocean continental margin (Broadhead et al., 1982; Klemme and Ulmishek, 1991; Gutschick and Sandberg, 1991; Ettensohn, 1992; Hamblin, 2010; Bingham-Koslowski et al., 2016). As discussed in section 3, the U and Mo isotope fractionation between seawater and sediments is influenced by both the degree of basin restriction and the local bottom water redox conditions.

The black shales of the Kettle Point Formation in the Gore of Chatham core have the geochemical features characteristic of deposition in a euxinic environment with Fe-limitation. The black shales have high TOC and TS contents. The high Mo concentrations (40–459 ppm; average = 121 ppm) in the Kettle Point black shales are similar to concentrations observed in organic-rich sediments from modern anoxic basins with persistent euxinia and in other Phanerozoic euxinic black shales (average = 164 ppm; Algeo and Lyons, 2006; Scott et al., 2008; Scott and Lyons, 2012). Similarly, U concentrations in the Kettle Point Formation (10-62 ppm; average = 27 ppm) are high and comparable to sediments from modern anoxic basins and other Phanerozoic black shales (average = 26 ppm; Partin et al., 2013).

The ratio of authigenic Mo to U enrichment in black shales compared with modern seawater can provide valuable information about local paleoredox and paleohydrographic conditions. Uranium is removed more efficiently than Mo to sediments in suboxic settings whereas Mo is removed more efficiently to sediments in euxinic settings (Crusius et al., 1996; Morford and Emerson, 1999; Morford et al., 2005; Algeo and Tribovillard, 2009). Exceptionally high Mo/U ratios can be related to the efficient operation of a local particulate Mn-Fe oxyhydroxide shuttle, which accelerates the transfer of Mo to the lower

part of the water column or seafloor via adsorption of Mo to sinking oxyhydroxide particles (Algeo and Tribovillard, 2009). Upon reaching the euxinic seafloor, the oxyhydroxide particles undergo reductive dissolution, thus releasing Mo into solution, which is followed by the sequestration of Mo by organic matter, clay minerals, and/or sulfide minerals.

The Kettle Point Formation is considerably more enriched in Mo relative to U, with a strong correlation between the two metals ($R^2 = 0.82$). As shown in Fig. 6, the samples plot well above the modern seawater Mo/U molar ratio and follow a positive covariation trend that is roughly equal to a Mo/U ratio about 3 times that of modern seawater. This observation is consistent with euxinic conditions, where the accumulation rate of Mo substantially exceeded that of U. In addition, the high Mo/U ratio may suggest operation of an Fe-Mn particulate shuttle that enhanced transfer of Mo to the seafloor, thus further increasing the enrichment of Mo over U (Algeo and Tribovillard, 2009). Significantly, none of the data plot along the strongly restricted basin trend of Algeo and Tribovillard (2009), consistent with moderately to weakly restricted conditions from the open ocean.

The Mo-TOC data from the core can be separated into two sections. Units 1–3 (135–64 m) have a smaller Mo/TOC slope (8.3 ppm/wt%) that is very similar to the Framvaren Fjord, which points to a moderately restricted basin. In contrast, Unit 4 (64–28 m) has a much steeper slope (34.8 ppm/wt%) that falls between the Saanich Inlet and Cariaco Basin slopes, indicating a weakly restricted basin. These observations suggest that during deposition of the Kettle Point Formation, there was a significant transition from a moderately restricted basin to a weakly restricted basin, which increased the supply of Mo and U to the euxinic bottom waters. This is consistent with the increased Mo and U EFs and slightly higher Mo EF / U EF ratios in Unit 4. Such an interpretation also implies a higher sea level during Unit 4 (thus increasing water exchange with the open ocean) compared with black shale deposition during Units 1-3. The grey-green shales reflect the lowest sea level, which permitted oxygenation of the entire water column at this locality (Bingham-Koslowski et al., 2016).

An alternative interpretation is that the change in Mo/TOC slope between Units 1–3 and Unit 4 reflects a change in the global oceanic Mo inventory as a result of changes in the global extent of anoxic versus oxic conditions. In this scenario, Units 1–3 were deposited during a time of more widespread ocean anoxia (lower seawater Mo inventory and thus the

black shales have a lower Mo/TOC slope), whereas Unit 4 was deposited at a time of more widespread ocean oxygenation (higher seawater Mo inventory and thus the black shales have a higher Mo/TOC slope). These two possibilities (local versus global control on the Mo/TOC ratios) can be more fully evaluated using the relationship between the Mo and U isotope data (see section 6.3).

A Fe-S-TOC ternary diagram evaluates variation in Fe/TOC, S/TOC, and S/Fe ratios in a series of samples that reveals the limiting factor on the precipitation of pyrite in a euxinic environment (Dean and Arthur, 1989). When a majority of samples plot on a line corresponding to a constant S/Fe ratio or to a constant S/TOC ratio, then Fe limitation and organic carbon limitation is implied, respectively. On the other hand, significant scatter on the ternary plot with highly variable S/Fe ratios would suggest sulfur limitation in the system. As shown in Fig. 10, there is no evidence of data distribution about a line of constant S/TOC ratio and TOC contents are high, thus ruling out organic carbon limitation. Instead, the majority of the Kettle Point data clusters along the line from TOC to S/Fe = 0.57, which suggests an Fe-limited system with an overall S/Fe ratio close to 0.57 (stoichiometric pyrrhotite FeS; i.e., not all of the Fe was reactive and converted into pyrite) (Dean and Arthur, 1989). However, a subset of samples have larger S/Fe ratios reaching up to 1.15. Samples with all of the reactive Fe fixed as pyrite will plot along the S/Fe = 1.15 line (Dean and Arthur, 1989). There is minimal correlation between TOC and TS contents, but there is a good correlation between TS and Fe contents, which supports an interpretation of Fe-limitation (Fig. 10). Moreover, the Kettle Point black shales have an average Fe/Al ratio of 0.49 ± 0.10 (Table 2), which is similar to the average continental crust (detrital) value of 0.5 (Taylor and McLennan, 1995; Lyons and Severmann, 2006). Units 1-3 generally have higher Fe/Al ratios over 0.5 (average = 0.6), whereas lower ratios (average = 0.4) are encountered in Unit 4 (Table 2 and Fig. 5A), which suggests a slightly greater detrital sediment load and/or lower availability of reactive Fe during Unit 4 deposition (Lyons and Severmann, 2006; Asael et al., 2013). The lower Fe/Al ratios in Unit 4 are consistent with more samples from this unit plotting along a line of S/Fe = 0.57.

A)

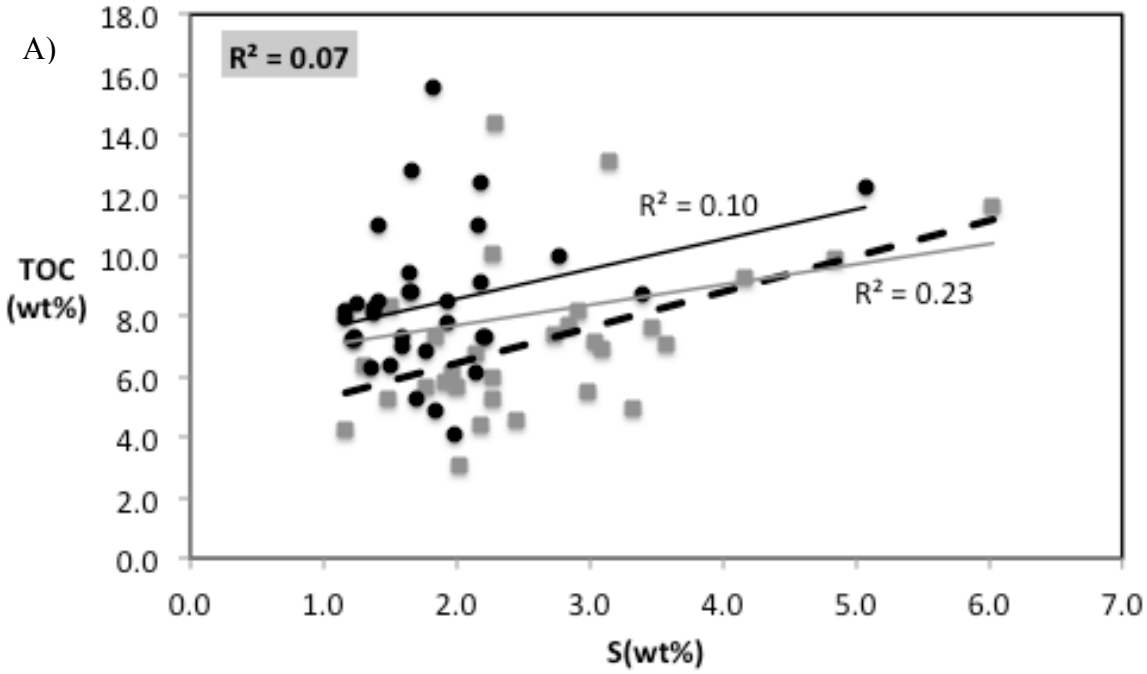
R² = 0.07
R² = 0.10
R² = 0.23
TOC (wt%)
S(wt%)
18.0
16.0
14.0
12.0
10.0
8.0
6.0
4.0
2.0
0.0
0.0
1.0
2.0
3.0
4.0
5.0
6.0
7.0

B)

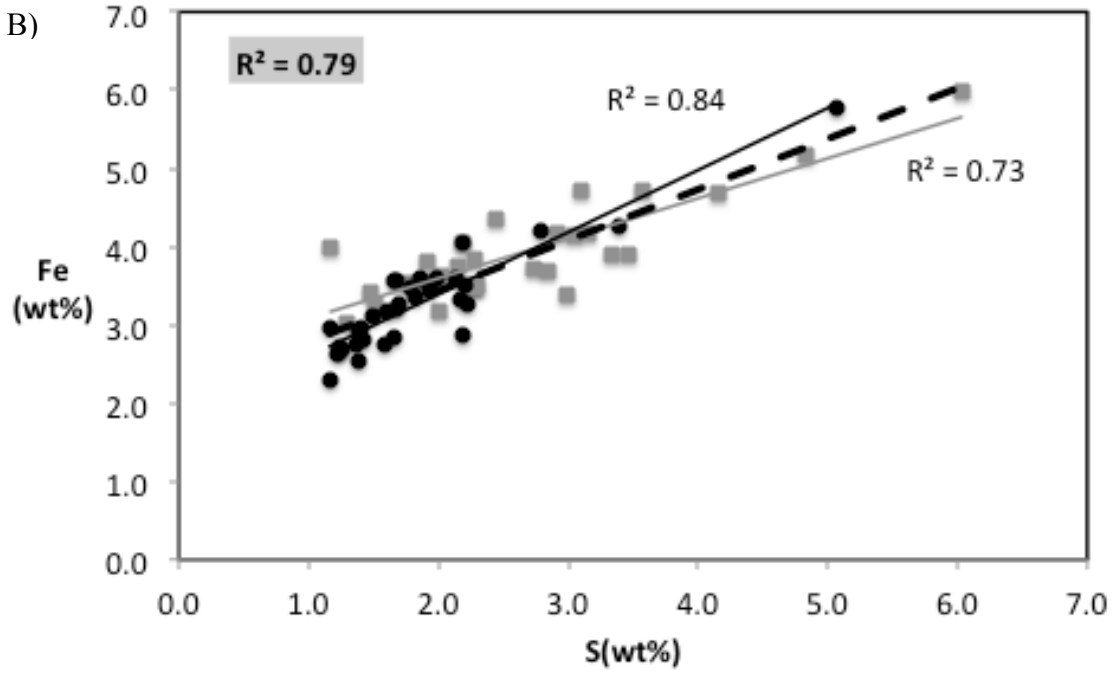
R² = 0.79
R² = 0.84
R² = 0.73
Fe (wt%)
S(wt%)
7.0
6.0
5.0
4.0
3.0
2.0
1.0
0.0
0.0
1.0
2.0
3.0
4.0
5.0
6.0
7.0

C)

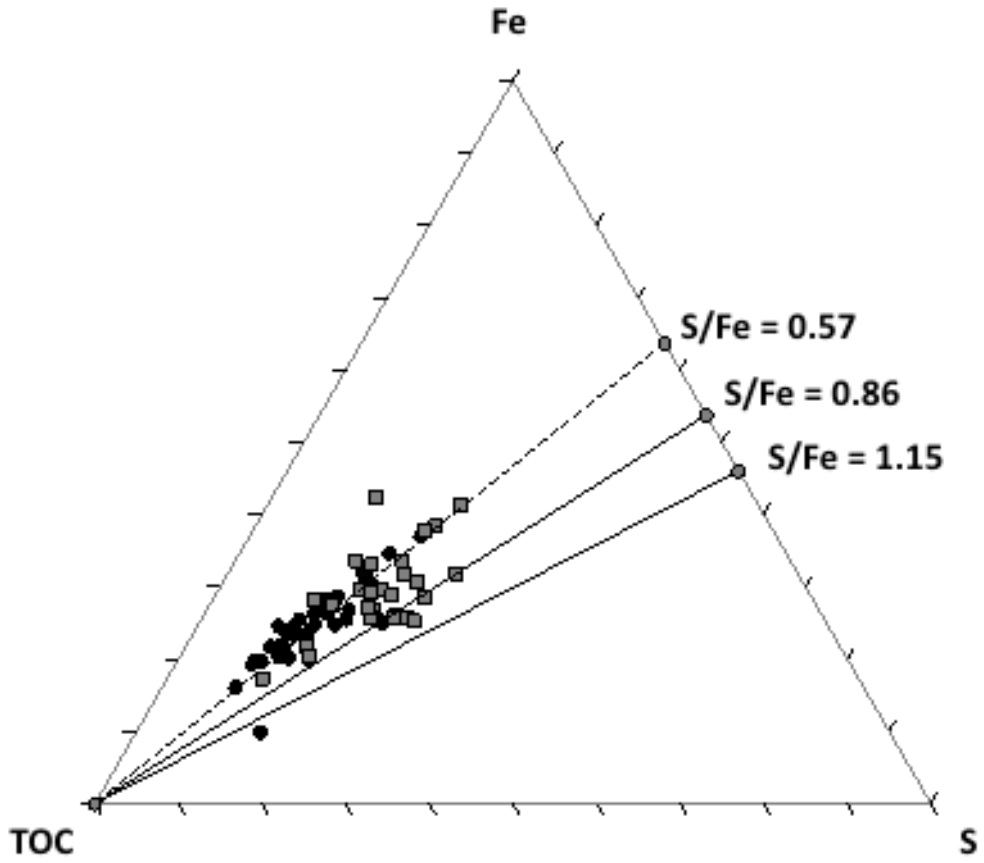

Fig 10. A. Comparison of total sulfur (S) and TOC contents. B. Comparison of total sulfur (S) and Fe contents. C. Fe-S-TOC ternary diagram, after Dean and Arthur (1989). In all three panels, grey squares and trendlines represent Units 1-3 (135-64 m); black circles and trendlines represent Unit 4 (64-28 m); and the dashed trendline and R^2 in the grey boxes are for all samples.

Hence, there are three major observations derived from the elemental data: 1) The Kettle Point Formation black shales were most likely deposited in a euxinic depositional environment with Fe-limitation; 2) The operation of a particulate shuttle may have further enhanced the transfer of Mo to the euxinic sediments; and 3) there may have been a transition from moderate to weak basin restriction during the deposition of the Kettle Point Formation.

6.2 Uranium isotope constraints on the extent of Frasnian-Famennian ocean anoxia

6.2.1 Calculation of authigenic $\delta^{238}U$

Because the bulk shale $\delta^{238}U$ reflects a mix of detrital-sourced U with low $\delta^{238}U$ and authigenic U with high $\delta^{238}U$, it is necessary to correct for the presence of local detrital $\delta^{238}U$ before inferring the global ocean redox conditions. The average value of detrital $\delta^{238}U$ would be similar to or lower than the average upper continental crust $\delta^{238}U$ (−0.29 ± 0.03‰; Tissot and Dauphas, 2015) if there is negligible to minor fractionation of U isotopes during weathering and transport of detrital siliciclastic sediments to the oceans (Andersen et al., 2016). However, Holmden et al. (2015) reported a value of −0.83 ± 0.12‰ for the detrital fraction of Saanich Inlet sediments, which suggests that detrital minerals can have their isotopic composition modified by weathering. Therefore, we use a range of –0.8‰ to –0.3‰ for detrital $\delta^{238}U$.

Authigenic $\delta^{238}U$ can be calculated by the following equation (Asael et al., 2013):

$$\Delta^{238}U_a = \delta^{238}U_S - (Al/U)_S \times \{(\delta^{238}U_d - \delta^{238}U_S) / [(Al/U)_d - (Al/U)_S]\}$$

where the average Al and U contents in the upper continental crust (8.04 wt% and 2.8 ppm, respectively; McLennan, 2001) are used to represent detrital Al and U concentrations, "a" represents authigenic, "s" represents total sample, and "d" represents detrital. The authigenic $\delta^{238}U$ for the entire Kettle Point Formation after correction for detrital U ranges from –0.06‰ to 0.80‰ (average = 0.41 ± 0.23‰, 2SD) and from –0.12‰ to 0.62‰ (average = 0.33 ± 0.22‰, 2SD), when detrital $\delta^{238}U$ values of −0.3‰ and −0.8‰ are assumed, respectively (Table 3). The detrital component comprises up to 45% of the bulk U in the Kettle Point black shales. Units 1-3 have a lower average authigenic $\delta^{238}U$ (0.18 ± 0.19‰ and 0.08 ± 0.13‰) than Unit 4 (0.54 ± 0.13‰ and 0.47 ± 0.12‰), using detrital $\delta^{238}U$ values of −0.3‰ and −0.8‰, respectively. Hence, correction for detrital U yields average authigenic $\delta^{238}U$ that is 0.1–0.2‰ higher compared with bulk shale $\delta^{238}U$. Authigenic U accounts for 55-95% of the total U in these samples. The authigenic $\delta^{238}U$ from Unit 4 contains some of the highest values reported thus far for black shales, and is higher than the average authigenic $\delta^{238}U$ from any modern anoxic basin (Weyer et al., 2008; Montoya-Pino et al., 2010; Andersen et al., 2014; Holmden et al., 2015; Noordmann et al., 2016).

Table 3. Authigenic $\delta^{238}U$ compositions for the Kettle Point Formation black shales

Sample	Al (wt%)	U (ppm)	$\delta^{238}U$[1] (‰)	2SD measured	2SD[2] reported	n[3]	$\delta^{238}U_{auth}$[4] (‰)	F_{auth}[5]	F_{det}[6]	$\delta^{238}U_{auth}$[7] (‰)	F_{auth}[5]	F_{det}[6]
							$\delta^{238}U_{det}$[8]= -0.8‰			$\delta^{238}U_{det}$[8]= -0.3‰		
KPZ-1	8.43	35.08	0.55	0.07	0.09	3	0.66	0.92	0.08	0.62	0.89	0.11
KPZ-2	7.50	40.82	0.40	0.02	0.09	3	0.48	0.94	0.06	0.45	0.90	0.10
KPZ-3	7.01	48.37	0.48	0.04	0.09	3	0.53	0.96	0.04	0.50	0.94	0.06
KPZ-4	6.79	39.01	0.40	0.01	0.09	3	0.48	0.94	0.06	0.45	0.90	0.10
KPZ-5	7.68	35.26	0.34	0.10	0.10	3	0.47	0.90	0.10	0.42	0.83	0.17
KPZ-6	7.52	13.23	0.19	0.03	0.09	3	0.42	0.81	0.19	0.30	0.68	0.32
KPZ-7	6.52	26.42	0.50	0.06	0.09	3	0.66	0.89	0.11	0.61	0.83	0.17
KPW6	7.04	22.78	0.43	0.06	0.09	3	0.59	0.88	0.12	0.53	0.82	0.18
KPW4	7.01	30.17	0.41	0.03	0.09	3	0.49	0.94	0.06	0.45	0.90	0.10
KPW5	7.62	27.16	0.37	0.04	0.09	3	0.54	0.87	0.13	0.49	0.80	0.20
KPW3	8.72	20.50	0.47	0.08	0.09	3	0.63	0.89	0.11	0.55	0.83	0.17
KPW2	9.22	13.75	0.34	0.07	0.09	3	0.66	0.78	0.22	0.51	0.67	0.33
KPW1	9.40	10.48	0.30	0.04	0.09	3	0.80	0.69	0.31	0.57	0.55	0.45
KPR2	7.82	15.09	0.27	0.14	0.14	3	0.59	0.77	0.23	0.48	0.64	0.36
KPR6	6.92	27.12	0.31	0.07	0.09	3	0.46	0.88	0.12	0.41	0.80	0.20
KPR8	5.85	17.71	0.33	0.11	0.11	3	0.49	0.88	0.12	0.42	0.80	0.20
KPR11	7.26	24.30	0.36	0.10	0.10	3	0.45	0.93	0.07	0.39	0.88	0.12
KPR14	7.09	21.58	0.23	0.06	0.09	3	0.33	0.91	0.09	0.26	0.84	0.16
KPR17	7.43	31.32	0.12	0.02	0.09	3	0.20	0.92	0.08	0.16	0.84	0.16
KPP11	7.79	22.07	0.15	0.11	0.11	3	0.24	0.91	0.09	0.17	0.83	0.17
KPP4	7.55	20.24	0.22	0.04	0.09	3	0.35	0.89	0.11	0.27	0.80	0.20
KPP3	8.67	7.62	0.05	0.04	0.09	3	0.59	0.61	0.39	0.26	0.39	0.61
KP18	8.28	16.11	-0.01	0.08	0.09	3	0.10	0.88	0.12	-0.01	0.73	0.28
KP15	6.74	14.44	0.03	0.07	0.09	3	0.17	0.86	0.14	0.07	0.70	0.30
KP10	6.30	19.11	-0.05	0.05	0.09	3	0.04	0.89	0.11	-0.03	0.74	0.26
KP8	6.81	18.69	-0.13	0.11	0.11	3	0.13	0.72	0.28	0.06	0.40	0.60
KP5	6.13	23.02	-0.04	0.03	0.09	2	0.02	0.93	0.07	-0.04	0.81	0.19
KP2	6.49	21.26	-0.11	0.02	0.09	2	-0.06	0.93	0.07	-0.12	0.79	0.21

1. U isotope data reported relative to CRM145
2. Reported uncertainty is the 2SD of replicate measurements or 0.09‰, whichever is greater
3. Number of times MC-ICP-MS analysis was carried out on the sample solutions
4. Authigenic $\delta^{238}U$ when detrital $\delta^{238}U = –0.8‰$
5. Fraction of authigenic U in the sample
6. Fraction of detrital U in the sample
7. Authigenic $\delta^{238}U$ when detrital $\delta^{238}U = –0.3‰$
8. Detrital $\delta^{238}U$

6.2.2 Interpretation of the increasing upward trend in authigenic $\delta^{238}U$

There are two possible scenarios that can explain the upward trend of increasing authigenic $\delta^{238}U$ in the Kettle Point Formation. The first scenario relates to a change in global ocean redox conditions, whereas the second scenario involves an invariant global ocean redox state but a change in local depositional conditions, namely the extent of basin restriction from the open ocean. These two possibilities are explored in detail below.

The trend towards heavier $\delta^{238}U$ (and higher U enrichments) upsection may reflect a greater global extent of ocean anoxia during Units 1-3, followed by a switch to a more oxygenated global ocean during Unit 4. Such an interpretation assumes that there was no significant change in the extent of basin restriction that would obscure the effect of global ocean redox changes on the U isotope signature of the Kettle Point black shales. If applying a U isotope fractionation factor of 0.60‰ for removal of U to euxinic sediments, similar to the weakly restricted Saanich Inlet (Holmden et al., 2015) then the global seawater $\delta^{238}U$ values in Unit 4 would be as high as 0‰, which is much higher than modern seawater $\delta^{238}U$ (–0.4‰). Such high seawater $\delta^{238}U$ would imply a significantly greater extent of ocean oxygenation during the Late Devonian compared with today, which is difficult to reconcile with the common occurrence of black shales in the rock record at this time (e.g., Smith and Bustin, 2000; Isaacson et al., 2008; Elkelani at al., 2014; Becker et al., 2016). Therefore, it is likely that the seawater-sediment U isotope fractionation factor during Unit 4 deposition was closer to 0.85‰, similar to the average U isotope fractionation during microbially mediated U(VI) reduction (Basu et al., 2014; Stirling et al., 2015; Stylo et al., 2015). If this fractionation factor was representative of U removal during all of Kettle Point Formation deposition, then the inferred global seawater $\delta^{238}U$ would be about –0.77‰ to –0.67‰ (i.e., for authigenic $\delta^{238}U$ = 0.08‰ to 0.18‰ in the shales, and subtracting 0.85‰) for Units 1-3, and –0.38‰ to –0.31‰ (i.e., for authigenic $\delta^{238}U$ = 0.47‰ to 0.54‰ in the shales, and subtracting 0.85‰) for Unit 4. The overall average seawater $\delta^{238}U$ for Units 1–3 would thus be –0.71‰; and for Unit 4, it would be –0.35‰ (i.e., taking the mid-points of the above ranges). It is noted, however, that variation in the U isotope fractionation factor associated with microbially mediated U(VI) reduction may have occurred during deposition of the Kettle Point Formation (e.g., over a range of 0.7–1.0‰; Basu et al., 2014; Stirling et al., 2015; Stylo et al., 2015).

As shown in Fig. 11, a simple steady-state U isotope mass balance model (Montoya-Pino et al., 2010) can be used to infer the extent of ocean anoxia across the Frasnian-Famennian boundary. The mass balance equation used is expressed as:

$$\delta^{238}U_{input} = (f_{anox} \times \delta^{238}U_{anox}) + (f_{other} \times \delta^{238}U_{other})$$

where "input" is the riverine input, "anoxic" denotes the anoxic and euxinic sink, and "other" represents U removal to sediments in all other marine settings, f_{anox} and f_{other} denote the fraction of U removed into each sink, and $f_{other} + f_{anox} = 1$. Combining $f_{other} + f_{anox} = 1$ with the above equation, and solving for f_{anox} yields:

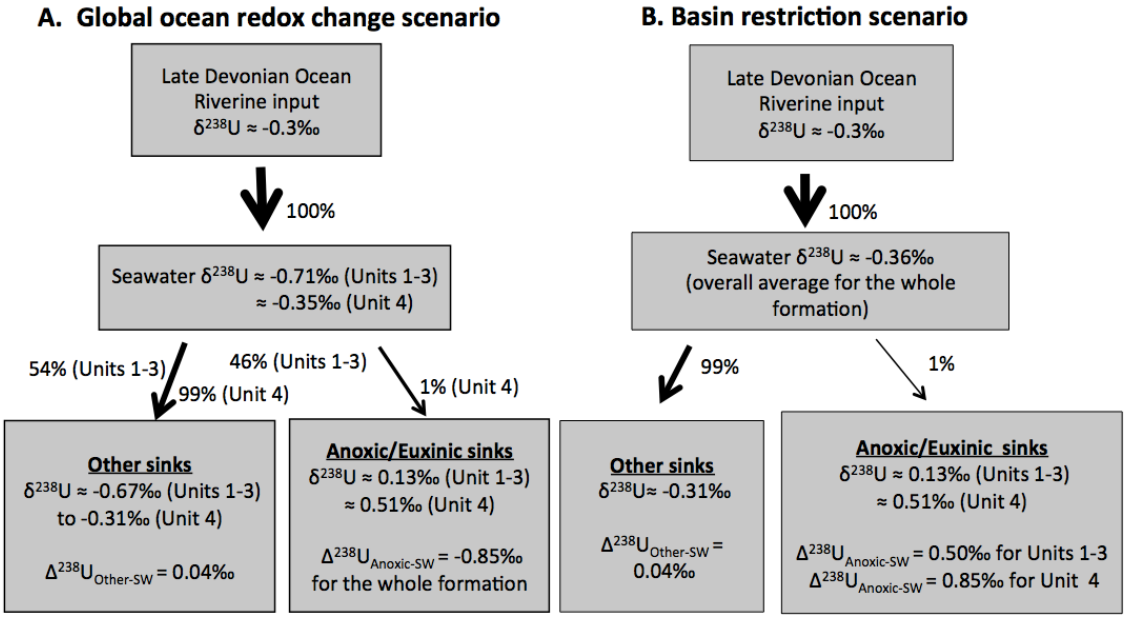

Fig. 11. Oceanic uranium isotope mass balance for A) the Late Devonian Ocean for the global ocean redox change scenario, and B) the Late Devonian Ocean for the basin restriction change scenario, and the associated estimates of the magnitude of the anoxic/euxinic sink in each scenario.

During Late Devonian time, the average riverine input $\delta^{238}U$ is assumed to be similar as the modern average of –0.3‰ (Tissot and Dauphas, 2015; Andersen et al., 2016), which is reasonable since the upper continental crust during the Late Devonian probably did not have a significantly different chemical composition from today. For the modern oceans, there is an overall average U isotope fractionation of 0.043‰ between seawater and the "other" sinks based on data from modern environments (Montoya-Pino et al., 2010; Andersen et al., 2014, 2016; Tissot and Dauphas, 2015; Tissot and Dauphas, 2015; Wang et al., 2016; Noordmann et al., 2016). Hence, the $\delta^{238}U_{other}$ during Units 1–3 and Unit 4 are inferred to be –0.667‰ and –0.307‰ for seawater $\delta^{238}U$ of –0.71‰ and –0.35‰,

respectively, assuming a similar U isotope fractionation factor during Late Devonian time. The average authigenic $\delta^{238}U$ from Units 1–3 (~0.13‰) and Unit 4 (~0.51‰) are assumed to be representative of relatively open-ocean euxinic sediments during deposition of these respective units. Hence, the calculated fractions of U being removed into the anoxic/euxinic sink and all other sinks are 46% and 54%, respectively, during Units 1–3, and 1% and 99%, respectively, during Unit 4. If the maximum observed U isotope fractionation of 1‰ for microbially mediated reduction of U(VI) was used instead of the 0.85‰ average (Basu et al., 2014; Stirling et al., 2015; Stylo et al., 2015), then the calculated fractions of U being removed into the anoxic/euxinic sink and all other sinks are 55% and 45%, respectively, during Units 1–3, and 16% and 84%, respectively, during Unit 4. Using more complex mass-balance models that couple the proportion of U burial into the different marine sinks with the seafloor area covered by each marine sink (Wang et al., 2016) suggests that during deposition of Units 1–3, at least a few percent and possibly even tens of percent of the seafloor was covered by anoxic waters. By comparison, the extent of anoxic seafloor contracted significantly to modern levels, or nearly so, during deposition of Unit 4.

In the second (alternative) scenario, the $\delta^{238}U$ of the Kettle Point black shales exhibits an increasing trend upsection because of a change in the isotope fractionation factor during U reduction/removal related to a change in the extent of basin restriction from the open ocean. In this case, Units 1–3 were deposited during a moderate extent of basin restriction (based on lower Mo/TOC ratios) that could be associated with a smaller U isotope fractionation between the euxinic sediments and seawater compared with Unit 4, which was deposited at a time of weaker basin restriction (based on higher Mo/TOC ratios). For the moderately restricted Units 1–3, a U isotope fractionation of 0.5‰ may be reasonable given that an average U isotope fractionation of ~0.4‰ is observed between global seawater and the euxinic sediments of the more restricted Black Sea (Weyer et al., 2008; Montoya-Pino et al., 2010). As noted previously, the most likely representative U isotope fractionation between global seawater and euxinic sediments during Unit 4 deposition is closer to 0.85‰ (because lower fractionation factors yield unrealistically high seawater $\delta^{238}U$). Applying the anoxic/euxinic fractionation factors of 0.50‰ to Units 1-3, and 0.85‰ to Unit 4, an average global seawater $\delta^{238}U$ of –0.31‰ to –0.38‰ (Unit 4) and –0.32‰ to –0.42‰ (Units 1–3) is obtained using detrital $\delta^{238}U$ values of −0.3‰ to −0.8‰. Hence, the $\delta^{238}U$ value for the Frasnian-Famennian ocean during Kettle Point deposition is suggested to be approximately –0.36‰, which is close to the

modern well-oxygenated seawater composition (–0.39‰). Hence, widespread ocean oxygenation is inferred for the Frasnian-Famennian ocean in the scenario where the $\delta^{238}U$ of the Kettle Point Formation black shales is controlled strictly by the extent of basin restriction from the open ocean.

In either of the above scenarios, it is likely that widespread ocean oxygenation existed during deposition of Unit 4. In the next section, we evaluate the two hypotheses for the extent of ocean anoxia across the Frasnian-Famennian boundary (i.e., Units 1-3) by considering the Mo isotope compositions of black shales from the Kettle Point Formation.

6.3 Mo isotope constraints on the extent of Frasnian-Famennian ocean euxinia

6.3.1 Mo isotope composition of Frasnian-Famennian seawater

The $\delta^{98}Mo$ values in the Kettle Point Formation span a wide range from 0.62‰ to 1.73‰ that falls between the modern seawater composition (~ 2.34‰; Barling et al., 2001; Siebert et al., 2003; Nakagawa et al., 2012) and the average upper crust composition (~0‰; Voegelin at al., 2014; Greber et al., 2015a; Breillat et al., 2016). Variability in the Mo isotope composition can be interpreted as evidence for fractionation between seawater and euxinic sediments, thus it is essential to evaluate if the $\delta^{98}Mo$ data from the Kettle Point Formation is representative of the coeval global seawater composition. There is minimal detrital impact to consider on the bulk $\delta^{98}Mo$ values from the Kettle Point black shales since the Mo concentrations are very high relative to the average crustal value of ~1.5 ppm (McLennan, 1991), resulting in the proportion of detrital Mo in these samples being < 5% using the Mo mass balance. Hence, the bulk $\delta^{98}Mo$ values were used in the following discussion.

In Units 1–3, the samples have a narrower range of heavier $\delta^{98}Mo$ (average = 1.21‰ ± 0.32‰, 2SD) with a maximum value of 1.73‰. Because the lighter Mo isotopes are always preferentially removed to sediments (i.e., due to operation of a particulate shuttle, non-quantitative removal of Mo from bottom waters, and/or incomplete conversion of molybdate to highly reactive tetrathiomolybdate if bottom waters were weakly euxinic), the highest $\delta^{98}Mo$ from euxinic black shales is most likely to reflect the capture of seawater $\delta^{98}Mo$ or at least capture the smallest amount of Mo isotope fractionation from seawater.

Hence, the highest δ^{98}Mo values of 1.6–1.7‰ from Unit 1 and Unit 2 provide a lower limit for global seawater δ^{98}Mo across the Frasnian-Famennian boundary.

The Mo isotope composition of a black shale is most likely to capture the seawater value where bottom waters are sulfidic enough (i.e., H_2S_{aq} >11 μM) to enable quantitative conversion of molybdate to tetrathiomolybdate and the degree of basin restriction is strong enough to permit quantitative removal of Mo from the bottom waters (Arnold et al., 2004; Neubert et al., 2008). The samples from Units 1-3 were most likely deposited in euxinic waters based on high Mo, TOC, and S contents as discussed before, but it is hard to distinguish if conditions were strongly euxinic or weakly euxinic. The lower bottom water Mo concentrations inferred from the lower Mo/TOC ratios in Units 1-3 suggests a greater chance of more quantitative removal of Mo from bottom waters (Algeo and Lyons, 2006). However, the average Mo/TOC ratio for Units 1-3 (8 ppm/wt%) is still higher than the Black Sea (4.5 ppm/wt%) where there is near-quantitative scavenging of Mo from euxinic bottom waters. The poor correlation between Mo EF and δ^{98}Mo (R^2 = 0.40) and the complete lack of correlation between δ^{98}Mo and Mo/TOC (R^2 = 0.0; Fig. 9) observed in Units 1-3 is consistent with non-quantitative scavenging of Mo. Hence, it is possible that sufficient dissolved Mo was available in the water column to enable preservation of a Mo isotope fractionation associated with non-quantitative Mo removal, thus shifting the δ^{98}Mo of the sediments to lighter values compared with seawater. Therefore, it is reasonable to infer that the coeval global seawater δ^{98}Mo was higher than 1.6–1.7‰ during deposition of Units 1-3. There is a 0.5 ± 0.3‰ fractionation between strongly euxinic bottom waters and sediments if Mo removal from the water column is not quantitative (Nagler et al., 2011). Applying this fractionation factor to the Kettle Point Formation black shales, the contemporaneous seawater δ^{98}Mo would be 2.23 ± 0.30‰ (i.e., 1.93-2.53‰). A broadly similar extent of Mo isotope fractionation is known to occur between weakly euxinic waters and sediments in the deep Cariaco Basin (Arnold et al., 2004). In either case, previously published mass balance models for the extent of ocean euxinia based on Mo concentrations and isotope compositions in euxinic black shales suggest that euxinic waters will cover <0.3% of the global ocean floor when black shales have δ^{98}Mo ≥ 1.6–1.7‰ and Mo concentrations in excess of 100 ppm, assuming that rivers had an average Mo concentration and δ^{98}Mo similar to today (Dahl et al., 2011; Reinhard et al., 2013).

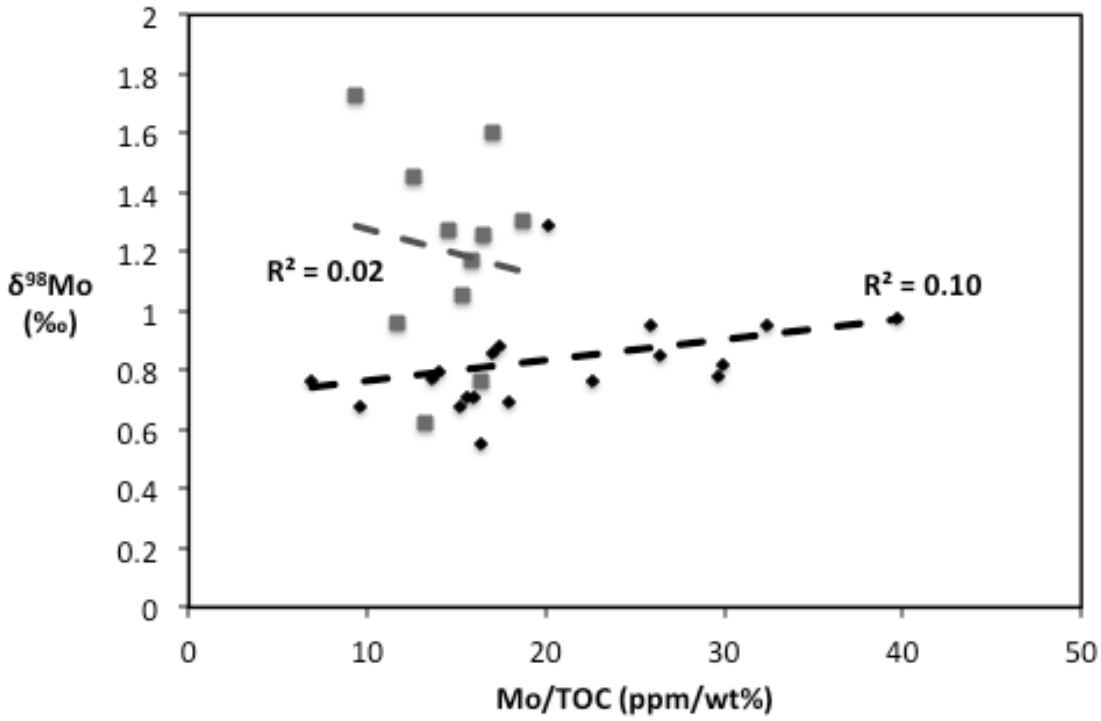

Fig. 12. Geochemical diagrams showing the relationship between δ^{98}Mo and Mo/TOC. The grey dashed trendline and grey dots represent Units 1–3 (135-64 m); the black trendline and black dots represent Unit 4 (64-28 m).

For Unit 4, δ^{98}Mo ranges from 0.55‰ to 0.98‰, which is lower than the values from Units 1-3. In addition, Unit 4 has a much steeper Mo/TOC slope (~35 ppm/wt%) compared with Units 1-3 (~8 ppm/wt%). Unit 4 has very high authigenic Mo enrichments and also preserves a poorer correlation between Mo EF and δ^{98}Mo (R^2 = 0.19) and between Mo/TOC and δ^{98}Mo (R^2 = 0.10), again implying non-quantitative scavenging of Mo. Low δ^{98}Mo could be interpreted as evidence for widespread ocean euxinia. However, the low δ^{98}Mo contradicts the high δ^{238}U and high Mo and U enrichments that point to widespread ocean oxygenation during Unit 4 deposition. These observations indicate a larger Mo isotope fractionation between the Unit 4 sediments and coeval seawater compared with between the Unit 1-3 sediments and coeval seawater. It is thus most likely Unit 4 was deposited from weakly euxinic waters. A similar interpretation was reached for euxinic black shales of the Ediacaran Doushantuo Formation (South China), which also had high δ^{238}U, high Mo and U enrichments, and generally low δ^{98}Mo (Kendall et al., 2015). The exact fractionation factor between Unit 4 sediments and seawater cannot be precisely quantified as modern weakly euxinic settings have a wide range of fractionation factors reaching up to 3‰ (Arnold et al., 2004; Neubert et al., 2008). The light δ^{98}Mo can also be caused by the operation of a particulate shuttle, but this possibility is not consistent with the

poor correlations between Mo concentration and δ^{98}Mo. If a particulate shuttle was the sole control on the δ^{98}Mo of the Kettle Point black shales, then the Fe-Mn particulates would deliver isotopically light Mo to sediments, and there should be a negative correlation observed between Mo EF and δ^{98}Mo. Therefore, both a particulate shuttle and weakly euxinic conditions could have existed, but weakly euxinic conditions must have played a leading role on controlling the Mo isotope signature. Operation of both processes may be responsible for the scattered distribution of Mo EF vs δ^{98}Mo and Mo/TOC vs δ^{98}Mo.

6.3.2 Coupled Mo-U isotope constraints on the extent of ocean oxygenation across the Frasnian-Famennian boundary

The coupled Mo-U isotope systematics shed important insights on global ocean redox conditions across the Frasnian-Famennian boundary during deposition of Units 1-3. In the first scenario inferred from U isotopes, namely a significantly greater extent of ocean anoxia, it is expected that the Mo isotope composition of Units 1-3 should be significantly lighter than modern seawater because of a greater extent of ocean euxinia compared with today. It is then expected that the stratigraphic shift upsection in Unit 4 to higher δ^{238}U should have been accompanied by a shift to higher δ^{98}Mo if there was a transition from a globally significant extent of ocean anoxia to widespread ocean oxygenation (see section 3). However, a positive covariation between δ^{98}Mo and δ^{238}U is not observed, suggesting that global redox changes are not the major factor controlling the δ^{98}Mo and δ^{238}U of the Kettle Point Formation black shales.

Instead, the negative correlation between δ^{98}Mo and δ^{238}U indicates that local changes in the depositional environment, including the degree of basin restriction and possibly the intensity of water column euxinia needs to be considered as an important control on the Mo-U isotope systematics of the black shales. As described above, it is possible that black shales from Units 1-3 were deposited under conditions of greater basin restriction (and potentially more euxinic bottom waters) than during deposition of Unit 4. Hence, during Units 1-3, there was a smaller Mo isotope fractionation between seawater and sediments (i.e., higher δ^{98}Mo in black shales), a smaller U isotope fractionation during U(VI) reduction and removal to sediments (i.e., lower δ^{238}U), and lower authigenic enrichments of Mo and U. Subsequently, the more open-ocean conditions (i.e., higher sea level) during Unit 4 deposition may have been accompanied by a larger Mo isotope fractionation between seawater and sediments (i.e., lower δ^{98}Mo in black shales), a larger U

isotope fractionation during U(VI) reduction and removal to sediments (i.e., higher $\delta^{238}U$), and higher authigenic enrichments of Mo and to a lesser extent U. The inverse correlation between $\delta^{98}Mo$ and $\delta^{238}U$ arises from the fact that lighter Mo isotopes and heavier U isotopes are preferentially removed from seawater to euxinic sediments.

Although the elemental and isotopic data from the Kettle Point Formation are consistent with a local depositional control on the shale geochemistry, the data do not require that the extent of ocean oxygenation was similar to today. A seawater $\delta^{98}Mo$ between 1.7‰ (the heaviest isotope composition in the Kettle Point Formation) and 2.3‰ (the modern value) is permitted by the data, and thus there could have been a slightly greater extent of ocean euxinia compared with today (but <0.3% of the ocean floor, as noted earlier). During Unit 4 deposition, a U isotope fractionation of 1‰ during U(VI) reduction would permit a global seawater $\delta^{238}U$ that is 0.1‰ lower than modern seawater, which would also be consistent with a slighter greater extent of ocean anoxia compared with today (but likely no more than a few percent of the seafloor based on the mass balance model of Wang et al., 2016). Such a scenario is more consistent with the common occurrence of epeiric sea black shales in the Late Devonian rock record than with modern-style widespread ocean oxygenation.

Overall, the coupled use of Mo and U abundances and isotopic compositions is shown in this study to represent a powerful approach that provides a more robust interpretation of both local and global ocean redox conditions. For example, it is worth noting that an erroneous interpretation could have been derived for the extent of ocean anoxia during Units 1-3 using U concentration and isotope data alone.

6.4. Implications for the Frasnian-Famennian mass extinction

Our geochemical data suggest that the Kettle Point black shales were deposited at a time of relatively widespread ocean oxygenation, with a slightly greater extent of ocean anoxia compared with today. This observation, coupled with the geological setting of many Late Devonian black shales, suggests that anoxic conditions were primarily confined to epeiric seas during sea level highstand conditions (Haq and Schutter, 2008; Harris et al., 2013; Alshahrani and Evans, 2014; Bush et al., 2015). Because the Kettle Point Formation

includes the Frasnian-Famennian boundary, it is of vital importance to test hypotheses regarding the role of ocean anoxia on the Late Devonian mass extinction events. In the Kettle Point Formation, the Frasnian-Famennian extinction may be marked by a decrease in the abundance of *Tasmanites* across the Unit 1-2 contact (Bingham-Koslowski et al., 2016).

The geochemical data from the Kettle Point Formation support other geological and geochemical data that point to an overall well-oxygenated atmosphere-ocean system in the Late Devonian Period, including the fossil charcoal record that indicates continuous and sustained fire events beneath a high-O_2 atmosphere (Rimmer et al., 2015). Other studies have suggested that ocean anoxia during the Late Devonian was largely localized in foreland basins and intracratonic epeiric seas (e.g., Harris et al., 2013; Bingham-Koslowski et al., 2016). Hence, global ocean anoxia is probably not a major trigger of the Frasnian-Famennian extinction event. Other researchers have found geochemical evidence for ocean anoxia around the time of the mass extinction (Wignall and Hallam, 1992; McGhee, 1996; Wignall and Twitchett, 1996; Jin et al., 2000; Tribovillard et al., 2004; Riquier et al., 2006; Carmichael et al., 2014; Formolo et al., 2014). Although it remains possible that epeiric sea anoxia was a contributing factor within individual intracratonic basins, further investigations into additional trigger mechanisms are encouraged.

Climate cooling is proposed to be one of the major reasons for the mass extinction (McGhee, 1982, 1996, 2013; Copper, 1977, 1986, 2002; Caputo, 1985; Algeo et al., 1995; Algeo and Scheckler, 1998; Streel et al., 2000; Joachimski and Buggisch, 2002; Dopieralska et al., 2016). For example, the mass extinction event particularly impacted the low-latitude tropical shallow water faunas during the late Frasnian, suggesting that repeated and significant temperature changes was one of the key drivers (Joachimski and Buggisch, 2002). Positive excursions in conodont apatite $\delta^{18}O$ paralleling with positive excursions in carbonate $\delta^{13}C$ from Frasnian-Famennian boundary sections were found by Joachimski and Buggisch (2002), which indicates enhanced organic carbon burial and a reduced atmospheric CO_2 concentration, consistent with climatic cooling. This cooling may also be related to the Devonian radiation of land plants, which increased the efficiency of weathering and thus enhanced the nutrient flux to the oceans (Algeo et al., 1995; Algeo and Scheckler, 1998). Despite evidence of a short-lived global eustatic sealevel fall around the Frasnian-Famennian boundary, evidence of glacial deposits of Frasnian to early Famennian age have not yet been found (Streel et al., 2000; Joachimski and Buggisch, 2002).

In addition, rapid, large-scale sea-level rises and falls and its consequences including eutrophication, microbial blooms, and photic zone euxinia are also suggested to be significant factors in the Late Devonian mass extinctions (Ji, 1989; Liao, 2002; Chen et al., 2002, 2013; Chen et al., 2002a; Chen and Tucker, 2003; Castle and Rodgers, 2009). A multiple-cause synthesis dominated by sea-level change is also inferred by Chen et al. (2013) through analysis of S isotope compositions in carbonate-associated sulfate and pyrite sulfide during the time interval. The data reflects a rapid sea-level fall in the latest Frasnian, and a subsequent long-lasting episode of photic-zone euxinia following a rapid sea-level rise in the earliest Famennian, while climate cooling also played an important role in delaying biological recovery after the extinction (Chen et al., 2013). This view of sea-level change associated with climate cooling is further supported by Ma et al. (2016) through integrating the related sea level record, isotope patterns, sea temperatures, and the extinction events.

Other explanations such as magmatism (Ricci et al., 2013) and bolide impacts (McLaren, 1970; McGhee, 1996; McGhee, 2001) are also argued to have a close correlation with the Kellwasser extinction event. Based on $^{40}Ar/^{39}Ar$ dating, the Frasnian–Famennian boundary (~372 Ma; Gradstein et al., 2012) and the emplacement of large igneous provinces in Eastern Siberia (i.e., Viluy traps; ranging from 362.3 ± 3.4 Ma to 379.7 ± 3.5 Ma) are found to be coeval (Ricci et al., 2013). The Viluy traps could be harmful to biodiversity because the emission of SO_2 and CO_2 gas, and the release/formation of sulfuric aerosols may have destabilized the climate by inducing rapid warming (enhanced CO_2) and/or cooling (formation of sulfur aerosols) (Retallack and Jahren, 2008; Ganino and Arndt, 2009; Svensen et al., 2009; Bond and Wignall, 2014). Our Mo and U concentration and isotope data imply that any warming associated with large igneous province emplacement did not result in widespread ocean stratification and anoxia. Bolide impacts can also result in earthquakes, tsunamis, wildfires, and dust clouds, which is a severe disruption to ecosystems (McLaren, 1970), however, there is no clear evidence of a link between a bolide impact and the Frasnian-Famennian extinction.

From the above discussion, it can be seen that the Late Devonian extinction events were probably not driven solely by one single factor. Multiple causes were probably linked together to cause the events, especially sea-level changes associated with climate cooling as

well as magmatism. Ocean anoxia may also play a role (such as development of photic zone euxinia in some areas), but our Mo and U evidence for relatively widespread oxygenation indicates that such a role was not at a global scale, but rather limited locally to shallow epeiric seas, intracratonic basins, and continental margins.

6.5 Implications for shale gas in Ontario

As discussed previously, bottom water euxinia was clearly present in the Chatham Sag, and played a major role in contributing to preservation of large amounts of organic matter in the black shales of the Kettle Point Formation. The high TOC content is consistent with high source rock potential (Loftsson, 1984; Powell et al., 1984; Delitala, 1984; Armstrong, 1986; Dusseault at al., 1986; Hamblin, 2006, 2010; Béland-Otis, 2013; Bingham-Koslowski et al., 2016) as previously suggested by many earlier studies. The Fe-TOC-S diagram indicates that the Kettle Point Formation is an Fe-limited euxinic system, with some of the sulfur likely being incorporated into the organic matter. Normally, this could be a concern for shale gas exploitation because thermal cracking of sulfur-rich organic matter could generate environmentally detrimental sour gas during catagenesis. However, the Kettle Point Formation organic matter is thermally immature to early mature, so it is possible that there was not a lot of thermogenic gas produced, thus limiting the production of sour gas. Light stable isotope analysis of the gas produced from the Kettle Point Formation suggests a predominantly microbial origin, rather than a thermogenic origin, and H_2S was not listed as an appreciable component of the gas composition (Beland-Otis, 2013). Nevertheless, it is recommended that gas composition be carefully monitored during any shale gas production. The issue of sour gas production in southern Ontario may be more relevant to the thermogenic gas produced by the more thermally mature upper Ordovician units (Collingwood Member of the Cobourg Formation and Rouge River Member of the Blue Mountain Formation; Beland-Otis, 2015) if these organic-rich source rocks were deposited from euxinic bottom waters. It is still of vital importance to consider the economic versus environmental impact of the production of shale gas in Ontario given significant concerns regarding anthropogenic greenhouse warming.

7.0 Conclusions

The geochemical data from the black shales of the Kettle Point Formation in the Gore of Chatham core provides valuable insights for ocean redox conditions during the Frasnian-Famennian mass extinction event. The high Mo and U enrichments, high TOC and S contents, and high Mo/U ratios together with the Fe-TOC-S systematics point to Fe-limited water column euxinia in the Chatham Sag. The Mo and U isotope compositions suggest two possible scenarios regarding ocean redox conditions during deposition of the Kettle Point Formation: 1) global ocean redox conditions changed from more anoxic to more oxygenated; or 2) a relatively invariant global ocean redox state but the extent of local basin restriction from the open ocean decreased. Based on a negative correlation between the Mo and U isotope compositions, it is concluded that changes in the extent of local basin restriction is the more likely scenario. Specifically, the black shales of the lower to middle Kettle Point Formation (Units 1-3) were probably deposited under conditions of greater basin restriction and potentially more euxinic bottom waters, while the upper Kettle Point Formation (Unit 4) was deposited in a less restricted basin (i.e., higher sea level) with less euxinic bottom waters. In Units 1-3, the highest δ^{98}Mo value of ~1.7‰ provides a lower limit for global seawater δ^{98}Mo across the Frasnian-Famennian boundary because the high Mo/TOC ratios from these black shales suggest non-quantitative removal of Mo from bottom waters and thus preservation of a Mo isotope fractionation between the euxinic sediments and seawater. The more open-ocean conditions during Unit 4 contributed to higher enrichment of U and especially Mo, a larger U isotope fractionation between the seawater and euxinic sediments, and thus a higher U isotope composition in the black shales. By contrast, the larger Mo isotope fractionation between seawater and sediments under weakly euxinic conditions, possibly accompanied by operation of an Fe-Mn particulate shuttle, resulted in the lighter δ^{98}Mo of Unit 4. In such a scenario where the U isotope composition of the Kettle Point Formation was primarily influenced by basin restriction, the δ^{238}U value for the Frasnian-Famennian ocean during Kettle Point deposition is suggested to be close to the modern seawater value, which implies widespread ocean oxygenation. The Mo and U isotope data do permit a slightly greater extent of global ocean anoxia and euxinia compared with today, but such conditions were likely confined locally to epeiric seas, intracratonic basins, and continental margins. Overall, the data suggests that widespread ocean anoxia was not the major cause of the Frasnian-Famennian mass extinction event.

References

Agrawal, A. (2009). *A technical and economic study of completion techniques in five emerging US gas shale plays* (Doctoral dissertation, Texas A and M University).

Algeo, T. J., Berner, R. A., Maynard, J. B., and Scheckler, S. E. (1995). Late Devonian oceanic anoxic events and biotic crises:"rooted" in the evolution of vascular land plants. GSA today, 5(3), 45.

Algeo, T. J., and Scheckler, S. E. (1998). Terrestrial-marine teleconnections in the Devonian: links between the evolution of land plants, weathering processes, and marine anoxic events. *Philosophical Transactions of the Royal Society of London B: Biological Sciences*, *353*(1365), 113-130.

Algeo, T. J. and Maynard, J. B. (2004). Trace-element behavior and redox facies in core shales of Upper Pennsylvanian Kansas-type cyclothems. *Chemical Geology*, *206*(3), 289-318.

Algeo, T. J., and Lyons, T. W. (2006). Mo–total organic carbon covariation in modern anoxic marine environments: Implications for analysis of paleoredox and paleohydrographic conditions. *Paleoceanography*, *21*(1).

Algeo, T. J. and Maynard, J. B. (2008). Trace-metal covariation as a guide to water-mass conditions in ancient anoxic marine environments. Geosphere, 4(5), 872-887.

Algeo, T. J. and Tribovillard, N. (2009). Environmental analysis of paleoceanographic systems based on molybdenum–uranium covariation. *Chemical Geology*, 268(3), 211-225.

Algeo, T. J. and Rowe, H. (2012). Paleoceanographic applications of trace-metal concentration data. *Chemical Geology*, *324*, 6-18.

Alroy, J., Aberhan, M., Bottjer, D. J., Foote, M., Fürsich, F. T., Harries, P. J. and Kosnik, M. A. (2008). Phanerozoic trends in the global diversity of marine invertebrates. *Science*, *321*(5885), 97-100. American Journal of Science, 315(8), 713-733.

Alshahrani, S. and Evans, J. (2014) Shallow-Water Origin of a Devonian Black Shale, Cleveland Shale Member (Ohio Shale), Northeastern Ohio, USA. *Open Journal of Geology*, 4, 636-653.

Anbar, A. D., and Knoll, A. H. (2002). Proterozoic ocean chemistry and evolution: a bioinorganic bridge?. *science*, *297*(5584), 1137-1142.

Anbar, A. D. (2004). Molybdenum stable isotopes: observations, interpretations and directions. *Reviews in Mineralogy and Geochemistry*, *55*(1), 429-454.

Andersen, M. B., Romaniello, S., Vance, D., Little, S. H., Herdman, R., and Lyons, T. W. (2014). A modern framework for the interpretation of 238 U/235 U in studies of ancient ocean redox. *Earth and Planetary Science Letters*, *400*, 184-194.

Anderson, R. F. (1987). Redox behavior of uranium in an anoxic marine basin. *Uranium*, *3*(2-4), 145-164.

Anderson, R. F., Fleisher, M. Q., and LeHuray, A. P. (1989). Concentration, oxidation state, and particulate flux of uranium in the Black Sea. *Geochimica et Cosmochimica Acta*, *53*(9), 2215-2224.

Anderson T. F. and Raiswell R. (2004). Sources and mechanisms for the enrichment of highly reactive iron in euxinic Black Sea sediments. *Am. J. Sci.* 304, 203–233.

Archer C. and Vance D. (2008). The isotopic signature of the global riverine molybdenum flux and anoxia in the ancient oceans. Nat. Geosci. 1, 597–600.

Ardakani, O. H., Chappaz, A., Sanei, H., and Mayer, B. (2016). Effect of thermal maturity on remobilization of molybdenum in black shales. *Earth and Planetary Science Letters*, *449*, 311-320.

Armstrong, D.K., (1986). Trace element geochemistry and petrology of the Kettle Point Formation (Upper Devonian), a black shale unit of southwestern Ontario. M.S.

Armstrong, D. K., and Dodge, J. E. P. (2007). Paleozoic geology of southern Ontario. *Ontario Geological Survey, Miscellaneous Release—Data*, *219*.

Armstrong, D. K., and Carter, T. R. (2010). The subsurface Paleozoic stratigraphy of southern Ontario. *Ontario Geological Survey.*

Arnold, G. L., Anbar, A. D., Barling, J. and Lyons, T. W. (2004). Molybdenum isotope evidence for widespread anoxia in mid-Proterozoic oceans. *Science*, *304*(5667), 87-90.

Asael, D., Tissot, F. L., Reinhard, C. T., Rouxel, O., Dauphas, N., Lyons, T. W., ... and Chéron, S. (2013). Coupled molybdenum, iron and uranium stable isotopes as oceanic paleoredox proxies during the Paleoproterozoic Shunga Event. *Chemical Geology*, *362*, 193-210.

Averbuch, O., Tribovillard, N., Devleeschouwer, X., Riquier, L., Mistiaen, B., and Vliet‐Lanoe, V. (2005). Mountain building‐enhanced continental weathering and organic carbon burial as major causes for climatic cooling at the Frasnian‐Famennian boundary (c. 376 Ma)?. Terra Nova, 17(1), 25-34.

Bajo, C., Rybach, L., and Weibel, M. (1983). Extraction of uranium and thorium from Swiss granites and their microdistribution: 1. Extraction of uranium and thorium. *Chemical Geology*, *39*(3-4), 281-297.

Barker, J. F., and Pollock, S. J. (1984). The geochemistry and origin of natural gases in southern Ontario. *Bulletin of Canadian Petroleum Geology*, *32*(3), 313-326.

Barling J., Arnold G. L. and Anbar A. D. (2001). Natural mass- dependent variations in the isotopic composition of molybde- num. Earth Planet. Sci. Lett. 193, 447–457.

Barling, J., and Anbar, A. D. (2004). Molybdenum isotope fractionation during adsorption by manganese oxides. *Earth and Planetary Science Letters,* 217(3), 315-329.

Barnes, C. E., and Cochran, J. K. (1990). Uranium removal in oceanic sediments and the oceanic U balance. *Earth and Planetary Science Letters*, *97*(1), 94-101.

Basu, A., Sanford, R.A., Johnson, T.M., Lundstrom, C.C., Löffler, F.E. (2014). Uranium isotopic fractionation factors during U (VI) reduction by bacterial isolates. *Geochim. Cosmochim*. Acta 136, 100–113.

Becker, R. T., Kaiser, S. I., and Aretz, M. (2016). Review of chrono-, litho-and biostratigraphy across the global Hangenberg Crisis and Devonian–Carboniferous Boundary. *Geological Society, London, Special Publications*, *423*, SP423-10.

Béland Otis, C. (2013). Gas assessment of the Devonian Kettle Point Formation; Ontario Geological Survey, Open File Report 6279, 63p.

Béland Otis, C. (2015). Upper Ordovician organic-rich mudstones of southern Ontario: Drilling project results; Ontario Geological Survey, Open File Report 6312, 59p.

Bertine, K. K., and Turekian, K. K. (1973). Molybdenum in marine deposits. *Geochimica et Cosmochimica Acta*, *37*(6), 1415-1434.

Bingham-Koslowski, N., Tsujita, C. C., Jin, J., & Azmy, K. (2016). Widespread Late Devonian marine anoxia in eastern North America; a case study of the black shale of the Kettle Point Formation, southwestern Ontario. *Canadian Journal of Earth Sciences*, (ja).

Biswas, K. C., Woodards, N. A., Xu, H., and Barton, L. L. (2009). Reduction of molybdate by sulfate-reducing bacteria. *Biometals*, *22*(1), 131-139.

Bond, D. P., Wignall, P. B., and Racki, G. (2004). Extent and duration of marine anoxia during the Frasnian–Famennian (Late Devonian) mass extinction in Poland, Germany, Austria and France. *Geological Magazine*, *141*(02), 173-193.

Bond, D. P., and Wignall, P. B. (2008). The role of sea-level change and marine anoxia in the Frasnian–Famennian (Late Devonian) mass extinction. *Palaeogeography, Palaeoclimatology, Palaeoecology*, *263*(3), 107-118.

Bond, D. P., and Wignall, P. B. (2014). Large igneous provinces and mass extinctions: an update. *Geological Society of America Special Papers*, *505*, SPE505-02.

Bostick, B. C., Fendorf, S., and Helz, G. R. (2003). Differential adsorption of molybdate and tetrathiomolybdate on pyrite (FeS2). *Environmental science and technology*, *37*(2), 285-291.

Brady, W. B. (1955). Palaeozoic geology of the Windsor-Sarnia area, Ontario. Queen's Printer.

Breillat, N., Guerrot, C., Marcoux, E., and Négrel, P. (2016). A new global database of δ 98 Mo in molybdenites: A literature review and new data. *Journal of Geochemical Exploration*, *161*, 1-15.

Brennecka, G. A., Wasylenki, L. E., Bargar, J. R., Weyer, S., and Anbar, A. D. (2011). Uranium isotope fractionation during adsorption to Mn-oxyhydroxides. *Environmental science and technology*, *45*(4), 1370-1375.

Broadhead, R. F., Kepferle, R. C. andPotter, P. E. (1982). Stratigraphic and sedimentologic controls of gas in shale--example from Upper Devonian of northern Ohio. *AAPG Bulletin*, *66*(1), 10-27.

Broecker, W. S., Peng, T. H., and Beng, Z. (1982). *Tracers in the Sea*. Lamont-Doherty Geological Observatory, Columbia University.

Brown, T. C., and Kenig, F. (2004). Water column structure during deposition of Middle Devonian–Lower Mississippian black and green/gray shales of the Illinois and Michigan Basins: a biomarker approach. *Palaeogeography, Palaeoclimatology, Palaeoecology*, *215*(1), 59-85.

Bush, A. M., Csonka, J. D., DiRenzo, G. V., Over, D. J., and Beard, J. A. (2015). Revised correlation of the Frasnian–Famennian boundary and Kellwasser Events (Upper Devonian) in shallow marine paleoenvironments of New York State. *Palaeogeography, Palaeoclimatology, Palaeoecology*, *433*, 233-246.

Caley, J. F. (1943). *Palaeozoic geology of the London area, Ontario*. Edmond Cloutier, Printer to the King's Most Excellent Majesty.

Caley, J. F., Sanford, B. V., and Brady, W. B. (1945). *Palaeozoic Geology of the Windsor Sarnia Area, Ontario*. La Commission.

Canfield, D. E. (1998). A new model for Proterozoic ocean chemistry. *Nature*, 396(6710), 450-453.

Caputo, M. V. (1985). Late Devonian glaciation in South America. *Palaeogeography, Palaeoclimatology, Palaeoecology*, *51*(1), 291-317.

Carmichael, S. K., Waters, J. A., Suttner, T. J., Kido, E., and DeReuil, A. A. (2014). A new model for the Kellwasser Anoxia Events (Late Devonian): Shallow water anoxia in an open oceanic setting in the Central Asian Orogenic Belt. *Palaeogeography, Palaeoclimatology, Palaeoecology*, *399*, 394-403.

Castle, J. W., and Rodgers Jr, J. H. (2009). Hypothesis for the role of toxin-producing algae in Phanerozoic mass extinctions based on evidence from the geologic record and modern environments. *Environmental Geosciences*, *16*(1), 1-23.

Chappaz, A., Lyons, T. W., Gregory, D. D., Reinhard, C. T., Gill, B. C., Li, C., and Large, R. R. (2014). Does pyrite act as an important host for molybdenum in modern and ancient euxinic sediments?. *Geochimica et Cosmochimica Acta*, *126*, 112-122.

Chen, D., and Tucker, M. E. (2003). The Frasnian–Famennian mass extinction: insights from high-resolution sequence stratigraphy and cyclostratigraphy in South China. *Palaeogeography, Palaeoclimatology, Palaeoecology*, *193*(1), 87-111.

Chen, D., Wang, J., Racki, G., Li, H., Wang, C., Ma, X., and Whalen, M. T. (2013). Large sulphur isotopic perturbations and oceanic changes during the Frasnian–Famennian transition of the Late Devonian. Journal of the Geological Society, 170(3), 465-476.

Chen, G., Chapron, B., Ezraty, R., and Vandemark, D. (2002). A global view of swell and wind sea climate in the ocean by satellite altimeter and scatterometer. *Journal of Atmospheric and Oceanic Technology*, *19*(11), 1849-1859.

Chen, X., Wu, Z., Xu, S., Wang, L., Huang, R., Han, Y., ... and Wang, Y. (2015). Probing the electron states and metal-insulator transition mechanisms in molybdenum disulphide vertical heterostructures. *Nature communications*, *6*.

Chen, X., Romaniello, S. J., Herrmann, A. D., Wasylenki, L. E., and Anbar, A. D. (2016). Uranium Isotope Fractionation During Coprecipitation with Aragonite and Calcite. *Geochimica et Cosmochimica Acta*.

Clark, S. K., and Johnson, T. M. (2008). Effective isotopic fractionation factors for solute removal by reactive sediments: A laboratory microcosm and slurry study. *Environmental science and technology*, *42*(21), 7850-7855.

Coleman, D. J., Nye, K. J., Chick, K. E., and Gagg, C. M. (1995). A comparison of immunomagnetic separation plus enrichment with conventional salmonella culture in the examination of raw sausages. *Letters in applied microbiology*, *21*(4), 249-251.

Collier, R. W. (1985). Molybdenum in the northeast Pacific Ocean. *Limnology and Oceanography*, *30*(6), 1351-1354.

Coniglio, M., and Cameron, J. S. (1990). Early diagenesis in a potential oil shale: evidence from calcite concretions in the Upper Devonian Kettle Point Formation, southwestern Ontario. *Bulletin of Canadian Petroleum Geology*, *38*(1), 64-77.

Copper, P. (1977). Paleolatitudes in the Devonian of Brazil and the Frasnian-Famennian mass extinction. *Palaeogeography, Palaeoclimatology, Palaeoecology*, *21*(3), 165-207.

Copper, P. (1986). Frasnian/Famennian mass extinction and cold-water oceans. *Geology*, *14*(10), 835-839.

Copper, P. (2002). Reef development at the Frasnian/Famennian mass extinction boundary. *Palaeogeography, Palaeoclimatology, Palaeoecology*, *181*(1), 27-65.

Crusius, J., Calvert, S., Pedersen, T., and Sage, D. (1996). Rhenium and molybdenum enrichments in sediments as indicators of oxic, suboxic and sulfidic conditions of deposition. *Earth and Planetary Science Letters*, *145*(1), 65-78.

Dahl, T. W., Hammarlund, E. U., Anbar, A. D., Bond, D. P., Gill, B. C., Gordon, G. W. and Canfield, D. E. (2010). Devonian rise in atmospheric oxygen correlated to the radiations of terrestrial plants and large predatory fish. *Proceedings of the National Academy of Sciences*, *107*(42), 17911-17915.

Dahl, T. W., Chappaz, A., Fitts, J. P., and Lyons, T. W. (2013). Molybdenum reduction in a sulfidic lake: Evidence from X-ray absorption fine-structure spectroscopy and implications for the Mo paleoproxy. *Geochimica et Cosmochimica Acta*, *103*, 213-231.

Dahl, T. W., Boyle, R. A., Canfield, D. E., Connelly, J. N., Gill, B. C., Lenton, T. M., and Bizzarro, M. (2014). Uranium isotopes distinguish two geochemically distinct stages during the later Cambrian SPICE event. *Earth and planetary science letters*, *401*, 313-326.

de Witt Jr, W. (1986). Devonian gas-bearing shales in the Appalachian basin.

Dean, W. E., and Arthur, M. A. (1989). Iron-sulfur-carbon relationships in organic-carbon-rich sequences I: Cretaceous Western Interior Seaway. *American Journal of Science*, *289*(6), 708-743.

Delitala, F. (1984). The mineralogy and geochemistry of the Kettle Point oil shale, S.W. Ontario; unpublished MSc thesis, *University of Western Ontario, London, Ontario*, 136p.

Droser, M. L., Bottjer, D. J., Sheehan, P. M., and McGhee, G. R. (2000). Decoupling of taxonomic and ecologic severity of Phanerozoic marine mass extinctions. *Geology*, *28*(8), 675-678.

Duan, Y., Anbar, A. D., Arnold, G. L., Lyons, T. W., Gordon, G. W., and Kendall, B. (2010). Molybdenum isotope evidence for mild environmental oxygenation before the Great Oxidation Event. *Geochimica et Cosmochimica Acta*, *74*(23), 6655-6668.

Dunk R. M., Mills R. A. and Jenkins W. J. (2002) A revaluation of the oceanic uranium budget for the Holocene. Chem. Geol. 190, 45–67.

Dusseault, M.B., Loftsson, M. and Russell, D. (1986). The mechanical behavior of the Kettle Point oil shale; *Canadian Geotechnical Journal*, v.23, p.87-93.

Elkelani, M. M. A., Sinninghe Damsté, J. S., Steemans, P., Reichart, G. J., and Smeenk, Z. (2014). Carbon isotope chemostratigraphy and palynology of Late Devonian black shales from the eastern Murzuq Basin. *Silurian and Devonian rocks and crude oil from the western part of Libya*, 71-108.

Emerson, S. R., and Huested, S. S. (1991). Ocean anoxia and the concentrations of molybdenum and vanadium in seawater. Marine Chemistry, 34(3), 177-196.

Erickson, B. E., and Helz, G. R. (2000). Molybdenum (VI) speciation in sulfidic waters:: stability and lability of thiomolybdates. *Geochimica et Cosmochimica Acta*, *64*(7), 1149-1158.

Ettensohn, F. R. (1992). Controls on the origin of the Devonian-Mississippian oil and gas shales, east-central United States. *Fuel*, *71*(12), 1487-1492.

Formolo, M. J., Riedinger, N. and Gill, B. C. (2014). Geochemical evidence for euxinia during the Late Devonian extinction events in the Michigan Basin (USA). *Palaeogeography, Palaeoclimatology, Palaeoecology*, *414*, 146-154.

Fractionation: Weyer S., Anbar A. D., Gerdes A., Gordon G. W., Algeo T. J. and Boyle E. A. (2008). Natural fractionation of $^{238}U/^{235}U$. *Geochim. Cosmochim. Acta 72*, 345–359.

Ganino, C., and Arndt, N. T. (2009). Climate changes caused by degassing of sediments during the emplacement of large igneous provinces. *Geology*, *37*(4), 323-326.

George, A. D., Chow, N. and Trinajstic, K. M. (2014). Oxic facies and the Late Devonian mass extinction, Canning Basin, Australia. *Geology*, *42*(4), 327-330.

Goldberg, T., Gordon, G., Izon, G., Archer, C., Pearce, C. R., McManus, and Rehkämper, M. (2013). Resolution of inter-laboratory discrepancies in Mo isotope data: an intercalibration. *Journal of Analytical Atomic Spectrometry*, *28*(5), 724-735.

Gordon, G. W., Lyons, T. W., Arnold, G. L., Roe, J., Sageman, B. B., and Anbar, A. D. (2009). When do black shales tell molybdenum isotope tales?. *Geology*, *37*(6), 535-538.

Goto, K. T., Anbar, A. D., Gordon, G. W., Romaniello, S. J., Shimoda, G., Takaya, Y. and Hanyu, T. (2014). Uranium isotope systematics of ferromanganese crusts in the Pacific Ocean: Implications for the marine 238 U/235 U isotope system. Geochimica et Cosmochimica Acta, 146, 43-58.

Gradstein, F. M., Ogg, J. G., Schmitz, M., and Ogg, G. (Eds.). (2012). *The geologic time scale 2012 2-volume set*. elsevier.

Gutschick, R. C. and Sandberg, C. A. (1991). Late Devonian history of Michigan basin. *Geological Society of America Special Papers*, *256*, 181-202.

Hamblin, A. P. (1998). *Upper Cambrian Strata of Southwestern Ontario: Summary of Literature*. Natural Resources Canada, Geological Survey of Canada.

Hamblin, A. P. (2006). *The" shale gas" concept in Canada: a preliminary inventory of possibilities*. Geological Survey of Canada.

Hamblin, A.P. (2010). Detailed outcrop and core measured sections of the Kettle Point formation, southwestern Ontario, with reference to shale gas potential, *Geological Survey of Canada*, Open File 6579, 26 p.

Haq, B. U., and Schutter, S. R. (2008). A chronology of Paleozoic sea-level changes. Science, 322(5898), 64-68.

Harris, N. B., Mnich, C. A., Selby, D. and Korn, D. (2013). Minor and trace element and Re–Os chemistry of the Upper Devonian Woodford Shale, Permian Basin, west Texas: Insights into metal abundance and basin processes. *Chemical Geology*, *356*, 76-93.

Helz, G. R., Miller, C. V., Charnock, J. M., Mosselmans, J. F. W., Pattrick, R. A. D., Garner, C. D., and Vaughan, D. J. (1996). Mechanism of molybdenum removal from the sea and its concentration in black shales: EXAFS evidence. *Geochimica et Cosmochimica Acta*, *60*(19), 3631-3642.

Helz, G. R., Vorlicek, T. P., and Kahn, M. D. (2004). Molybdenum scavenging by iron monosulfide. *Environmental science and technology*, *38*(16), 4263-4268.

Helz, G. R., Bura-Nakić, E., Mikac, N. and Ciglenečki, I. (2011). New model for molybdenum behavior in euxinic waters. *Chemical Geology*, *284*(3), 323-332.

Hinojosa, J. L., Stirling, C. H., Reid, M. R., Moy, C. M., and Wilson, G. S. (2016). Trace metal cycling and 238 U/235 U in New Zealand's fjords: Implications for reconstructing global paleoredox conditions in organic-rich sediments. *Geochimica et Cosmochimica Acta*, *179*, 89-109.

Holmden, C., Amini, M. and Francois, R. (2015). Uranium isotope fractionation in Saanich Inlet: A modern analog study of a paleoredox tracer. *Geochimica et Cosmochimica Acta*, *153*, 202-215.

Huang, C., and Gong, Y. (2016). Timing and patterns of the Frasnian–Famennian event: Evidences from high-resolution conodont biostratigraphy and event stratigraphy at the Yangdi section, Guangxi, South China. Palaeogeography, Palaeoclimatology, Palaeoecology, 448, 317-338.

Isaacson, P. E., Diaz-Martinez, E., Grader, G. W., Kalvoda, J., Babek, O., and Devuyst, F. X. (2008). Late Devonian–earliest Mississippian glaciation in Gondwanaland and its biogeographic consequences. *Palaeogeography, Palaeoclimatology, Palaeoecology*, *268*(3), 126-142.

Jaffey, A. H., Flynn, K. F., Glendenin, L. E., Bentley, W. T., and Essling, A. M. (1971). Precision measurement of half-lives and specific activities of U 235 and U 238. *Physical Review C*, *4*(5), 1889.

Jenkyns, H. C. (2010). Geochemistry of oceanic anoxic events. *Geochemistry, Geophysics, Geosystems*, *11*(3).

Ji, Q. (1989). On the Frasnian-Famennian mass extinction event in South China. *Courier Forschungsinstitut Senckenberg*, *117*, 275-301.

Jin, Y. G., Wang, Y., Wang, W., Shang, Q. H., Cao, C. Q., and Erwin, D. H. (2000). Pattern of marine mass extinction near the Permian-Triassic boundary in South China. *Science*, *289*(5478), 432-436.

Joachimski, M. M., and Buggisch, W. (1993). Anoxic events in the late Frasnian—Causes of the Frasnian-Famennian faunal crisis?. *Geology*, *21*(8), 675-678.

Joachimski, M. M. (1997). Comparison of organic and inorganic carbon isotope patterns across the Frasnian–Famennian boundary. *Palaeogeography, Palaeoclimatology, Palaeoecology*, *132*(1), 133-145.

Joachimski, M. M., Ostertag-Henning, C., Pancost, R. D., Strauss, H., Freeman, K. H., Littke, R., ... and Racki, G. (2001). Water column anoxia, enhanced productivity and concomitant changes in δ 13 C and δ 34 S across the Frasnian–Famennian boundary (Kowala—Holy Cross Mountains/Poland). *Chemical Geology*, *175*(1), 109-131.

Joachimski, M. M., and Buggisch, W. (2002). Conodont apatite δ18O signatures indicate climatic cooling as a trigger of the Late Devonian mass extinction. *Geology*, *30*(8), 711-714.

John, E. H., Wignall, P. B., Newton, R. J. and Bottrell, S. H. (2010). $\delta^{34}S$ and $\delta^{18}O$ records during the Frasnian–Famennian (Late Devonian) transition and their bearing on mass extinction models. *Chemical geology*, *275*(3), 221-234.

Johnson, M. D., Russell, D. J., and Telford, P. G. (1983). Oil shale assessment project, v. 1: Shallow drilling results 1981/82. *Ontario Geological Survey, Open File Report*, *5458*, 36.

Kashiwabara, T., Takahashi, Y. and Tanimizu, M. (2009). A XAFS study on the mechanism of isotopic fractionation of molybdenum during its adsorption on ferromanganese oxides. *Geochemical Journal*, *43*(6), e31-e36.

Kaufmann, B. (2006). Calibrating the Devonian time scale: a synthesis of U–Pb ID–TIMS ages and conodont stratigraphy. Earth-Science Reviews, 76(3), 175-190.

Kazmierczak, J., Kremer, B., and Racki, G. (2012). Late Devonian marine anoxia challenged by benthic cyanobacterial mats. *Geobiology*, *10*(5), 371-383.

Kendall B., Creaser R. A., Gordon G. W. and Anbar A. D. (2009). Re–Os and Mo isotope systematics of black shales from the Middle Proterozoic Velkerri and Wollogorang Formations, McArthur Basin, northern Australia. Geochim. Cosmochim. Acta 73, 2534–2558.

Kendall B., Brennecka G. A., Weyer S. and Anbar A. D. (2013) Uranium isotope fractionation suggests oxidative uranium mobilization at 2.50 Ga. *Chem. Geol*. 362, 105–114.

Kendall B., Dahl T.W., Anbar A.D., in press. Good golly, why moly? The stable isotope geochemistry of molybdenum. *Reviews in Mineralogy and Geochemistry: Non-traditional stable isotopes*. Mineralogical Society of America and Geochemical Society. *These authors contributed equally.

Kendall, B., Gordon, G. W., Poulton, S. W. andAnbar, A. D. (2011). Molybdenum isotope constraints on the extent of late Paleoproterozoic ocean euxinia. *Earth and Planetary Science Letters*, *307*(3), 450-460.

Kendall, B., Komiya, T., Lyons, T.W., Bates, S.M., Gordon, G.W., Romaniello, S.J. and Jiang, G. (2015). Uranium and molybdenum isotope evidence for an episode of widespread ocean oxygenation during the late Ediacaran Period. *Geochimica et Cosmochimica Acta*, *156*, 173-193.

Klemme, H. D., and Ulmishek, G. F. (1991). Effective petroleum source rocks of the world: stratigraphic distribution and controlling depositional factors (1). *AAPG Bulletin*, *75*(12), 1809-1851.

Klinkhammer, G. P., and Palmer, M. R. (1991). Uranium in the oceans: where it goes and why. *Geochimica et Cosmochimica Acta*, *55*(7), 1799-1806.

Koslowski, B.N. (2015). High resolution stratigraphy and paleoenvironmental reconstruction of the Upper Devonian Kettle Point Formation, southwestern Ontario, Canada, (Doctoral thesis, University of Western Ontario).

Langmuir, D. (1978). Uranium solution-mineral equilibria at low temperatures with applications to sedimentary ore deposits. *Geochimica et Cosmochimica Acta*, *42*(6), 547-569.

Lau, K. V., Maher, K., Altiner, D., Kelley, B. M., Kump, L. R., Lehrmann, D. J., ... and Payne, J. L. (2016). Marine anoxia and delayed Earth system recovery after the end-Permian extinction. *Proceedings of the National Academy of Sciences*, *113*(9), 2360-2365.

Levman, B. G., and Bitter, P. H. V. (2002). The Frasnian-Famennian (mid-Late Devonian) boundary in the type section of the Long Rapids Formation, James Bay Lowlands, northern Ontario, Canada. *Canadian Journal of Earth Sciences*, *39*(12), 1795-1818.

Liao, W. (2002). Biotic recovery from the Late Devonian FF mass extinction event in China. *Science in China Series D: Earth Sciences*, *45*(4), 380-384.

Loftsson, M. (1984). Engineering geology of the Kettle Point oil shales; unpublished MSc thesis, *University of Waterloo, Waterloo, Ontario*, 149p.

Lyons, T. W., and Severmann, S. (2006). A critical look at iron paleoredox proxies: new insights from modern euxinic marine basins. *Geochimica et Cosmochimica Acta*, *70*(23), 5698-5722.

Lyons, T. W., Reinhard, C. T., and Planavsky, N. J. (2014). The rise of oxygen in Earth/'s early ocean and atmosphere. *Nature,* 506(7488), 307-315.

Ma, X., Gong, Y., Chen, D., Racki, G., Chen, X., and Liao, W. (2016). The Late Devonian Frasnian–Famennian Event in South China—Patterns and causes of extinctions, sea level changes, and isotope variations. *Palaeogeography, Palaeoclimatology, Palaeoecology*, *448*, 224-244.

Macdonald, W.D. (1960). The Upper Devonian Kettle Point Formation of Ontario; *Canadian Mining and Metallurgical Bulletin*, v.53, p.844-847.

Martini, A. M., Walter, L. M., Budai, J. M., Ku, T. C. W., Kaiser, C. J., and Schoell, M. (1998). Genetic and temporal relations between formation waters and biogenic methane: Upper Devonian Antrim Shale, Michigan Basin, USA. *Geochimica et Cosmochimica Acta*, *62*(10), 1699-1720.

Marynowski, L., Narkiewicz, M., and Grelowski, C. (2000). Biomarkers as environmental indicators in a carbonate complex, example from the Middle to Upper Devonian, Holy Cross Mountains, Poland. *Sedimentary Geology*, *137*(3), 187-212.

Marynowski, L., and Filipiak, P. (2007). Water column euxinia and wildfire evidence during deposition of the Upper Famennian Hangenberg event horizon from the Holy Cross Mountains (central Poland). *Geological Magazine*, *144*(03), 569-595.

Marynowski, L., Kurkiewicz, S., Rakociński, M., and Simoneit, B. R. (2011). Effects of weathering on organic matter: I. Changes in molecular composition of extractable organic compounds caused by paleoweathering of a Lower Carboniferous (Tournaisian) marine black shale. *Chemical Geology*, *285*(1), 144-156.

McDonough, W. F., and Sun, S. S. (1995). The composition of the Earth. Chemical geology, 120(3), 223-253.

McGhee Jr., G.R., Clapham, M.E., Sheehan, P.M., Bottjer, D.J., Droser, M.L., (2013). A new ecological-severity ranking of major Phanerozoic biodiversity crises. *Palaeogeogr. Palaeoclimatol. Palaeoecol.* 370, 260–270.

McGhee, G. R. (1982). The Frasnian-Famennian extinction event: A preliminary analysis of Appalachian marine ecosystems. *Geological Society of America Special Papers*, *190*, 491-500.

McGhee, G. R. (1996). *The late Devonian mass extinction: the Frasnian/Famennian crisis*. Columbia University Press.

McGhee, G. R. (2001). Late Devonian extinction. *Palaeobiology II*, 223-226.

McLaren, D. J. (1970). Time, life, and boundaries. *Journal of Paleontology*, 801-815.

McLennan, S. M., and Taylor, S. R. (1991). Sedimentary rocks and crustal evolution: tectonic setting and secular trends. *The Journal of Geology*, 1-21.

McLennan, S. M. (2001). Relationships between the trace element composition of sedimentary rocks and upper continental crust. *Geochemistry, Geophysics, Geosystems*, 2(4).

McManus, J., Nägler, T. F., Siebert, C., Wheat, C. G., and Hammond, D. E. (2002). Oceanic molybdenum isotope fractionation: Diagenesis and hydrothermal ridge-flank alteration. *Geochemistry, Geophysics, Geosystems*, *3*(12), 1-9.

McManus, J., Berelson, W. M., Klinkhammer, G. P., Hammond, D. E., and Holm, C. (2005). Authigenic uranium: relationship to oxygen penetration depth and organic carbon rain. *Geochimica et Cosmochimica Acta*, *69*(1), 95-108.

Melendez, I., Grice, K., Trinajstic, K., Ladjavardi, M., Greenwood, P., and Thompson, K. (2013). Biomarkers reveal the role of photic zone euxinia in exceptional fossil preservation: An organic geochemical perspective. *Geology*, *41*(2), 123-126.

Miller, K. G., MouNtaiN, G. S., WriGht, J. D., and BroWNiNG, J. V. (2011). Sea level and ice Volume Variations. *Oceanography*, *24*(2), 40-53.

Montoya-Pino, C., Weyer, S., Anbar, A. D., Pross, J., Oschmann, W., van de Schootbrugge, B., and Arz, H. W. (2010). Global enhancement of ocean anoxia during Oceanic Anoxic Event 2: A quantitative approach using U isotopes. *Geology*, *38*(4), 315-318.

Morford, J. L., and Emerson, S. (1999). The geochemistry of redox sensitive trace metals in sediments. *Geochimica et Cosmochimica Acta*, 63(11), 1735-1750.

Morford, J. L., Emerson, S. R., Breckel, E. J., and Kim, S. H. (2005). Diagenesis of oxyanions (V, U, Re, and Mo) in pore waters and sediments from a continental margin. *Geochimica et Cosmochimica Acta*, *69*(21), 5021-5032.

Nägler, T. F., Neubert, N., Böttcher, M. E., Dellwig, O., and Schnetger, B. (2011). Molybdenum isotope fractionation in pelagic euxinia: Evidence from the modern Black and Baltic Seas. *Chemical Geology*, 289(1), 1-11.

Nägler, T. F., Anbar, A. D., Archer, C., Goldberg, T., Gordon, G. W., Greber, N. D., ... and Vance, D. (2014). Proposal for an international molybdenum isotope measurement standard and data representation. *Geostandards and Geoanalytical Research*, *38*(2), 149-151.

Nakagawa Y., Takano S., Firdaus M. L., Norisuye K., Hirata T., Vance D. and Sohrin Y. (2012). The molybdenum isotopic composition of the modern ocean. Geochem. J. 46, 131–141.

Neubert, N., Nägler, T. F., and Böttcher, M. E. (2008). Sulfidity controls molybdenum isotope fractionation into euxinic sediments: Evidence from the modern Black Sea. *Geology*, *36*(10), 775-778.

Noordmann, J., Weyer, S., Montoya-Pino, C., Dellwig, O., Neubert, N., Eckert, S., ... and Böttcher, M. E. (2015). Uranium and molybdenum isotope systematics in modern euxinic basins: Case studies from the central Baltic Sea and the Kyllaren fjord (Norway). *Chemical Geology*, *396*, 182-195.

Noordmann, J., Weyer, S., Georg, R. B., Jöns, S., and Sharma, M. (2016). 238U/235U isotope ratios of crustal material, rivers and products of hydrothermal alteration: new insights on the oceanic U isotope mass balance. *Isotopes in environmental and health studies*, *52*(1-2), 141-163.

Obermajer, M., Fowler, M. G., Goodarzi, F., and Snowdon, L. R. (1997). Organic petrology and organic geochemistry of Devonian black shales in southwestern Ontario, Canada. *Organic Geochemistry*, *26*(3), 229-246.

Ontario Geological Survey, and Harris, D. C. (1985). *Graphic Logs of Oil Shale Intervals-Ordovician Collingwood Member and the Devonian Kettle Point and Marcellus Formations*.

Partin, C. A., Lalonde, S. V., Planavsky, N. J., Bekker, A., Rouxel, O. J., Lyons, T. W., and Konhauser, K. O. (2013). Uranium in iron formations and the rise of atmospheric oxygen. *Chemical Geology*, *362*, 82-90.

Poulson, R. L., Siebert, C., McManus, J., and Berelson, W. M. (2006). Authigenic molybdenum isotope signatures in marine sediments. *Geology*, 34(8), 617-620.

Poulson Brucker, R. L., McManus, J., Severmann, S., and Berelson, W. M. (2009). Molybdenum behavior during early diagenesis: Insights from Mo isotopes. *Geochemistry, Geophysics, Geosystems*, *10*(6).

Poulton, S. W., and Canfield, D. E. (2011). Ferruginous conditions: a dominant feature of the ocean through Earth's history. *Elements, 7(2),* 107-112.

Powell, T.G., Macqueen, R.W., Barker, J.F. and Bree, D.G. (1984). Geochemical character and origin of Ontario oils. *Bulletin of Canadian Petroleum Geology*, v.32, p.289-312.

Racki, G., Racka, M., Matyja, H., and Devleeschouwer, X. (2002). The Frasnian/Famennian boundary interval in the South Polish–Moravian shelf basins:

integrated event-stratigraphical approach. *Palaeogeography, Palaeoclimatology, Palaeoecology*, *181*(1), 251-297.

Rakociński, M., Pisarzowska, A., Janiszewska, K., and Szrek, P. (2016). Depositional conditions during the Lower Kellwasser Event (Late Frasnian) in the deep-shelf Łysogóry Basin of the Holy Cross Mountains Poland. *Lethaia*.

Reinhard, C. T., Planavsky, N. J., Robbins, L. J., Partin, C. A., Gill, B. C., Lalonde, S. V., Bekker, A., Konhauser, K.O. and Lyons, T. W. (2013). Proterozoic ocean redox and biogeochemical stasis. Proceedings of the National Academy of Sciences, 110(14), 5357-5362.

Requejo, A. G., Allan, J., Creaney, S., Gray, N. R., and Cole, K. S. (1992). Aryl isoprenoids and diaromatic carotenoids in Paleozoic source rocks and oils from the Western Canada and Williston Basins. *Organic Geochemistry*, *19*(1), 245-264.

Retallack, G. J., and Jahren, A. H. (2008). Methane release from igneous intrusion of coal during Late Permian extinction events. *The Journal of Geology*, *116*(1), 1-20.

Ricci, J., Quidelleur, X., Pavlov, V., Orlov, S., Shatsillo, A., and Courtillot, V. (2013). New 40 Ar/39 Ar and K–Ar ages of the Viluy traps (Eastern Siberia): Further evidence for a relationship with the Frasnian–Famennian mass extinction. *Palaeogeography, Palaeoclimatology, Palaeoecology*, *386*, 531-540.

Rimmer, S. M., Hawkins, S. J., Scott, A. C., and Cressler, W. L. (2015). The rise of fire: Fossil charcoal in late Devonian marine shales as an indicator of expanding terrestrial ecosystems, fire, and atmospheric change. *American Journal of Science*, *315*(8), 713-733.

Riquier, L., Tribovillard, N., Averbuch, O., Devleeschouwer, X., and Riboulleau, A. (2006). The Late Frasnian Kellwasser horizons of the Harz Mountains (Germany): two oxygen-deficient periods resulting from different mechanisms. *Chemical Geology*, *233*(1), 137-155.

Roen, J. B. (1984). Geology of the Devonian black shales of the Appalachian Basin. *Organic Geochemistry*, *5*(4), 241-254.

Romaniello, S. J., Herrmann, A. D., and Anbar, A. D. (2013). Uranium concentrations and 238 U/235 U isotope ratios in modern carbonates from the Bahamas: Assessing a novel paleoredox proxy. *Chemical Geology*, *362*, 305-316.

Ross, D. J., and Bustin, R. M. (2008). Characterizing the shale gas resource potential of Devonian–Mississippian strata in the Western Canada sedimentary basin: Application of an integrated formation evaluation. *AAPG bulletin*, *92*(1), 87-125.

Russell, D. J. (1985). Depositional analysis of a black shale by using gamma-ray stratigraphy: The Upper Devonian Kettle Point formation of Ontario. *Bulletin of Canadian Petroleum Geology*, *33*(2), 236-253.

Russell, D. J., and Barker, J. F. (1983, November). Stratigraphy and geochemistry of the Kettle Point shale, Ontario. In *Proceedings of Third Eastern Oil Shale Symposium. Institute of Mining and Minerals Research, Lexington, Kentucky* (pp. 169-180).

Ryder, R. T. (1996). Fracture patterns and their origin in the upper Devonian Antrim Shale gas reservoir of the Michigan basin; a review (No. 96-23). *US Geological Survey.*

Samson. (2007). Core Lab gas shale study, Canister and sorbed gas characterization data, Final Report. June 28 2007.

Sandberg, C. A., Morrow, J. R., and Ziegler, W. (2002). Late Devonian sea-level changes, catastrophic events, and mass extinctions. *Special papers-geological society of america*, 473-488.

Schauble, E. A. (2007). Role of nuclear volume in driving equilibrium stable isotope fractionation of mercury, thallium, and other very heavy elements. *Geochimica et Cosmochimica Acta*, *71*(9), 2170-2189.

Scott, C., Lyons, T. W., Bekker, A., Shen, Y. A., Poulton, S. W., Chu, X. L., and Anbar, A. D. (2008). Tracing the stepwise oxygenation of the Proterozoic ocean. *Nature*, *452*(7186), 456-459.

Scott, C., and Lyons, T. W. (2012). Contrasting molybdenum cycling and isotopic properties in euxinic versus non-euxinic sediments and sedimentary rocks: refining the paleoproxies. *Chemical Geology*, *324*, 19-27.

Sepkoski Jr, J. J. (1986). Phanerozoic overview of mass extinction. In *Patterns and Processes in the History of Life* (pp. 277-295). Springer Berlin Heidelberg.

Shiel, A. E., Laubach, P. G., Johnson, T. M., Lundstrom, C. C., Long, P. E., and Williams, K. H. (2013). No measurable changes in 238U/235U due to desorption–adsorption of U (VI) from groundwater at the Rifle, Colorado, integrated field research challenge site. *Environmental science and technology*, *47*(6), 2535-2541.

Shimmield, G. B., and Price, N. B. (1986). The behaviour of molybdenum and manganese during early sediment diagenesis—offshore Baja California, Mexico. *Marine Chemistry*, *19*(3), 261-280.

Siebert C., Na¨gler T. F., von Blanckenburg F. and Kramers J. D. (2003) Molybdenum isotope records as a potential new proxy for paleoceanography. Earth Planet. Sci. Lett. 211, 159–171.

Siebert C, McManus J, Bice A, Poulson R, Berelson WM. (2006) Molybdenum isotope

Smith, M. G., and Bustin, R. M. (2000). Late Devonian and Early Mississippian Bakken and Exshaw black shale source rocks, Western Canada Sedimentary Basin: a sequence stratigraphic interpretation. *AAPG bulletin*, *84*(7), 940-960.

Snowdon, L. R. (1984). A comparison of RockEval pyrolysis and solvent extract results from the Collingwood and Kettle Point oil shales, Ontario. *Bulletin of Canadian Petroleum Geology*, *32*(3), 327-334.

Stearn, C. W. (1987). Effect of the Frasnian-Famennian extinction event on the stromatoporoids. *Geology*, *15*(7), 677-679.

Sternbeck, J., Sohlenius, G., and Hallberg, R. O. (2000). Sedimentary trace elements as proxies to depositional changes induced by a Holocene fresh-brackish water transition. *Aquatic Geochemistry*, *6*(3), 325-345.

Stigall, A. L. (2012). Speciation collapse and invasive species dynamics during the Late Devonian "Mass Extinction". *GSA Today*, *22*(1), 4-9.

Stirling, C. H., Andersen, M. B., Potter, E. K., and Halliday, A. N. (2007). Low-temperature isotopic fractionation of uranium. *Earth and Planetary Science Letters*, *264*(1), 208-225.

Stirling, C. H., Andersen, M. B., Warthmann, R., and Halliday, A. N. (2015). Isotope fractionation of 238 U and 235 U during biologically-mediated uranium reduction. *Geochimica et Cosmochimica Acta*, *163*, 200-218.

Streel, M., Caputo, M. V., Loboziak, S., and Melo, J. H. G. (2000). Late Frasnian–Famennian climates based on palynomorph analyses and the question of the Late Devonian glaciations. *Earth-Science Reviews*, *52*(1), 121-173.

Stromquist, J.K., Dickhout, R. and Barker, J.F. (1984). Oil Shale Assessment Project, Volume 4, Analytical geochemistry of selected potential oil shales (Ontario and New Brunswick), *Ontario Geological Survey, Open File Report* 5461, 46p.

Stylo, M., Neubert, N., Wang, Y., Monga, N., Romaniello, S. J., Weyer, S., and Bernier-Latmani, R. (2015). Uranium isotopes fingerprint biotic reduction. *Proceedings of the National Academy of Sciences*, *112*(18), 5619-5624.

Summons, R. E., and Powell, T. G. (1986). Chlorobiaceae in Palaeozoic seas revealed by biological markers, isotopes and geology. *Nature*, *319*(6056), 763-765.

Summons, R. E., and Powell, T. G. (1987). Identification of aryl isoprenoids in source rocks and crude oils: biological markers for the green sulphur bacteria. *Geochimica et Cosmochimica Acta*, *51*(3), 557-566.

Svensen, H., Planke, S., Polozov, A. G., Schmidbauer, N., Corfu, F., Podladchikov, Y. Y., and Jamtveit, B. (2009). Siberian gas venting and the end-Permian environmental crisis. *Earth and Planetary Science Letters*, *277*(3), 490-500.

Taylor, S. R., and McLennan, S. M. (1985). The continental crust: its composition and evolution.thesis, *Univ. of Waterloo, Waterloo, Ontario, Canada*, 234 pp.

Telus, M., Dauphas, N., Moynier, F., Tissot, F. L., Teng, F. Z., Nabelek, P. I., ... and Groat, L. A. (2012). Iron, zinc, magnesium and uranium isotopic fractionation during continental crust differentiation: The tale from migmatites, granitoids, and pegmatites. *Geochimica et Cosmochimica Acta*, 97, 247-265.

Tissot, B. P., and Welte, D. H. (1978). *Petroleum Formation and Occurance: A New Approach to Oil and Gas Exploration*. Springer.

Tissot, F. L., and Dauphas, N. (2015). Uranium isotopic compositions of the crust and ocean: Age corrections, U budget and global extent of modern anoxia. *Geochimica et Cosmochimica Acta*, 167, 113-143.

Tribovillard, N., Averbuch, O., Devleeschouwer, X., Racki, G., and Riboulleau, A. (2004). Deep water anoxia over the Frasnian–Famennian boundary (La Serre, France): a tectonically induced oceanic anoxic event?. *Terra Nova*, 16(5), 288-295.

Tribovillard, N., Algeo, T. J., Lyons, T., and Riboulleau, A. (2006). Trace metals as paleoredox and paleoproductivity proxies: an update. *Chemical Geology*, *232*(1), 12-32.

Tulipani, S., Grice, K., Greenwood, P. F., Haines, P. W., Sauer, P. E., Schimmelmann, A., ... and Schwark, L. (2015). Changes of palaeoenvironmental conditions recorded in Late Devonian reef systems from the Canning Basin, Western Australia: A biomarker and stable isotope approach. *Gondwana Research*, *28*(4), 1500-1515.

Tyson, R. V., and Pearson, T. H. (1991). Modern and ancient continental shelf anoxia: an overview. Geological Society, London, *Special Publications*, 58(1), 1-24.

Uyeno, T., Telford, P. G., and Sanford, B. V. (1982). *Devonian conodonts and stratigraphy of southwestern Ontario* (Vol. 332). Geological Survey of Canada.

Vorlicek, T. P., Kahn, M. D., Kasuya, Y., and Helz, G. R. (2004). Capture of molybdenum in pyrite-forming sediments: role of ligand-induced reduction by polysulfides. *Geochimica et Cosmochimica Acta*, *68*(3), 547-556.

Wang, X., Johnson, T. M., and Lundstrom, C. C. (2015). Isotope fractionation during oxidation of tetravalent uranium by dissolved oxygen. *Geochimica et Cosmochimica Acta*, *150*, 160-170.

Wang, X., Planavsky, N. J., Reinhard, C. T., Hein, J. R., & Johnson, T. M. (2016). A Cenozoic seawater redox record derived from 238U/235U in ferromanganese crusts. *American Journal of Science*, *316*(1), 64-83.

Waples, D. W. (2013). Geochemistry in petroleum exploration. *Springer Science and Business Media.*

Weyer S., Anbar A. D., Gerdes A., Gordon G. W., Algeo T. J. and Boyle E. A. (2008) Natural fractionation of 238U/235U. *Geochim. Cosmochim.* Acta 72, 345–359.

Wheat, C. G., Mottl, M. J., and Rudnicki, M. (2002). Trace element and REE composition of a low-temperature ridge-flank hydrothermal spring. *Geochimica et Cosmochimica Acta*, *66*(21), 3693-3705.

Wignall, P. B., and Hallam, A. (1992). Anoxia as a cause of the Permian/Triassic mass extinction: facies evidence from northern Italy and the western United States. *Palaeogeography, Palaeoclimatology, Palaeoecology*, *93*(1), 21-46.

Wignall, P. B. (1994). *Black shales* (Vol. 30, p. 144). Oxford: Clarendon Press.

Wignall, P. B., and Twitchett, R. J. (1996). Oceanic anoxia and the end Permian mass extinction. *Science*, *272*(5265), 1155.

Wignall, P. B., and Newton, R. (1998). Pyrite framboid diameter as a measure of oxygen deficiency in ancient mudrocks. *American Journal of Science*, 298(7), 537-552.

Winder, C. G. (1966). Conodont zones and stratigraphic variability in Upper Devonian rocks, Ontario. *Journal of Paleontology*, 1275-1293.

Wright, J., and Colling, A. (1995). Open University Course Team. *Seawater: Its Composition, Properties and Behaviour,*.

Yudina, A. B., Racki, G., Savage, N. M., Racka, M., and Malkowski, K. (2002). The Frasnian-Famennian events in a deep-shelf succession, Subpolar Urals: biotic, depositional, and geochemical records. *Acta Palaeontologica Polonica*, *47*(2).

Zheng, Y., Anderson, R. F., van Geen, A., and Kuwabara, J. (2000). Authigenic molybdenum formation in marine sediments: a link to pore water sulfide in the Santa Barbara Basin. *Geochimica et Cosmochimica Acta*, *64*(24), 4165-4178.

Zheng, Y., Anderson, R. F., van Geen, A., and Fleisher, M. Q. (2002). Preservation of particulate non-lithogenic uranium in marine sediments. *Geochimica et Cosmochimica Acta*, *66*(17), 3085-3092.